$\mathcal{R}$ESALAB

FINAL REPORT

FOR

TECHNICAL, ANALYTICAL AND COMPUTER SUPPORT

Contract No. 952808

18 February 1970 - 30 September 1972

Prepared For
Jet Propulsion Laboratory
Pasadena, California

Prepared By
Resalab Energy Conversion
Sunnyvale, California

TABLE OF CONTENTS

I. INTRODUCTION

This is the final report of work performed by Resalab Energy Conversion for the Jet Propulsion Laboratory during the time period 18 February 1970 to 30 September 1972 in support of JPL's efforts in thermoelectrics. Most of the work has involved analytical and experimental work on silicon-germanium alloys and related technology. The aim of Resalab's efforts has been the development of a better understanding of power generators that use silicon-germanium alloys. The work performed by Resalab on this contract, Contract No. 952808, can be categorized by four specific tasks. These tasks are the RTG Design Study, Material Study, Sublimation of Silicon-Germanium Alloys and Special Studies. The results achieved on each task of this contract are discussed separately.

The RTG Design Study task involves the development of a rigorous mathematical model for the design and performance analysis of cylindrical silicon-germanium thermoelectric generators (RTG's) and consists of two parts, a steady-state (static) and a transient (dynamic) part. The Material Study task involves the definition and implementation of a material study that aims to experimentally characterize the long-term behavior of the thermoelectric properties of silicon-germanium alloys as a function of temperature. The Sublimation of Silicon-Germanium Alloys task consists of analytical and experimental efforts aimed at the determination of the sublimation characteristics of silicon-germanium alloys and the study of sublimation effects on RTG performance. The Special Studies task involves studies performed at JPL's request on a variety of specific topics on thermoelectric energy conversion.

II. RTG DESIGN STUDY

A. Intoduction

The objectives of this task are the development of an improved mathematical model for the design and performance of silicon-germanium RTG's, the programming of the resultant mathematical model for solution on a high speed computer and the application of the computer program to the performance evaluation of representative and/or specific RTG's in a variety of deep space missions. The mathematical model is specifically oriented towards silicon-germanium RTG's that use the Air-Vac thermocouple concept because existing models of RTG's of this type are inadequate and because RTG's using silicon-germanium Air-Vac thermocouples are presently contemplated for use in most future deep space probes.

Most existing RTG design and performance analysis techniques are either highly approximate or else are complicated and unwieldy combinations of independent generator component design subroutines, many of which are frequently of questionable rigor. A comprehensive and accurate analytical technique therefore offers a presently unavailable tool for conveniently investigating the role of RTG's in either general or specific space applications. A more rigorous mathematical model of RTG performance is of obvious necessity to overall spacecraft designers as well as to workers associated with components that directly interface with the RTG, not to mention people involved with the design and performance analysis of the RTG.

The mathematical model and associated computer program for the analysis of silicon-germanium RTG performance developed on the present contract consider the static as well as the dynamic performance of such a RTG. For computational convenience the models and computer programs depicting static and dynamic RTG

2.

performance have been separated. Each model is discussed in some detail below, with the bulk of the discussion devoted to the static model because it is the static operating mode of a RTG that generally dictates RTG design and long term performance. Although the RTG operates throughout its life dynamically because of radioisotope fuel decay, the time constant of fuel decay is generally so long that at any given operating time the RTG operates quasi-statically.

B.   Static RTG Performance Analysis

The mathematical model used to describe the performance of a RTG was separated into steady-state and transient parts following the small-signal transient analysis of a thermoelectric generator first proposed by Gray[1]. Following this analysis, the temperature and performance variations of a thermoelectric generator may be assumed to consist of large steady-state and relatively smaller transient components. Thus,

$$T_n (x,t) = T_{nS}(x) + \phi_n(x,t)$$

$$T_p (x,t) = T_{pS}(x) + \phi_p(x,t)$$

$$T_H (t) = T_{HS} + \phi_H (t)$$

$$T_C (t) = T_{CS} + \phi_C (t) \tag{1}$$

$$I (t) = I_S + i (t)$$

$$V (t) = V_S + v (t)$$

$$Q_H (t) = Q_{HS} + q_H(t)$$

$$Q_C (t) = Q_{CS} + q_C(t)$$

where the T's and ϕ's pertain to temperatures, I and i are currents, V and v are voltages and Q's and q's are heat input terms. Subscripts n and p identify the n-and p-type thermoelements, H and C pertain to thermoelement hot and cold junctions

3.

and S indicates steady-state. The independent variables x and t refer to distance along the thermoelements and time respectively.

There are five basic equations that generally describe the behavior of a thermoelectric device for both statis and dynamic conditions. These equations consist of the heat balance relationships at thermocouple hot and cold junctions, the differential equations for the temperature distribution along the n-and p-type thermoelements, and the relationship between generator output voltage and the current and thermoelement temperatures. Substitution of Equation (1) into these five basic equations enables the separation of the resultant equations into two sets of five equations each, the first set involving only the steady-state variables and the second set involving for the most part only the transient variables with some of the steady-state variables as coefficients. The set of equations involving only steady-state variables may be listed as follows:

$$Q_{HS} = -S_{HS}T_{HS}I_S - k_pA_p \frac{dT_{pS}}{dx} \quad x = H \quad -k_nA_n \frac{dT_{nS}}{dx} \quad x = H$$

$$Q_{CS} = S_{CS}T_{CS}I_S + k_pA_p \frac{dT_{pS}}{dx} \quad x = C + k_nA_n \frac{dT_{nS}}{dx} \quad x = C$$

$$k_pA_p \frac{d^2T_{pS}}{dx^2} + \tau_pI_S \frac{dT_{pS}}{dx} + \frac{\rho_p}{A_p} I_S^2 = 0 \tag{2}$$

$$k_nAn \frac{d^2T_{nS}}{dx^2} - \tau_nI_S \frac{dT_{nS}}{dx} = \frac{\rho_n}{A_n} I_S^2 = 0$$

$$V_S = S_{CS}T_{CS} - S_{HS}T_{HS} - \tau_p - \tau_n T_{CS} - T_{HS} - I_S \frac{\rho_n\ell}{A_n} + \frac{\rho_n\ell}{A_p}$$

where S ($S = S_p - S_n$) refers to the Seebeck coefficient, k to the thermal conductivity, τ to the Thomson coefficient and ρ to the electrical resistivity of the thermoelements. The cross-sectional areas and length of the thermoelements are given

by A and ℓ respectively. The solution of Equations (2) with appropriate boundary conditions leads to a method for generator performance analysis essentially similar to that already discussed in detail for a solar thermoelectric generator[2]. The application of Equations (2) to the case of a RTG has also been previously considered[3]. The present application of Equations (2) to the analysis of a silicon-germanium RTG, although not demonstrated in detail here, is however more complete than that of Reference 3 in that possible anisotropy of insulation thermal conductivity is considered in detail and generator end losses are more accurately taken into account.

It is noted that Equations (2) pertain only to the thermoelements and thus represent only the outline of the overall calculational sequence required to evaluate RTG performance. Heat losses through the thermal insulation surrounding the thermoelements are formally taken into account by the addition of an equation. The appropriate equation that, in general, accounts for insulation heat loss is

$$\frac{\partial}{\partial x} k_I A_i \frac{\partial T_I}{\partial x} - C_I A_I \frac{\partial T_I}{\partial t} = 0 \quad , \tag{3}$$

where the subscript I identifies insulation. As before, Equation (3) may be separated into steady-state and transient components through the introduction of the relationship

$$T_I(x,t) = T_{IS}(x) + \phi_I(x,t) \quad . \tag{4}$$

It is also noted that Equations (1) to (4) assume one space-dimensional heat flow. In the case of the RTG schematically illustrated in Figure 1, the space-variable x pertains to the radial direction. Because of the parallelepipedal configuration of the thermoelements, Equations (1) and (2) have been written in

Figure 1 Longitudinal View of RTG

6.

terms of the Cartesian coordinate. The use of an effective average insulation

area A_I permits the use of the same Cartesian coordinate even in the case of the

thermal insulation, although the corresponding cylindrical coordinate may appear

more appropriate. The assumption of one-dimensional heat flow implicit in

Equations (1) to (4) indicates the lack of heat exchange between the lateral

surfaces of the thermoelements and the surrounding thermal insulation. While

the introduction of Equations (3) and (4) into the analysis permits the appor-

tionment of total radial input heat into components flowing through the thermo-

elements and through the insulation, it does not allow for an accounting of the

continuous heat interchange between thermoelements and insulation at their inter-

face. This latter heat transfer phenomenon is taken into account by comparing

the detailed temperature gradients in each realm at a finite number of points at

the interface and through the use of the physical make-up of the interface region

actually calculating the heat interchange between the thermoelements and the in-

sulation. The iterative nature of the overall calculational sequence, as dis-

cussed in Reference 3, enables the continuous heat interchange between insula-

tion and thermoelements to be factored into the analysis such that in the final

limit of calculational convergence the temperature gradients for the total gen-

erator are taken into account in a self-consistent way. Generator end losses

are calculated in much the same manner. In essence then, although all starting

equations are assumed one-space dimensional, the temperatures and performance

of the two dimensional RTG (assuming rotational symmetry about the axis of the

generator) are calculated in a self-consistent manner through the method of suc-

cessive approximations; an n dimensional problem is reduced to n one-dimensional

problems through successive approximations such that self-consistency obtains.

The steady-state mathematical model developed for the RTG in the present

analysis assumes an overall RTG configuration represented by an upright Polygon

with radiation fins protruding from the intersections of the sides of the polygon. The radiation fins are assumed to extend the axial length of the RTG, and to possess a triangular cross-section, with the base of the triangle placed adjacent to the RTG in each case. The RTG is assumed to contain a cylindrical radio-isotope fuel capsule. Silicon-germanium Air-Vac thermocouples are assumed to surround the lateral surface of the fuel capsule, with a gap separating thermo-couple hot shoes and the fuel capsule surface. It is moreover assumed that the far edges of the end-most thermocouples line up exactly with the ends of the fuel capsule. Individual Air-Vac thermocouple hot shoes are assumed to be sep-arated by gaps in both the axial and the circumferential directions. The model also makes allowance for a gap between the centermost thermocouples, such that one half of the axial thermocouples are on each side of the center gap. Each thermocouple has a rectangular hot shoe, with the possibility of making adjacent sides either equal or different in length. Each thermocouple consists of n-and p-type thermoelements and a cold stack in addition to the hot shoe. The fuel capsule is assumed to be supported at its ends by cups and end supports. The void volume between thermocouples is filled with thermal insulation, as is the volume around the fuel capsule end supports at the ends of the RTG. Figure 1 shows a cross-section of the assumed RTG configuration in the axial direction. A section of the circumferential cross-section of the RTG is shown in Figure 2.

The sequence of steady-state RTG performance calculations starts with the input of the geometrical description of the generator and all pertinent prop-erties of the materials of construction. A list of all input items into the steady-state calculational sequence is given in Table I.

At the start of the calculational sequence a first approximation value is arbitrarily assigned to the thermocouple hot junction temperatures; in the
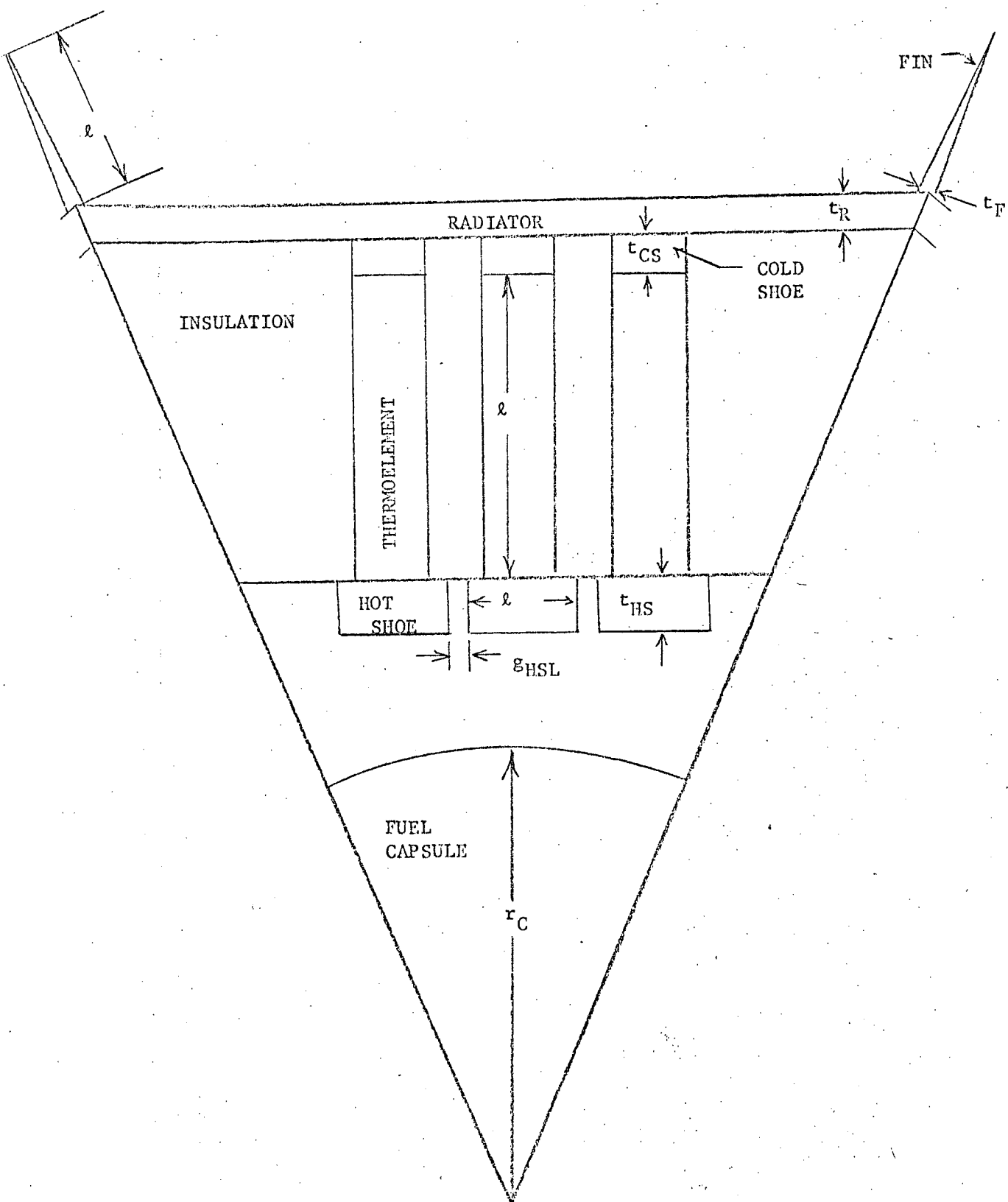
Figure 2: Lateral Section of RTG

Table I

Input Items Into Steady-State RTG Performance Code

Ambient Temperature for Lateral Radiator
Ambient Temperature for RTG Ends
Area of N Type Thermoelement
Area of P Type Thermoelement
Capsule End Emissivity
Convergence Criterion
Density of End Support
Density of Fin
Density of Fuel Capsule
Density of Hot Shoe
Density of Insulation
Density of Radiator
Density of Thermoelements
End Heat Conduction Coefficient
End Radiator Emissivity
End Support Emissivity
Extraneous Resistance Factor
Fin Tip to Fin Root Thickness Ratio
Fuel Cap Emissivity
Gap Between Adjacent Hot Shoes in Axial Direction
Gap Between Adjacent Hot Shoes in Lateral Direction
Hot Shoe Emissivity
Initialization Value of T(HOT)
Insulation Conduction Coefficient C1
Insulation Conduction Coefficient C2
Insulation Conduction Coefficient C3
Insulation Emissivity
Length From End of Capsule to End of RTG
Length of Fin
Length of Hot Shoe in Axial Direction
Length of Hot Shoe in Lateral Direction
Length of Thermocouple Material
Load Voltage
Miscellaneous Weight
Number of Parallel Paths
Number of Sides of Polygon
Number of Thermocouples in RTG
Number of Thermocouples Per Side of Polygon
Radiator Emissivity
Radius of End Support
Radius of Fuel Capsule

Table I (Cont.)

Thermal Conductivity of Capsule
Thermal Conductivity of Capsule End
Thermal Conductivity of Cold Stack
Thermal Conductivity of End Support
Thermal Conductivity of Hot Shoe
Thermal Conductivity of Radiator
Thickness of Capsule End
Thickness of Cold Stack
Thickness of End Insulation
Thickness of Fin
Thickness of Hot Shoe
Thickness of Radiator
Transverse Thermal Conductivity of Insulation
Total Heat Input
Width of Center Gap

first approximation it is thereby assumed that all thermocouples operate at identical hot junction temperatures. First approximation RTG cold side, including thermocouple cold junction temperatures are calculated from the heat input. Pertinent thermoelectric property data for the thermoelements are integrated, using these temperatures, along with the initialized values of thermocouple hot junction temperatures. Various geometric parameters are also calculated for use in the program.

The first estimate temperature distribution assumes that there is no axial temperature gradient in the generator and it is calculated by means of adjusting thermocouple hot junction temperatures until the total heat transferred through the generator agrees with the heat input within any arbitrary convergence criterion. The calculation that arrives at the first approximation temperatures for the generator thereby involves an iterative sequence. After the attainment of convergence in this first iterative loop, the calculation is continued in a second iterative loop that no longer assumes the lack of an axial temperature gradient in the generator. The results of the calculations in the first iterative loop therefore serve as inputs to the second loop. The second loop computes the temperature distribution in the generator and also accounts for axial heat flow; it also considers the heat interchange between thermoelements and the surrounding thermal insulation along the length of the thermoelements. Because the overall calculational sequence computes the performance of a RTG at a specified value of load voltage, the value of load current is set equal to zero in both loops if the calculated open circuit voltage is less than the voltage specified. This procedure prevents the load from acting as a current source that would drive current through the RTG when the specified load voltage exceeds the voltage available from the generator. In case the voltage generated by the RTG is

12.

less than the specified load voltage, the computations are therefore performed for the RTG in an open circuit operating mode. As a useful by-product, this procedure provides a method of calculating the open circuit performance of the RTG regardless of the heat input; this is accomplished by setting the load voltage to an arbitrary high value.

Four minor iterative loops are contained within the second major loop. The first of these minor loops computes the heat interchange between the thermo-elements and the surrounding thermal insulation along thermoelement lengths in the generator. The second loop computes the heat flow and temperature distribution through RTG end supports and end thermal insulation. The third minor loop calculates the heat flow characteristics between the lateral outer surface and the ends of the RTG. The fourth minor loop computes the heat flow characteristics and temperature distribution in the gap at the center of the RTG. Convergence to within any desired degree of accuracy is achieved in all of these four minor iterative loops by means of the Newton-Raphson technique. After achieving convergence in the minor loops, the total heat passing through the various components of the RTG is calculated and the sum of the individual values is compared to the total heat input to the RTG. If the calculated value of total heat input is not within any arbitrarily small desired increment, RTG fuel capsule temperatures are adjusted to new values and the whole calculational process repeated.

Normally about two to five iterations are required for convergence of the first major loop. The corresponding number of iterations required for convergence for the second major loop is usually three to seven. At the completion of the total calculational process, the output data are printed. Although any characteristic of RTG performance can be finally displayed as output data, it is

common to print values pertaining to the heat flowing through various RTG components, component temperatures and electrical performance characteristics of the RTG. The logic diagram for the steady-state portion of the presently developed steady-state RTG design code is displayed in Figure 3. It should be noted that the code name RATEG is used for the code and that the code is available on paper tape or punch-cards.

The computer program RATEG was made operational on a computer at the Jet Propulsion Laboratory and the results of this task were documented in detail as a memorandum and issued as Memorandum #14, Mathematical Model and Computer Program for the Design and Analysis of Silicon-Germanium Air-Vac RTG's. The documentation of the RTG model and computer code discussed in Memorandum #14 pertains only to the steady-state (static) operation of a RTG using silicon-germanium Air-Vac thermocouples. The steady-state part of the mathematical model is, of course, of considerably greater utility than the transient part in the design and analysis of thermoelectric generators. The code depicting the steady-state operation of a silicon-germanium RTG has been used on the present program in the performance of parametric analyses and the determination of operating characteristics of generators such as the MHW-RTG. The results of some such analyses are discussed under V - Special Studies of the present program.

C. Dynamic RTG Performance Analysis

As the transient (dynamic) operation of a RTG is relatively rare in most instances and because it is the steady-state operation that normally determines RTG design, the bulk of the efforts on RTG Design Study were devoted to the mathematical model and computer program depicting steady-state RTG operation. Nevertheless, a program for somewhat simplified RTG geometry was also adopted* for the calculation of RTG performance in transient operation. This program has been checked and debugged and is presently operational.

---

* The program for dynamic RTG operation was orginally developed by W. D. Leonard at JPL
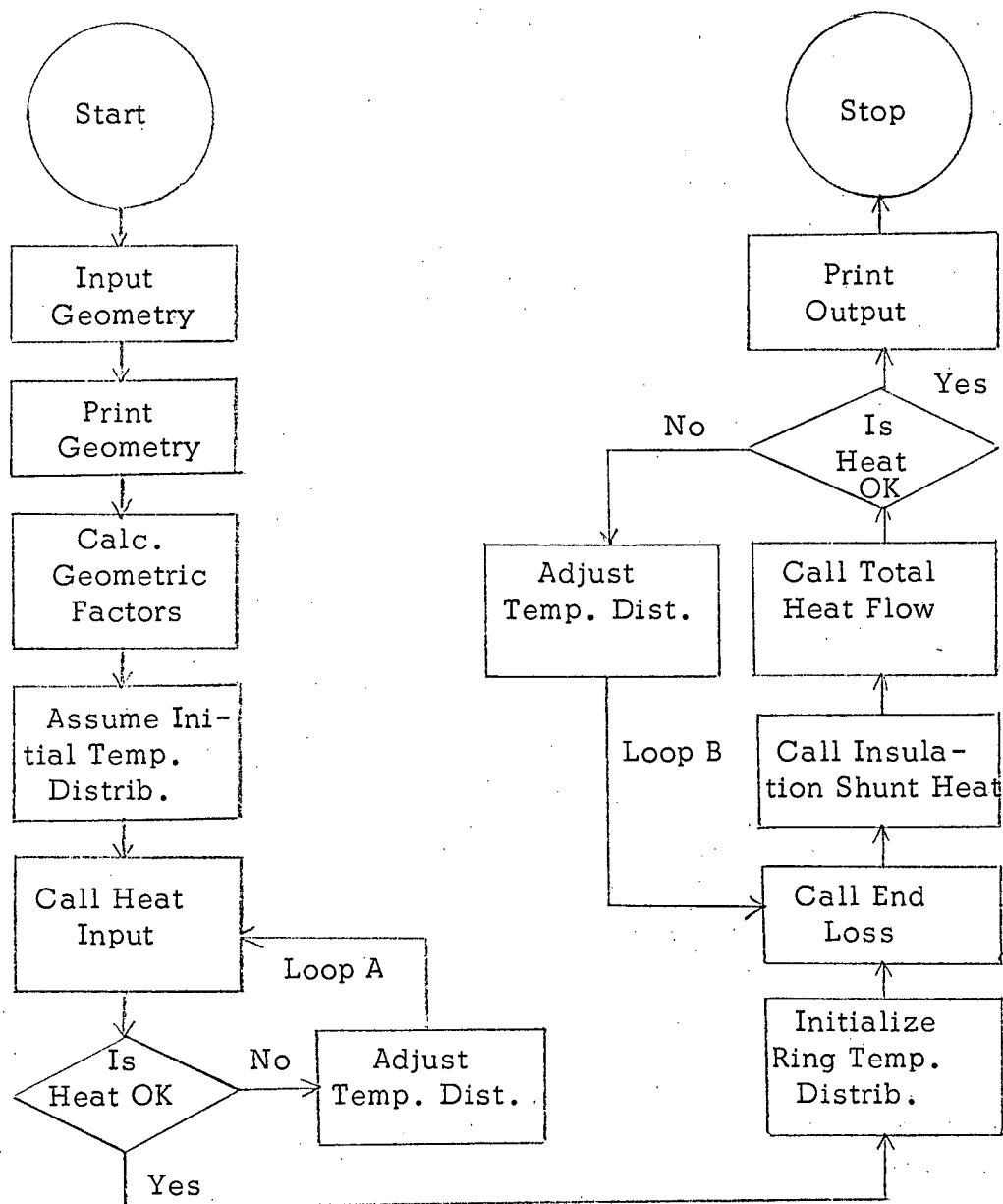
14.

Figure 3: RATEG Logic Diagram

The solution of the differential equations on which RTG design analyses are based results in the separation of the equations into static and dynamic portions. The set of equations involving only steady-state variables was given in the preceding section. The set of equations involving time dependent variables defined in Equations (1) of the preceeding section may be listed as follows

$$q_H = -S_{HS}T_{HS}i - S_{HS}I_S\phi_H - \tau I_S\phi_H - k_pA_p \left.\frac{\partial\phi_p}{\partial x}\right|x = H$$

$$- k_nA_n \left.\frac{\partial\phi_n}{\partial x}\right|x = H$$

$$q_C = S_{SC}T_{CS}i + S_{SC}I_S\phi_C + \tau I_S\phi_C + k_pA_p \left.\frac{\partial\phi_p}{\partial x}\right|x = C$$

$$+ k_nA_n \left.\frac{\partial\phi_n}{\partial x}\right|x = C \tag{5}$$

$$k_pA_p \frac{\partial^2\phi_p}{\partial x^2} + \tau_pI_S \frac{\partial\phi_p}{\partial x} + \tau_p \frac{dT_{pS}}{dx} i - C_pA_p \frac{\partial\phi_p}{\partial t}$$

$$+ 2 \frac{\rho_p}{A_p} I_S i = 0$$

$$k_nA_n \frac{\partial^2\phi_n}{\partial x^2} - \tau_nI_S \frac{\partial\phi_n}{\partial x} - \tau_n \frac{dT_{nS}}{dx} - C_nA_n \frac{\partial\phi_n}{\partial t}$$

$$+ 2 \frac{\rho_n}{A_n} I_S i = 0$$

$$V = \left(S_{CS}\phi_C - S_{HS}\phi_H\right) - i\left(\frac{\rho_n\ell}{A_n} + \frac{\rho_n\ell}{A_p}\right)$$

where $\tau = \tau_p - \tau_n$ and C_n and C_p are the specific heats of the n-and p-type thermoelements. All of the coefficients of Equations (5) are independent of time and only the coefficient dT_{pS}/dx and dT_{nS}/dx are functions of the space variable x.

The latter coefficients may be fixed by setting them equal to $\Delta T_s / \ell$; this procedure enables the treatment of all Equations (5) as equations with constant coefficients. The solution of Equations (5) requires the solution of two partial differential equations, the third and fourth of Equations (5).

A logic diagram of the transient program, called TRANS, is shown in Figure 4. The calculation starts with the geometry and initial temperature distribution. Based on the initial temperature distribution the program computes the integrated average property data of the thermoelements. This is done using a special subroutine which does the integration by a trapezoidal method.

Once the thermoelectric properties are calculated, the thermoelectric performance of the generator is computed. This includes the current, open circuit voltage and power output. If the load voltage is equal to or greater than the instantaneous open circuit voltage the current and power are set equal to zero. This prevents current from flowing through the generator backwards and in essence does not close the generator circuit until there is sufficient positive temperature drop across the thermoelements to drive current through the load.

The initial electrical performance of the generator and pertinent temperatures are printed as outputs. Time is incremented by a step the length of which is input to the program. The choice of the time increment requires some discretion. A time increment too small will require a large computer running time. A time increment too large will result in oscillating and diverging model temperatures. For RTG's of the MHW type, a time increment of 0.25 minutes is about optimum. A new calculated temperature distribution results. This calculation is described below. The thermoelectric properties are recalculated and the new performance is computed.

The total running time is examined to see if it is equal to the input value. If it is not, the print time is examined. If it is not time to print,
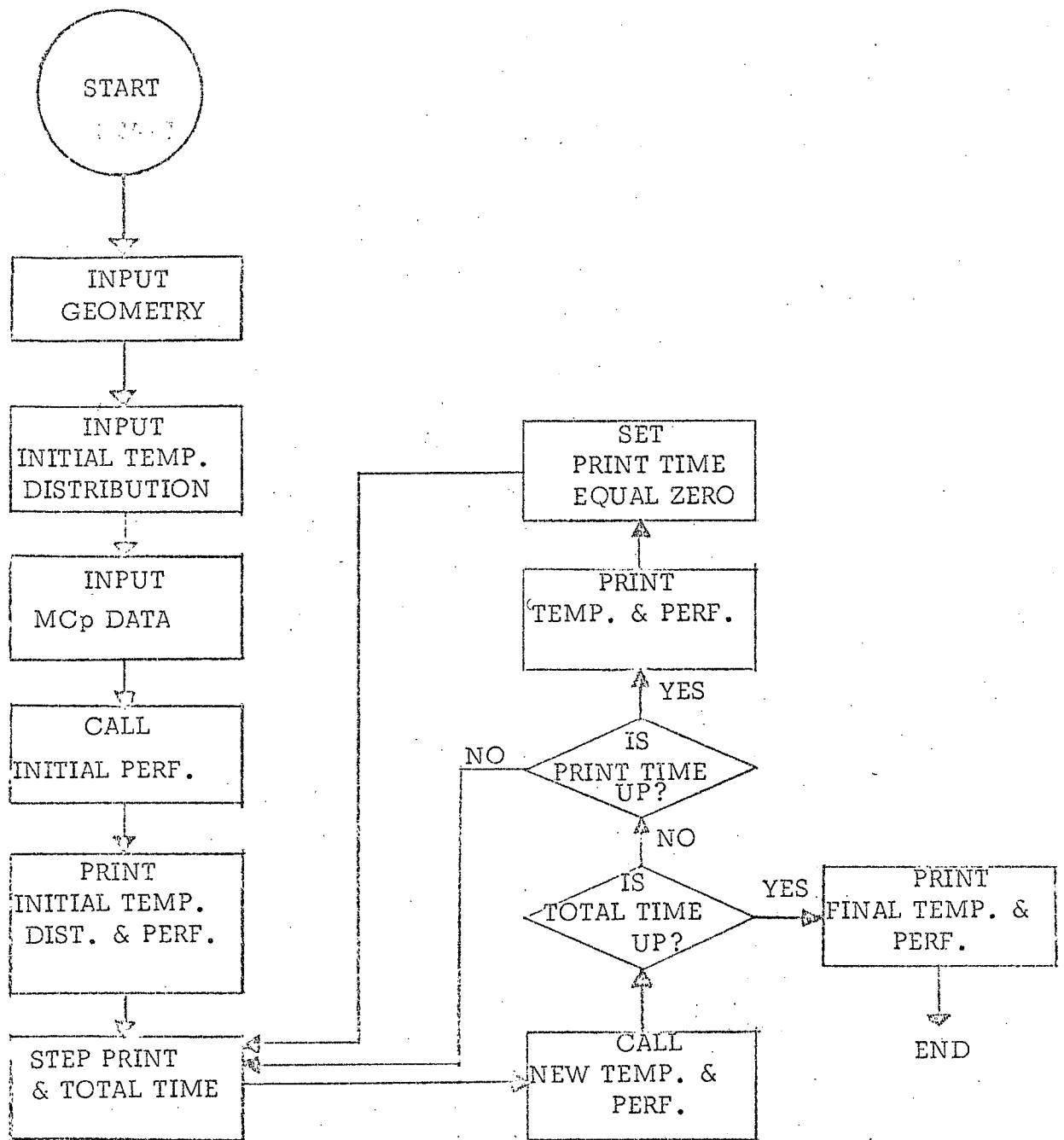
17.

FIGURE 4 DYNAMIC PROGRAM LOGIC DIAGRAM

18.

the running time and print time are stepped again and the calculational proce-
dure repeated. This cycle is repeated until the total running time has been
exhausted. At each print increment, as well as at the beginning and end of the
total time, the pertinent performance parameters are printed. In addition, at
the end of the run the final temperature at each model point is printed. This
makes it possible to start another run by using the final temperature distribu-
tion of the preceding run as the initial temperature distribution for the suc-
ceeding run. Thus, for example, one can observe the transient for one period
of time with the load voltage at some value and then observe what happens when
the load voltage is stepped to any other value.

The calculation of the new temperature distribution after each incre-
ment of time is done by performing an energy balance on each node. Figure 5
shows the nodal model used in TRANS. It consists of eight nodes including two
each in the thermoelectric material and insulation between the thermoelements.
In addition to the average temperature of the eight nodes, several interface
temperatures are used. An energy balance of the following from is applied to
each node:

$$Q_{in} = Q_{out} + E + M \frac{dT}{dt} \ , \tag{6}$$

where Q_{in} is the thermal energy into node, Q_{out} is the thermal energy out of
node, E is the electrical energy out of node, M is the mass-specific heat pro-
duct of node, $\frac{dT}{dt}$ is the rate of temperature change of node. For the thermoelec-
tric nodes the heat input and output account for the Fourier, Joule, Thomson and
Peltier heating in the materials. The remainder of the nodes have only Fourier
heating. Heat transfer between nodes can occur by radiation, convection and/or
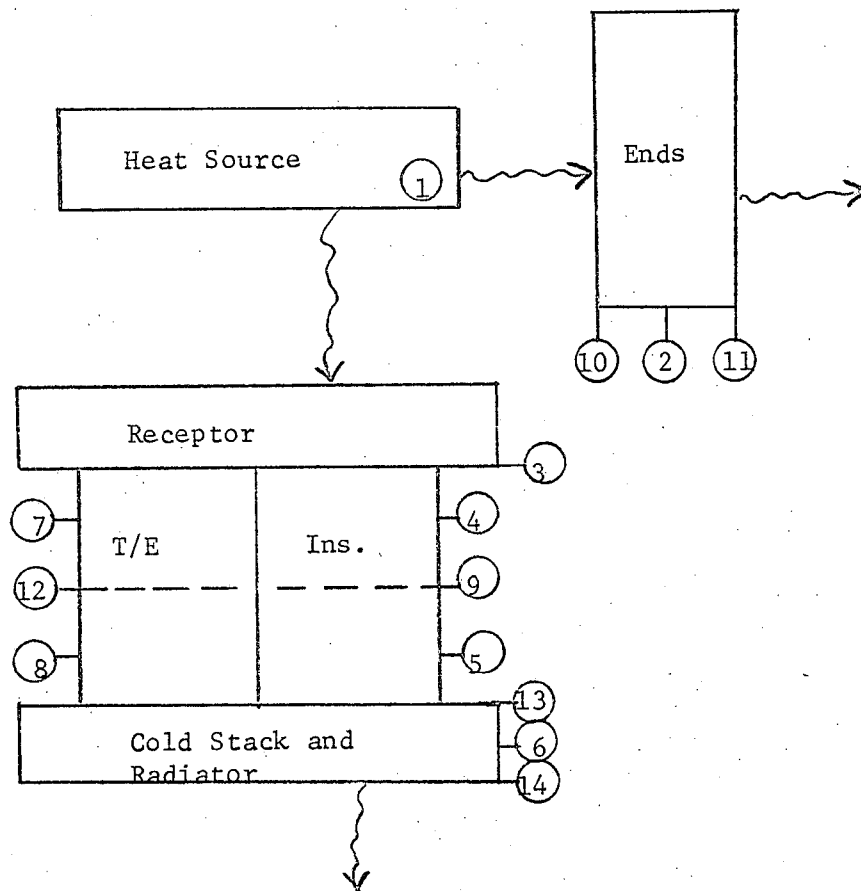conduction. Fin effects in the receptor and radiator are computed by the program

Figure 5 - Trans Nodal Model

Circled Numbers Refer to
Temperature Locations in Model

and are based upon the temperature of the particular node in question. The

internodal temperatures are computed from the nodal temperatures by simultan-

eous solution of the two heat balance equations that apply to that junction.

Where one or both of these equations is non-linear, the Newton-Raphson techni-

que is used.

The computer program for the analysis of transient RTG performance,

TRANS, has been fully debugged and is operational. A copy of it was made opera-

tional on a computer at JPL. TRANS has been used to perform selected analyses

on the transient performance of the MHW-RTG.

III.   MATERIAL STUDY

A.   Introduction

The objectives of this task were the characterization of the long-term thermoelectric properties of silicon-germanium alloys and the establishment of a solid-state dopant precipitation model to explain observed thermoelectric property changes.

It is generally known that the thermoelectric properties of n-type silicon-germanium alloys undergo modification as a function of operating time and temperature because of dopant precipitation. While many data have been collected, most of these data are for relatively short periods of time when compared to deep space probe missions now contemplated. Thus, a quantitative understanding of the long-term behavior of the thermoelectric properties of silicon-germanium alloys is important because it contributes directly to the ability to accurately design thermoelectric power generators optimized for applications requiring long operating times.

This task has attempted to characterize the thermoelectric properties of silicon-germanium alloys by considering the operation of a variety of test samples at temperatures in the range at which it is known that thermoelectric property modification occurs. The experimental efforts of this task have consisted of three types of experiments. The bulk of the effort has been devoted to the isothermal annealing of silicon-germanium alloy test specimens at temperatures in the range of 320 and 960°C. Some effort has been devoted to the investigation of silicon-germanium alloy properties in in-gradient operation. Preliminary work has been done on the measurement of the thermoelectric properties of silicon-germanium alloys as a function of temperature between 200 and 700°C.

The experimental efforts of the Material Study task have primarily concerned themselves with the study of the n-and p-type 80 a/o Si - 20 a/o Ge alloy.

The bulk of the effort has been devoted to material prepared by the hot pressing

technique at the RCA Corporation. The reason for the emphasis of the studies on

the silicon-germanium alloy with this composition has been due to the fact that

it is this alloy that is being used in the MHW-RTG. Moreover, the hot pressed

material made by the RCA Corporation is the specific material used in this gen-

erator. JPL plans to use the MHW-RTG on outer planetary spacecraft and as such

is required to know the detailed performance of the generator within projected

mission times.

The work done by Resalab on the Material Study task of this contract is

discussed below in terms of the three main areas of effort.

B.   Isothermal Annealing Tests

Early in the program it was envisioned that a large number of n-and p-type

80 a/o Si - 20 a/o Ge test samples would be isothermally annealed over a wide

range of operating temperatures with continuous monitoring of electrical resist-

ance and sample temperature. Because of this, an isothermal test furnace was

designed. This test furnace permits the concurrent testing of 84 parallelepipedal

samples of dimensions of 0.25 x 0.25 x 1.5 inch at any temperature in the range

of room temperature to some 1000°C. As designed, the isothermal test furnace

fits into an 18 inch bell-jar. Because of the use of refractory metal lead wires

and instrumentation probes all testing was planned to be performed in vacuum.

The isothermal annealing furnace consists of 42 independently heated

quartz tubes that are wrapped with Kanthal "A" heater wire. The tubes are

linearly tapered with the heater wire wrapping density increasing toward the

outer edges to account for end-losses. This procedure permits flattening of the

axial temperature profiles along the tubes. The furnace tubes are inserted into

the "honeycomb" furnace rack which is constructed of 316 stainless steel and

Marimet-45* thermal insulation. Whereas the stainless steel furnace rack is used only as a structural member, the insulating board forms the individual compartments for the quartz furnace tubes. Insulation is used to minimize thermal coupling between adjacent furnace units.

An isometric view of the stainless steel rack structure is shown in Figure 6. The rack is designed to accept sheets of insulating board to form an enclosed structure with 42 individual compartments. A partial full-scale front view of the complete furnace is shown in Figure 7. The insulated compartments are somewhat larger than the furnace tubes in order to allow the insertion of thermally conductive metal tubes, should additional flattening of the axial temperature profile be required. Elementary heat transfer considerations indicate this additional temperature flattening will not be required when samples of 1.5 inch length are being heated. The addition of metal tubes is almost certainly required, however, in the case of longer test samples.

A simple variac arrangement that uses well regulated input power is utilized to heat the furnace tubes. The input power is obtained from a 3KVA regulator which is mounted within the heater power rack. The regulator is capable of maintaining an output accuracy of plus or minus two percent while the input line may vary from 90 to 140 volts. It has been determined that the two ampere heater capacity will provide sufficient power for temperature levels of 300, 400 and 500°C; while, three and four ampere heater capacity will be required for the higher temperatures. Heater current and voltage measurements will be recorded by panel meters located near the heater adjustment variac.

Since it is desired to determine the long-term thermoelectric property changes that occur in a vacuum environment, a vacuum system suitable for the tests had to be provided. Of primary importance is the capability of the system

---

* Johns-Manville tradename

24.

ONLY FRONT
BRACES SHOWN
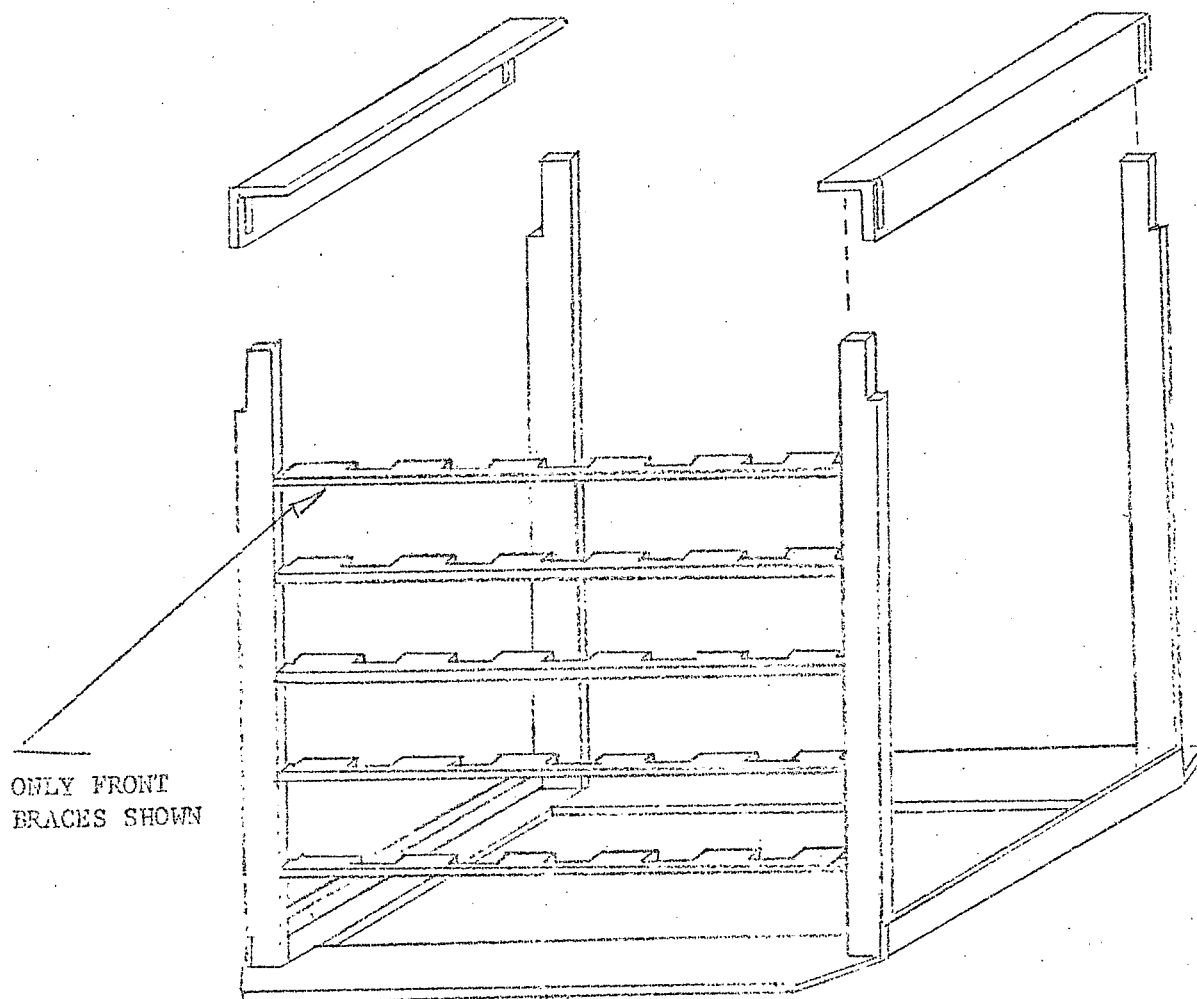
ISOTHERMAL ANNEALING FURNACE RACK
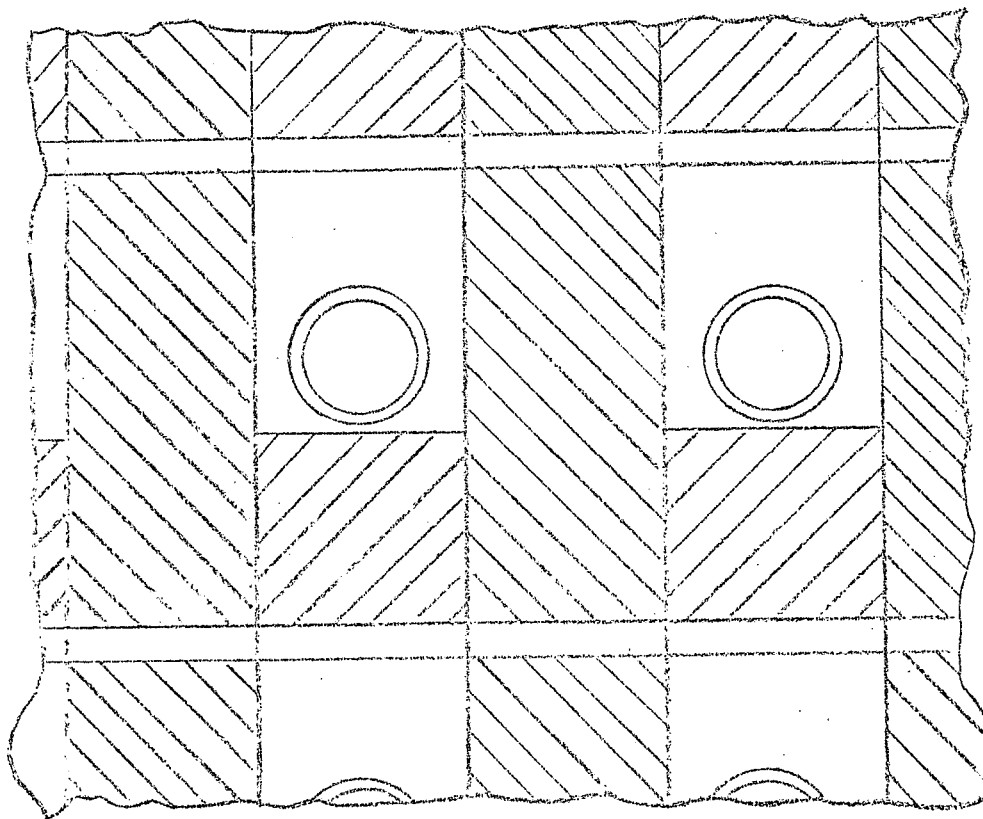
OVERALL VIEW

Figure 6

25.

Figure 7 – ISOTHERMAL ANNEALING FURNACE RACK

CLOSE-UP VIEW OF END

to handle the gas load at temperature as well as provide adequate interlock protection should some anomaly occur. A high capacity oil diffusion system employing a stainless steel bell jar was used with interlocking provision. The vacuum system was protected from the loss of chamber cooling, over pressure, and loss of diffusion pump cooling.

An automatic data system was used exclusively to monitor sample temperatures and resistance. Temperature readings were made hourly and the resistance measurements were, in general, performed on a weekly schedule unless rapid changes occurred. Early in the test, the frequency of resistance measurements was extended to a weekly interval because of the semi-automatic method used in data collection. In addition, the measurements required rather lengthly data reduction even though processing was accomplished on a time-sharing computer.

The isothermal annealing furnace was completed fairly early during the present program. It was not possible to start annealing tests with hot pressed n-and p-type 80 a/o Si - 20 a/o Ge samples because of the unavailability of sufficient quantities of this material from the RCA Corporation. An initial shipment of eight machined samples were received from RCA in March of 1971. Five of the eight samples had n-type and three had p-type polarity. In anticipation of a greater number of samples shortly afterward, the first eight samples were used to check-out the instrumentation and measurement techniques of isothermal testing. Each sample was instrumented with two tungsten/niobium thermocouples and a niobium current lead was attached to both ends of each sample. The average room temperature electrical resistivity of the five n-type samples was 0.986 milliohm-cm and of the three p-type samples was 1.061 milliohm-cm.

Because of the relatively few samples involved in the check-out tests, a special test furnace was fabricated. This furnace consisted of four 5/8 inch diameter quartz tubes, each wound with molybdenum heater wire. The four tubes were

placed in machined slots in a block of Marinite insulation board and were heated by passing current through the molybdenum furnace windings. Each tube could be operated at a different temperature and, in fact, the nominal temperatures of 300, 400, 500 and 600°C were selected for the preliminary test. Two samples were placed in each furnace tube, with the furnaces operating in a two inch diffusion pumped vacuum test station.

Initial data on the isothermal annealing of the eight silicon-germanium alloy test samples indicated the characteristic increase of the electrical resistivity of the n-type material. Although relatively more stable than the n-type material, it was found that the electrical resistivity of the highest temperature p-type alloy samples also increased with time. Although this phenomenon has been observed before, it has not previously been studied in any detail; the assumption that p-type silicon-germanium has properties that remain constant with time is commonly made in device performance calculations. The characteristic increase of the electrical resistivity of the n-type alloy reflects the precipitation of phosphorus from solid solution. Because of the combined effects of the degree of dopant super-saturation and the rates of dopant diffusion, the greatest changes in the electrical properties of n-type silicon-germanium alloys occured in the temperature range used in the preliminary annealing tests.

After a few hundred hours of testing, some difficulty was experienced with the instrumentation lead wires on the samples being annealed at the highest temperature of the preliminary annealing test. Both of the samples at 600°C lost one or more of their instrumentation lead wires and the circuits for passing current through the samples developed infinite resistance. Because of the loss of instrumentation wires from these samples, special tests were undertaken to determine more reliable methods of affixing instrumentation lead wires to the test

samples. In the test as originally started, all lead wires were attached by means of spot welding. Based on the results of the special tests, it was determined that spot welded lead wires additionally cemented to the samples at the point of contact with a high temperature alumina ceramic cement exhibited desired behavior at all test temperatures being considered. The spot welding that precedes cementing of wires assures good electrical contact between the wires and the test samples. The cement accords mechanical strength to the junction of wires and test sample. It should be noted that although many insulators and ceramics, such as SiO_2 and Al_2O_3 are believed to be unstable in a silicon-germanium environment at elevated temperatures, this has not been found to be the case at temperatures below some 900°C. It is thus expected that no noticeable interaction will occur between the ceramic cement and the silicon-germanium test samples even after extended operating times.

Because all tests had to be temporarily interrupted as a result of the Resalab Energy Conversion facility relocation from Menlo Park to Sunnyvale in June of 1971, the preliminary isothermal annealing of the eight silicon-germanium alloy test samples was interrupted. Inasmuch as the highest temperature test samples had lost their instrumentation lead wires and consequently had experienced various lengths of time of isothermal annealing without yielding any experimental data, it was decided to restart the test completely in the new facility. This was accomplished by isothermally annealing the n-type samples at 1000°C for an hour in vacuum. The initial dopant concentration of the alloy was thereby restored because the solid-solubility of dopant in silicon-germanium alloys attains a maximum near 1000°C. From previous experience it was known that all dopant adjustments occur very rapidly at high temperatures this was the reason for the selection of the 1000°C annealing temperature. The instrumentation

methods selected on the basis of the independent tests mentioned above were used to attach lead wires to the samples prior to the restart of the eight sample isothermal annealing test in the Sunnyvale facility. As before, the temperatures of this test were maintained at nominal values of 300, 400, 500 and 600°C with two samples at each nominal test temperature.

Because of continuing delays in the receipt of material from RCA, and specifically material made by a newly acquired hot press that will supply material to the MHW-RTG program in the future, it was decided, in July of 1971, to no longer delay the start of the large isothermal annealing test and to start this test with material already on hand. The material in question was made on RCA's old hot press and consisted of samples machined from ingots of n-and p-type 80 a/o Si - 20 a/o Ge alloy. Fourteen n-type and six p-type samples were accordingly machined from this material. The test samples had parallelepipedal configurations of dimensions 1.5 x 0.25 x 0.25 inch. As with the samples in the eight sample preliminary isothermal test, each test sample was instrumented with two tungsten/niobium thermocouples and a niobium current lead at both ends of each sample. The large scale isothermal annealing test was started in July of 1971 with all test samples at temperatures in the range 300 to 760°C.

Although precautions were taken and special instrumentation techniques used, after a few months of testing it was nevertheless found that of the total number of 28 samples on test, eight in one test and 20 in the other test, several samples exhibited anomalous behavior. Specifically, it was found that of the total of nine p-type samples on test, three had lost one or more of their instrumentation lead wires through the end of the reporting period and one yielded erratic data. Of the total of 19 n-type samples on test, two had lost one or more of their lead wires and another two exhibited erratic behavior. All other

30.

samples appeared to operate normally and yielded meaningful data. Inasmuch as this left 15 n-type and five p-type samples yielding good data, it was decided to continue the test.

Upon the loss of additional lead wires and instrumentation probes from isothermal test samples, in February of this year it was decided to interrupt both isothermal tests and to reinstrument all samples with defective instrumentation probes. The isothermal annealing tests were accordingly interrupted. During the reinstrumentation, it was further decided to combine the two tests in the larger of the two separate test facilities and to add additional samples to the test. The isothermal annealing test originally covered the range of temperatures of 322 to 760°C. Because changes observed in the higher temperature n-type samples exceeded those originally anticipated, it was decided to add more n-type samples to the test in the range of temperatures of 800 to 950°C. For a similar reason, it was decided to add additional p-type samples in the same range of temperatures. Additionally, a sample of zone levelled p-type alloy was also added to the test in order to obtain a preliminary indication of the effect of material preparation method on the behavior of its properties; all other samples in the isothermal annealing test are made from material prepared by hot pressing. As reworked, the isothermal annealing test included 34 samples, of which 22 were n-type and 12 were p-type. The test was restarted in March of this year. Table II lists the samples in the test facility, identifying the polarity type, the test temperature and the total test time of each sample through the end of the contract. The test is continuing. It is noted from Table II that the bulk of all samples have been tested for either 7695 or 8922 hours. The approximately 1200 hours difference in these two test times reflects the fact that the so-called large scale isothermal annealing tests were started at different times during last summer.

TABLE II

SAMPLES UNDERGOING ISOTHERMAL ANNEAL

Polarity Type	Temperature °C	Total Time in Hours
n	317	7695
n	330	7695
n	342	8922
n	351	8922
n	353	8922
n	360	8922
n	405	8922
n	417	7695
n	481	8922
n	503	8922
n	518	8922
n	526	7695
n	536	7695
n	606	8922
n	635	8922
n	637	8922
n	738	8922
n	765	8922
n	775	8922
n	876	4153
n	894	4153
n	1000	4153
p	440	8922
p	465	8922
p	536	7695
p	586	7695
p	623	8922
p	626	4153
p	645	8922
p	697	8922
p	728	8922
p	863	4153
p	887	4153
p	1053	4153

Difficulties with instrumentation probes and lead wires similar to those previously experienced were also experienced prior to the end of the contract. Ten of the 34 samples placed on test during the reinstrumentation lost one or more lead wires before the end of the contract. This means that at the end of the contract only 24 samples retained a full complement of instrumentation probes. Most instances of instrumentation failure resulted from an opening of the circuit used for passing electrical current through the test samples. This, of course, made it impossible to perform electrical resistance measurements on these samples. In most cases thermocouples spot welded on the samples still maintained integrity and continuous temperature measurements were still possible. Of the ten samples with failed instrumentation probes, six were the ones being annealed at temperatures in excess of 800°C. The remaining four were lower temperature samples.

Even though a number of the samples being isothermally annealed no longer yielded complete data, the isothermal test was continued. It is expected at a future time to interrupt the test once more and to reinstrument the failed samples. Even though they may provide data for relatively short periods of time, these samples nevertheless contribute to an overall understanding of the long-term behavior of the thermoelectric properties of the silicon-germanium alloy. Even intermittent electrical resistivity data are sufficient to characterize the time behavior of the electrical resistance of these samples.

The data obtained from the isothermal annealing tests pertain to the electrical resistance of the samples on test. The actual measured data were converted to values of electrical resistivity in order to determine the effect of time and temperature on the properties of silicon-germanium alloys. Typical plots of such data are shown in Figures 8 and 9. Figure 8 shows electrical
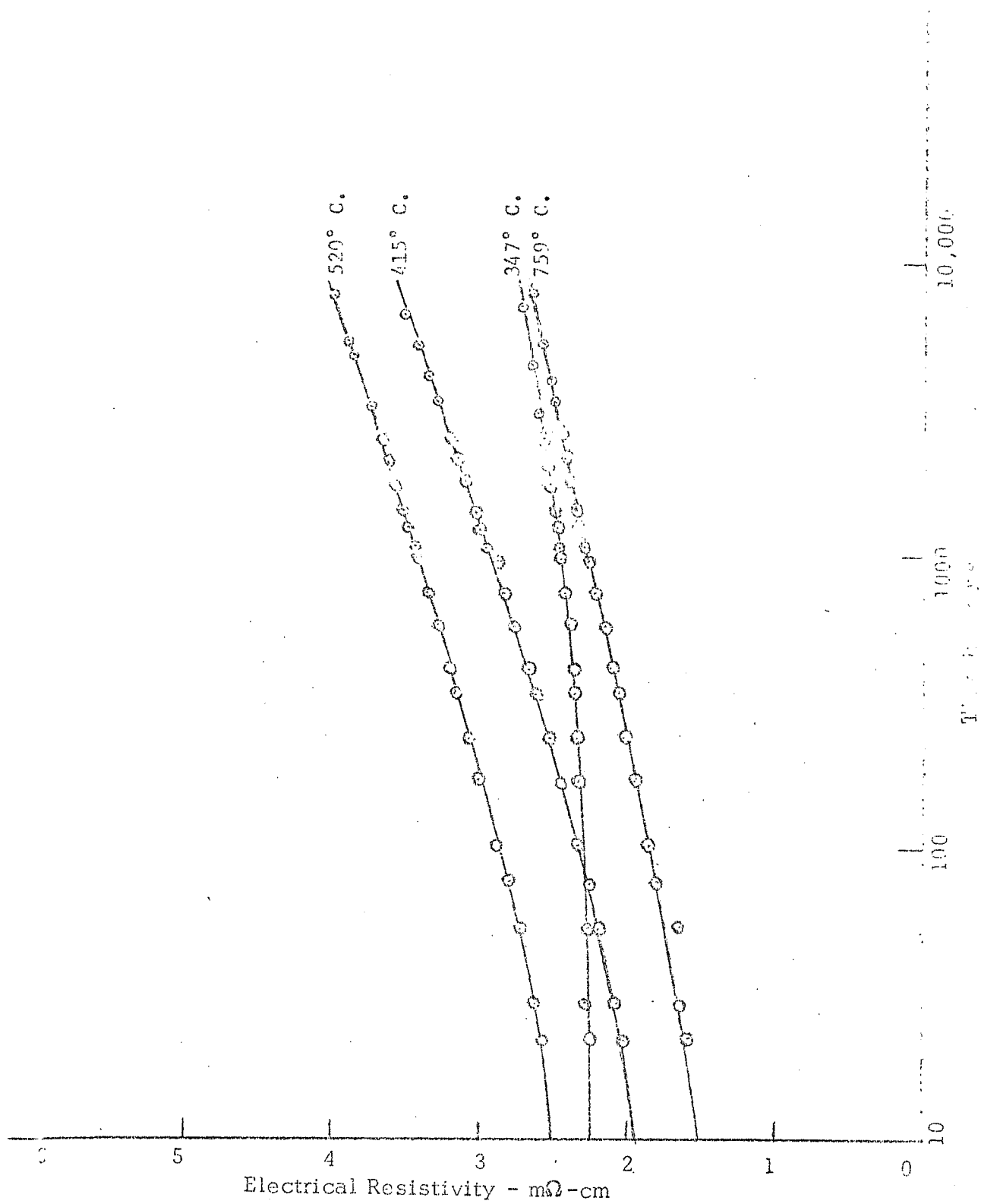
Figure 8. Electrical Resistivity as a Function of Time, n-type 80 a/o - 20 a/o Ge alloy
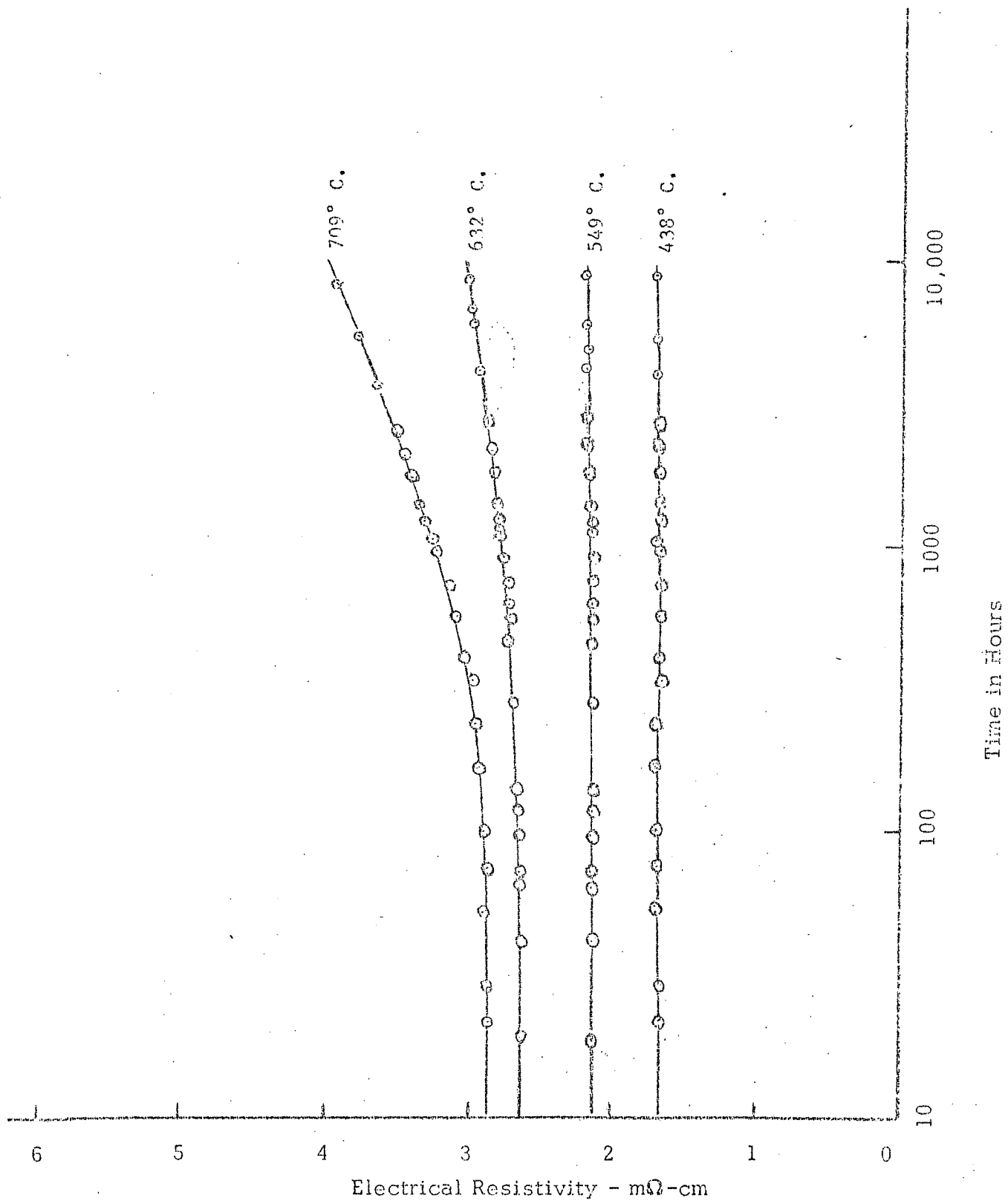
34.

Figure 9: Electrical Resistivity as a Function of Fine,
p-type 80 a/o Si - 20 a/o Ge alloy

resistivity as a function of time for four representative n-type samples of 80 a/o Si – 20 a/o Ge alloy. Corresponding plots of electrical resistivity as a function of time for the p-type alloy are shown in Figure 9. It is noted that the plots are in terms of the logarithm of time. The reason for plotting the data in this manner is that changes in electrical resistivity that occur later in life are thus accentuated. Moreover, in chemical kinetics it is found that diffusion limited precipitation processes exhibit an elongated S-shaped configuration when thus plotted. It is apparent in Figures 8 and 9 that if a diffusion limited precipitation process underlies the presently observed electrical resistivity changes in the silicon-germanium alloy on test, the process has obtained only partial completion through the end of current test time. Because it is expected that after very long annealing times the dopant concentration in the silicon-germanium alloys will asymptotically approach the equilibrium solid solubility of dopant in the alloy at any given temperature, it is assumed that upon further testing the electrical resistivity values will level off at asymptotes that correspond to the solid solubility. It is significant that changes as large as those seen in Figure 8 are observed in the highest temperature p-type silicon-germanium alloy test sample.

The analysis of isothermal annealing test data on silicon-germanium alloys obtained after some 5000 hours of test was started during the present contract. Underlying the analysis is the assumption that the observed changes in the electrical resistivity of silicon-germanium alloys are due to a diffusion limited dopant precipitation phenomenon. Whereas conventional models of dopant precipitation do not adequately agree with the observed electrical resistivity changes in silicon-germanium alloys, it was found[4] that a model due to Lifshitz and Slyozov does reasonably represent observed test data.

The dopant precipitation model of Lifshitz and Slyozov presupposes a critical radius in the precipitate phase; precipitate particles with radii smaller than the critical radius tend to dissolve in the matrix of the alloy and precipitate particles with radii larger than a critical radius tend to grow upon the addition of precipitating species from the alloy. The critical radius of the precipitate particles is a temperature dependent function and involves the surface energy of the particles. The dopant precipitation model of Lifshitz and Slyozov is given by

$$\left[\frac{C_i - C_e}{C_t - C_e}\right] = \left[\frac{4}{9}\left(\frac{C_e}{C_p}\right)\left(\frac{C_i - C_e}{C_e}\right)^3 \frac{D}{\beta^2}\right] t + B \quad , \tag{7}$$

where B is a constant and β is given by

$$\beta = \frac{2M\sigma}{\delta RT} \quad . \tag{8}$$

In the above relationship it should be noted that C_i represents the initial concentration of dopant in solution, C_t is the concentration of dopant in solution at any time t, C_e is the equilibrium concentration of dopant in solution, C_p is the concentration of dopant in the precipitate phase, D is the diffusion coefficient of dopant diffusion in the alloy, t is time, M is the mean atomic weight of the alloy, σ is the interphase surface energy, δ is the density of the alloy, R is the universal gas constant, and T is the absolute temperature. Because many of the terms that enter the above relationship are not known, it is convenient to lump them into unknown constants and to rewrite the expression as

$$\left[\frac{C_e}{C_t - C_e}\right]^3 = k_1 T^2 t + k_2 \quad , \tag{9}$$

where k_1 and k_2 are assumed to be unknown temperature dependent constants. This last relationship can be further simplified and related to electrical resistivity by means of the well known relationship

$$C = \frac{1}{\rho e \mu} \, , \tag{10}$$

where ρ is the electrical resistivity, e is electronic charge and μ is charge carrier mobility. Substitution of this relationship in the preceeding one enables the latter to be rewritten as

$$\left[\frac{\rho_t}{\rho_e - \rho_t} \right]^3 = k_1 T^2 t + k_2 \, . \tag{11}$$

where ρ_t is the electrical resistivity at any time t and ρ_e is the electrical resistivity at equilibrium carrier concentration. In rewriting the Lifshitz and Slyozov precipitation model in the last given form not only has it been assumed that many terms can be combined into the temperature dependent constants k_1 and k_2, but it has also been assumed that charge carrier mobility does not depend on charge carrier concentration. Although the latter assumption is known not to be exact, it holds reasonably for relatively small variations in charge carrier concentration. For example, it has been experimentally determined[5] that the Hall mobility of holes in p-type silicon-germanium alloys varies by less than a factor of two for hole concentration variations of two orders of magnitude. Carrier concentration changes due to dopant precipitation in silicon-germanium alloys rarely exceed a factor of two; charge carrier mobility is not therefore expected to change by more than a percent or so as a result of dopant precipitation. The assumption inherent in the last relationship that charge carrier mobility stays constant is therefore considered to be well justified.

In order to use the last given above relationship in the prediction of electrical resistivity as a function of time for any time, it is obviously necessary to substitute appropriate values for the three unknown constants, ρ_e, k_1 and k_2. This is best done by applying the relationship to a given set of electrical resistivity data experimentally determined for a time t at some temperature T. The precise procedure for doing this is to select the resistivity ρ_t at three different times t and write a set of three simultaneous equations. This set of simultaneous equations can then be solved for the three unknown constants. Insertion of values for these constants, along with the appropriate temperature in the above relationship enables the electrical resistivity to be calculated for any time t. Corresponding values of Seebeck coefficient can be determined from the previously established relationship between electrical resistivity and the Seebeck coefficient[6]. Although Seebeck coefficient data obtained in this manner are considered to be reasonably accurate, the relationship between electrical resistivity and Seebeck coefficient given in the referenced report will be confirmed by means of subsequent in-gradient tests.

The data obtained in the isothermal annealing test through February of this year were analyzed and reduced into thermoelectric property curves for the n-type 80 a/o Si - 20 a/o Ge alloy. The data on p-type samples were not sufficient to enable complete projection of the thermoelectric properties; considerably greater changes than originally anticipated had been observed in the p-type alloy at temperatures in excess of 700°C. When additional data become available from the higher temperature test samples placed on test during the present contract, projections will be made on the properties of the p-type alloy. The reduction of test data on the n-type samples made use of the equations given above.

The experimental data obtained on the isothermal annealing of n-type 80 a/o Si - 20 a/o Ge alloy were reduced by means of the given relationship. It is noted that the relationship contains three unknowns: ρ_e, k_1 and k_2. In order to solve for these three unknown constants, three values of electrical resistivity at three different times at any given temperature are required. The solution is effected by standard techniques for simultaneous equations. Through February of this year, each isothermally annealed n-type sample was characterized by a total of 29 data points. If all combinations and permutations of these data points for each sample were to be used in reducing the experimental data, several thousand sets of the three unknown constants would be evaluated for each. In view of the obvious impracticality of this procedure, it was decided that the use of 12 sets of three data points each would be used to characterize the be- havior of each sample. A random number sequence was used to select the 12 sets of three data points for each sample. The resultant 12 sets of the three unknown constants were averaged to yield the most probable value for each constant for any given sample. The standard deviation of the calculated constants has been computed for each sample. Any values of the constants outside the three σ-limit was discarded and a new average computed. This latter value for each of the three unknown constants for each test sample was inserted in Equation (11) and the electrical resistivity of each sample calculated as a continuous function of time by that equation. The relationship between the Seebeck coefficient and the electrical resistivity of n-type silicon-germanium alloys was then used to es- timate the value of Seebeck coefficient of each sample as a function of time. This relationship is shown in Figure 10. The thus determined values of Seebeck coefficient and electrical resistivity of the n-type 80 a/o Si - 20 a/o Ge alloy are shown in Figures 11 and 12 for a number of different operating times in terms
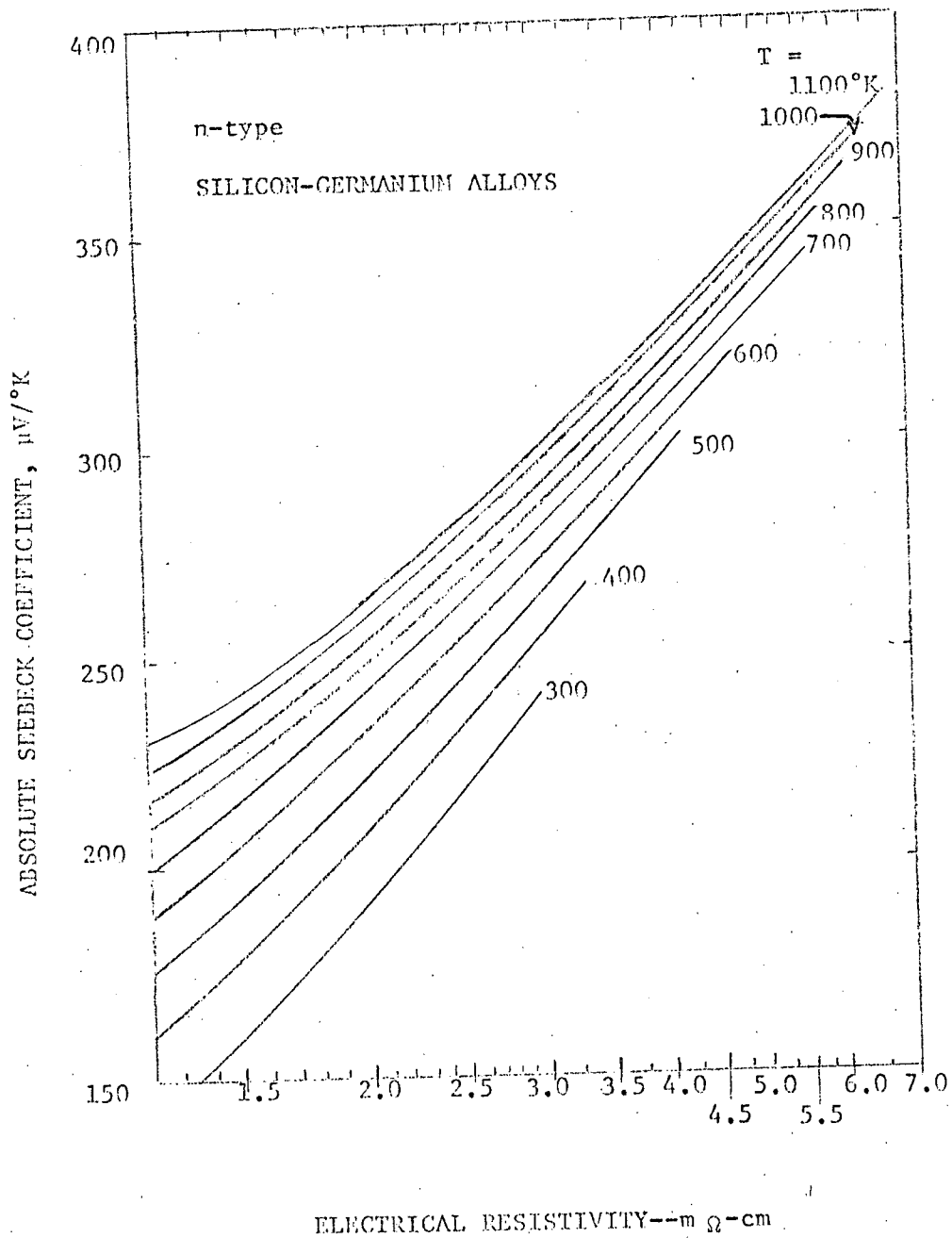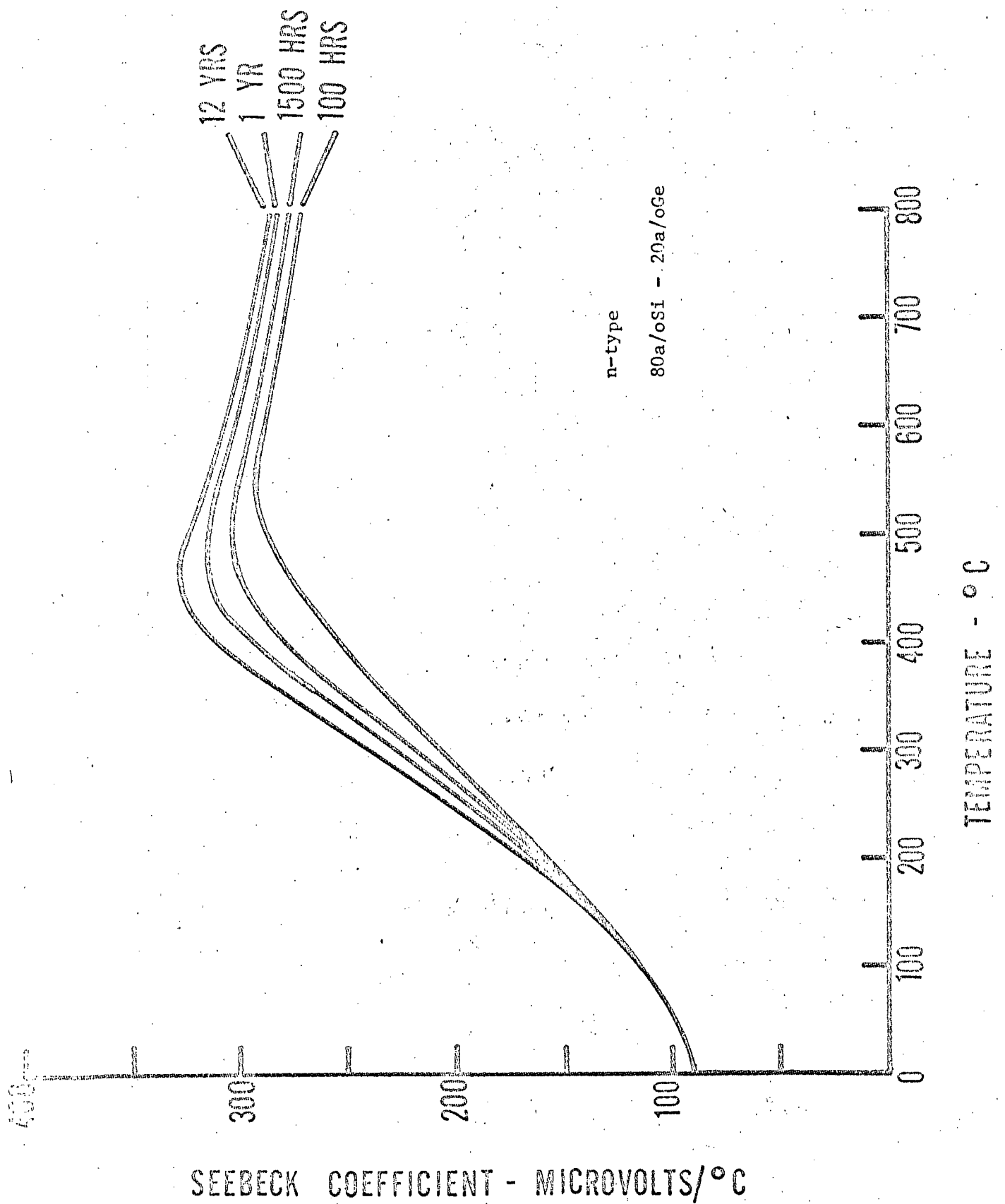
n-type

SILICON-GERMANIUM ALLOYS

ELECTRICAL RESISTIVITY--m Ω-cm

Figure 10.

41.

Figure 11

n-type
80a/oSi — 20a/oGe

12 YRS
1 YR
1500 HRS
100 HRS

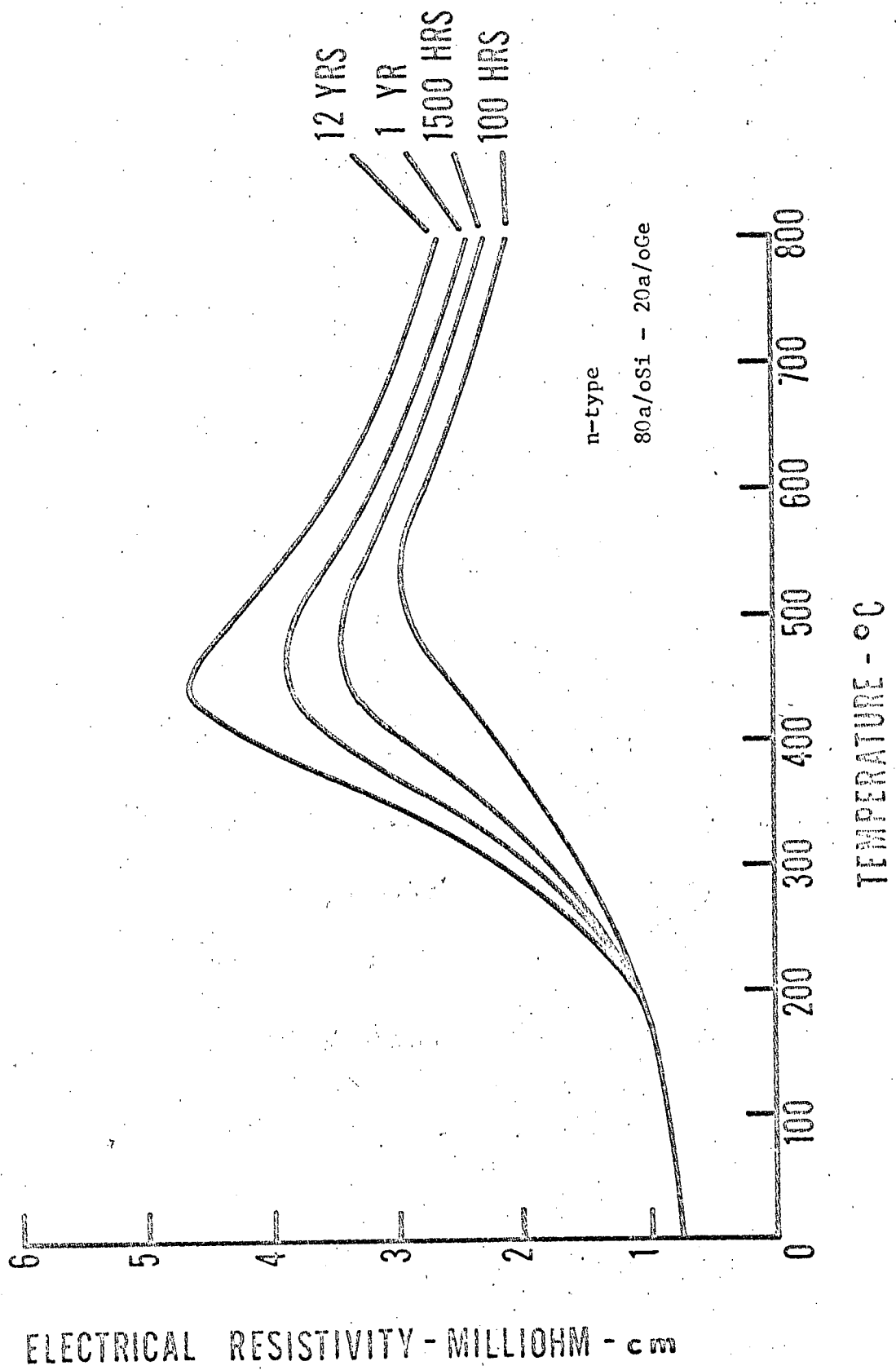ELECTRICAL RESISTIVITY - MILLIOHM - cm

TEMPERATURE - °C

Figure 12

43.

of best fit functions of temperature. It will be noted that the present thermo-electric property projections only extend to 800°C. The reason for this, of course, is that the longest time experimental data have been obtained up to only 760°C.

To complete the present characterization of the thermoelectric properties and their behavior as a function of time of the n-type 80 a/o Si - 20 a/o Ge alloy, Figure 13 reproduces the thermal conductivity of the alloy as a function of temperature previously given in Resalab Memorandum #8 to the Jet Propulsion Laboratory. It will be noted that, unlike the electrical resistivity and the Seebeck coefficient, a single time independent curve is given for the thermal conductivity. Although it may be anticipated that the thermal conductivity of the alloy is also a time dependent function, experimental data of a quantitative nature is nearly totally lacking; any changes in the thermal conductivity would be expected to be substantially smaller than those in the other two properties. Accordingly, a single temperature dependent function has been assumed for the thermal conductivity of the alloy.

The data shown in the Figures 11 to 13 have been combined in Figure 14 to indicate the latest projections on the time and temperature dependence of the figure-of-merit of n-type 80 a/o Si - 20 a/o Ge alloy. As seen in the corres-ponding curves of the electrical resistivity and Seebeck coefficient, it is noted in Figure 14 that the biggest changes in the figure-of-merit of the alloy occur at temperatures of the order of 400 to 500°C. It is also noted that sub-stantial change in the figure-of-merit occurs at temperatures in excess of 600°C.

In order to illustrate the relation of actual and calculated values of electrical resistivity to the best fit curves shown in Figure 12, the data points
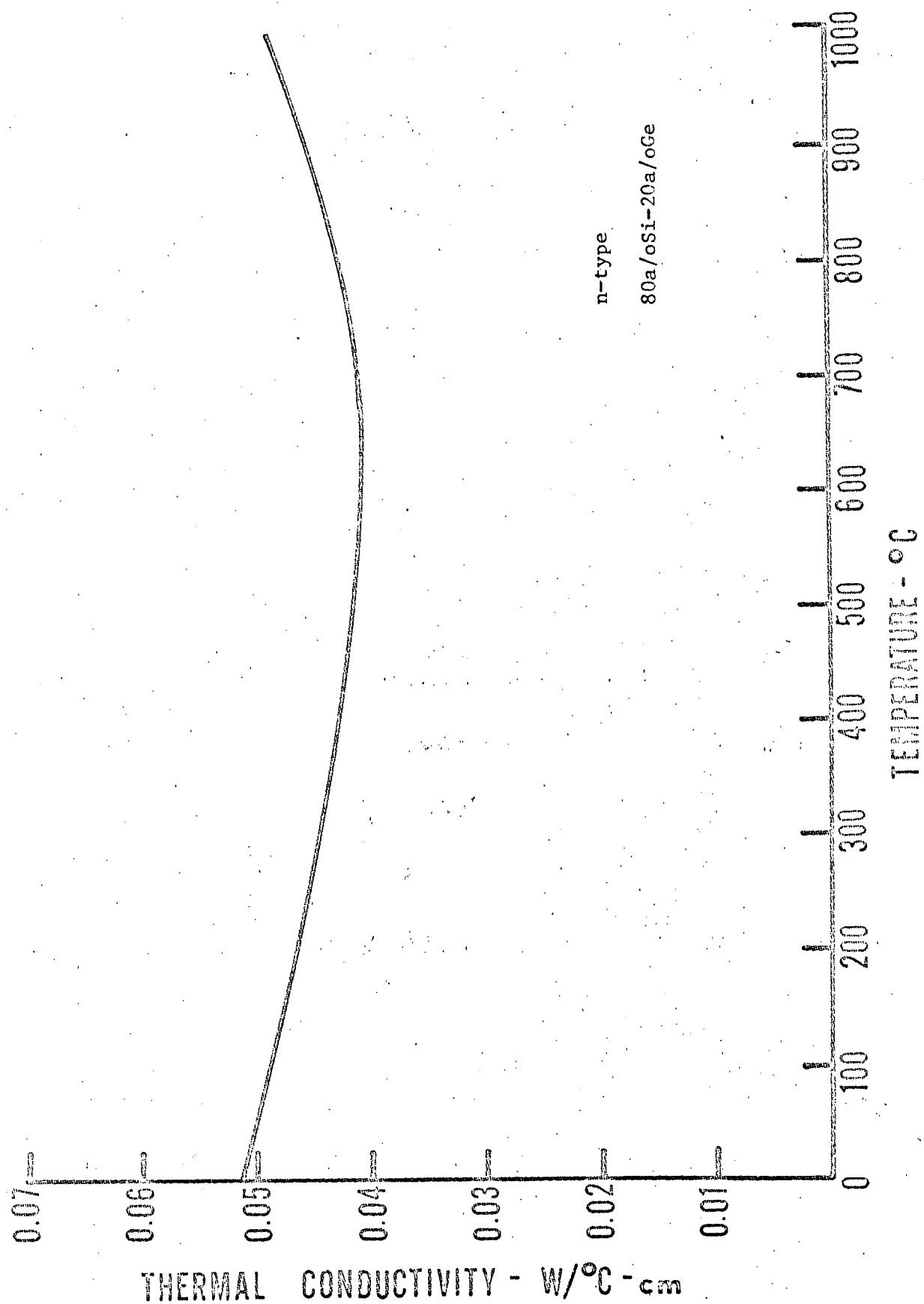
THERMAL CONDUCTIVITY - W/°C - cm

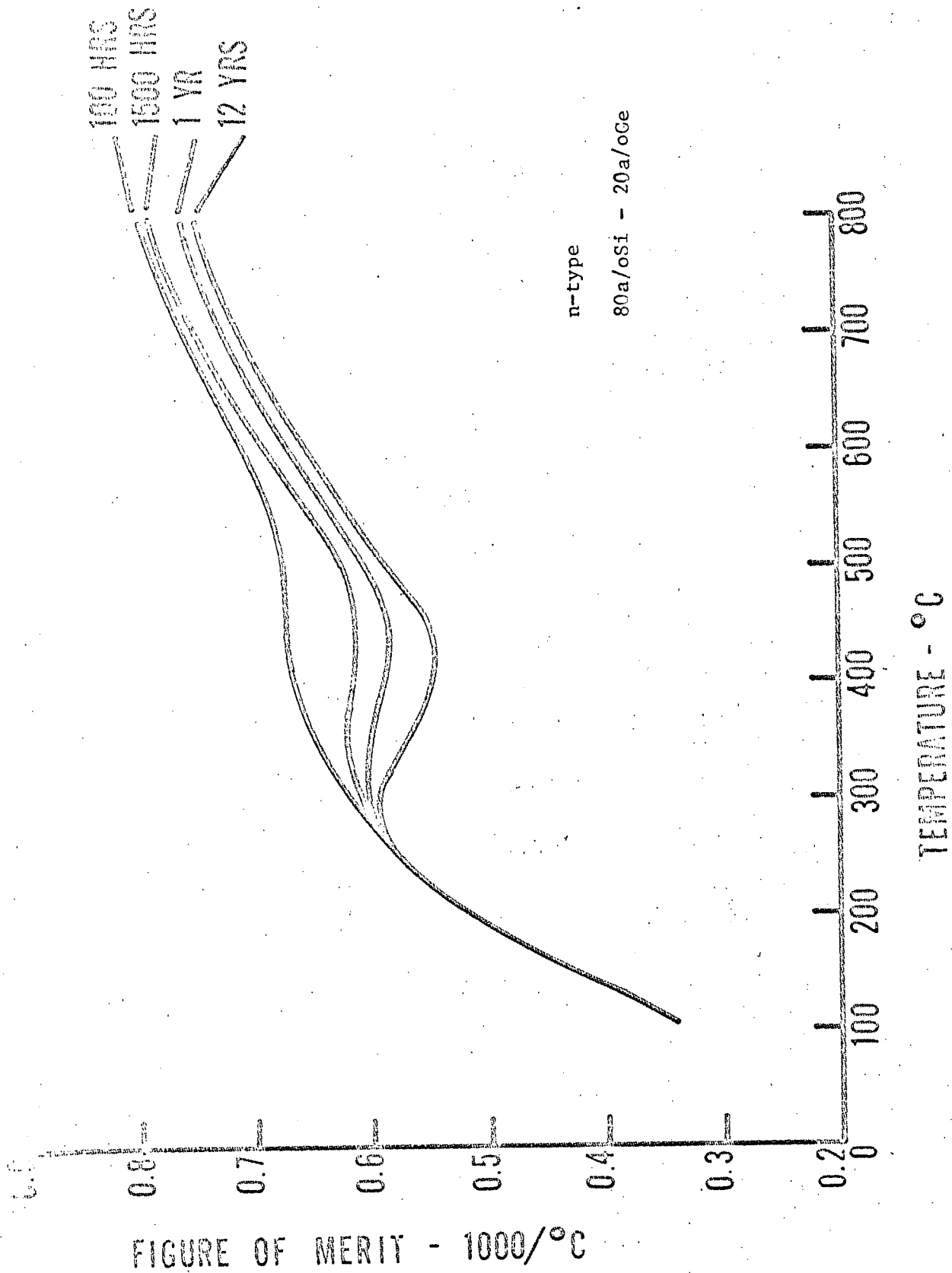TEMPERATURE - °C

n-type

80a/oSi-20a/oGe

Figure 13

45.

Figure 14

46.

superimposed on the resistivity curves representative of the material after 100 hours, 1500 hours and 12 years of operation. The data points shown for the 100 hour and 1500 hour curves pertain to best fit data for each sample and the data points for 12 years pertain to calculated data. The curves drawn through the data points are best fit curves to the data shown. The two data points on the 100 hour curve at temperatures below 300°C represent average initial data on all test samples obtained while the samples were being heated to their eventual operating temperatures. The reason for including those data points on the 100 hour curve is that little change in electrical resistivity is expected at such low operating temperatures at short times. The data point shown at 30°C represents the average room temperature electrical resistivity of all samples prior to start of testing. All of the samples were found to have initial electrical resistivity values within about ten percent of the average values.

In order to see how the present results compare to the previous projections of the long-term behavior of n-type 80 a/o Si – 20 a/o Ge alloy made in Memorandum #8[7], the results shown in Figure 12 for 100 hours and 12 years of operating time have been replotted in Figure 15 along with the corresponding curves from Memorandum #8. It is noted that the temperature of greatest thermoelectric property change is some 100°C higher than previously thought and that the temperature dependence of the electrical resistivity curves at temperatures higher than 600°C is different for the two cases. The present results are considered to be more accurate because of the greater number of test samples used and the longer time for which test data have been obtained. The fact that the room temperature resistivity values of the two curves do not coincide is not considered especially significant because this is primarily a reflection of the previous thermal history of the test samples. On the other hand, some of the differences
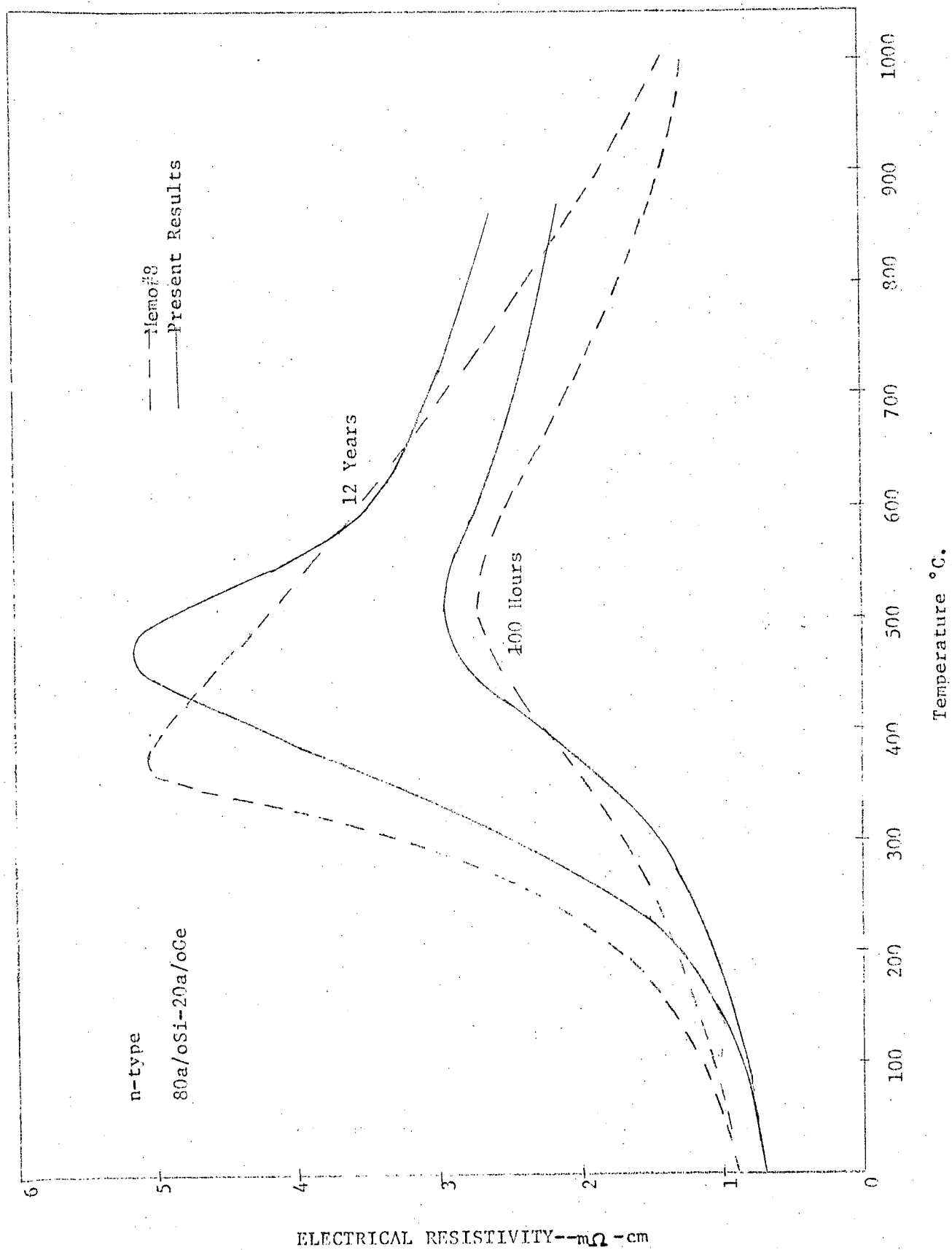
ELECTRICAL RESISTIVITY--mΩ-cm

n-type

80a/oSi-20a/oGe

12 Years

100 Hours

Temperature °C.

———Memo⁸⁹
———Present Results

Figure 15

48.

noted in the two sets of data may be due to the fact that the projections made in Memorandum #8 were based on experimental data on zone levelled material and the present projections are made on hot pressed material.

The 100 hour and 12 year figure-of-merit plots of Figure 14 have been replotted in Figure 16 along with the corresponding curves from Memorandum #8, in order to compare the present results to those previously obtained. Just as in the case of the electrical resistivity comparison shown above, it is noted that the temperature of greatest figure-of-merit change occurs at a somewhat higher temperature than previously thought. Similarly, at temperatures in excess of 600°C the temperature dependence of the figure-of-merit appears to be smaller than previous results had indicated. Because it appears that at still higher temperatures the figure-of-merit of the n-type 80 a/o Si - 20 a/o Ge alloy may be significantly lower than previously projected, it may be concluded that additional high temperature property data are definitely required.

Because of the lack of high temperature test data, it has been possible to only generate thermoelectric property data for the n-type 80 a/o Si - 20 a/o Ge alloy at temperatures below 800°C. Most applications of silicon-germanium alloys to thermoelectric power generation however extent to significantly higher temperatures, temperatures of the order of 1000°C. Until further isothermal annealing data at higher temperatures becomes available, the property curves as presented in this report can not be used for most performance analyses unless they are extrapolated to higher temperatures. This has been done in a preliminary manner. In order to reduce the arbitrariness in the extrapolation of the property data, it was decided to obtain initial data on the temperature dependence of the thermoelectric properties of the n-type alloy at temperatures higher than 800°C. A parallelepipedal sample of n-type 80 a/o Si - 20 a/o Ge alloy of
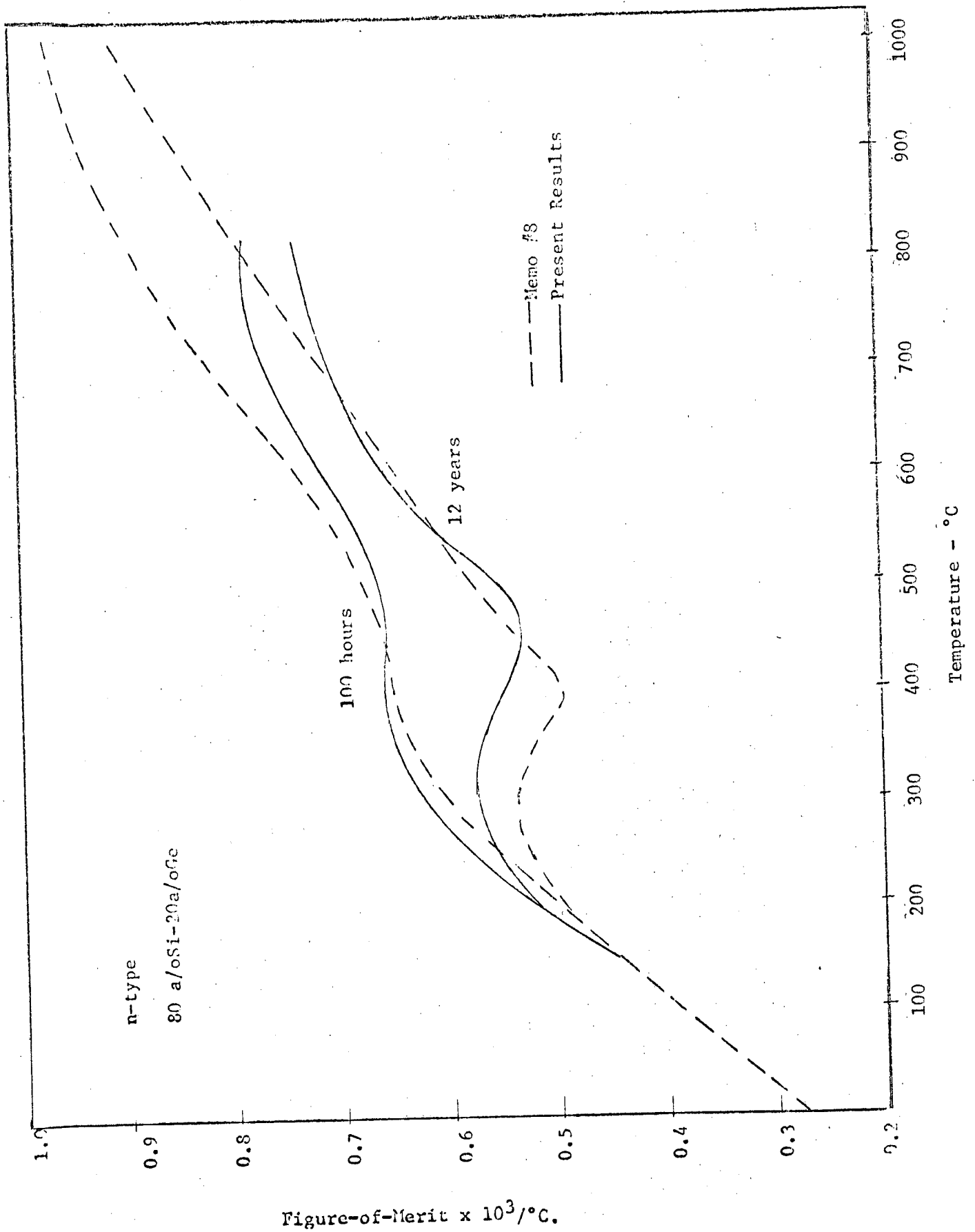
Figure 16

n-type

80 a/oSi-20a/oGe

100 hours

12 years

Memo #8

Present Results

Figure-of-Merit x 10^3/°C.

Temperature - °C

50.

dimensions of 0.25 x 0.25 x 1.5 inch was accordingly instrumented with thermo-couples, current leads and voltage probes and short term measurements of elec-trical resistance were performed as a function of temperature between room tem-perature and 970°C in a vacuum furnace. The electrical resistance data were converted to those of electrical resistivity by using known sample geometry. The results of this experiment are shown in Figure 17 in terms of electrical resistivity as a function of temperature. Superimposed in the figure are the curves of electrical resistivity as a function of temperature at different operating times. It is noted that the results of the present measurements fit well into the overall pattern of the temperature dependence of the electrical resistivity. It appears that the shortest time resistivity curve, that at 100 hours, asymptotically approaches the initial electrical resistivity curve. Whereas all of the projected electrical resistivity curves appear to be nearly parallel at 800°C, it may be concluded that either the projected data are some-what in error or that all of the curves approach the initial curve asymptotically, each curve doing so at a different temperature. If all of the curves should ap-proach the initial curve at the same temperature, then the former conclusion would be appropriate. This, in fact, may be so, although conclusive proof does not as yet exist because the silicon-germanium alloy sample measured during the present contract was maintained at its highest test temperature of 970°C for a period of several hours while continuous electrical resistance measurements were performed. Only minimal changes in electrical resistance were observed during that time. This appears to indicate that 970°C is close to the temperature of the maximum solid solubility of n-type dopant in the alloy. Whether this is so must nevertheless be established by more detailed and longer time tests in the future.
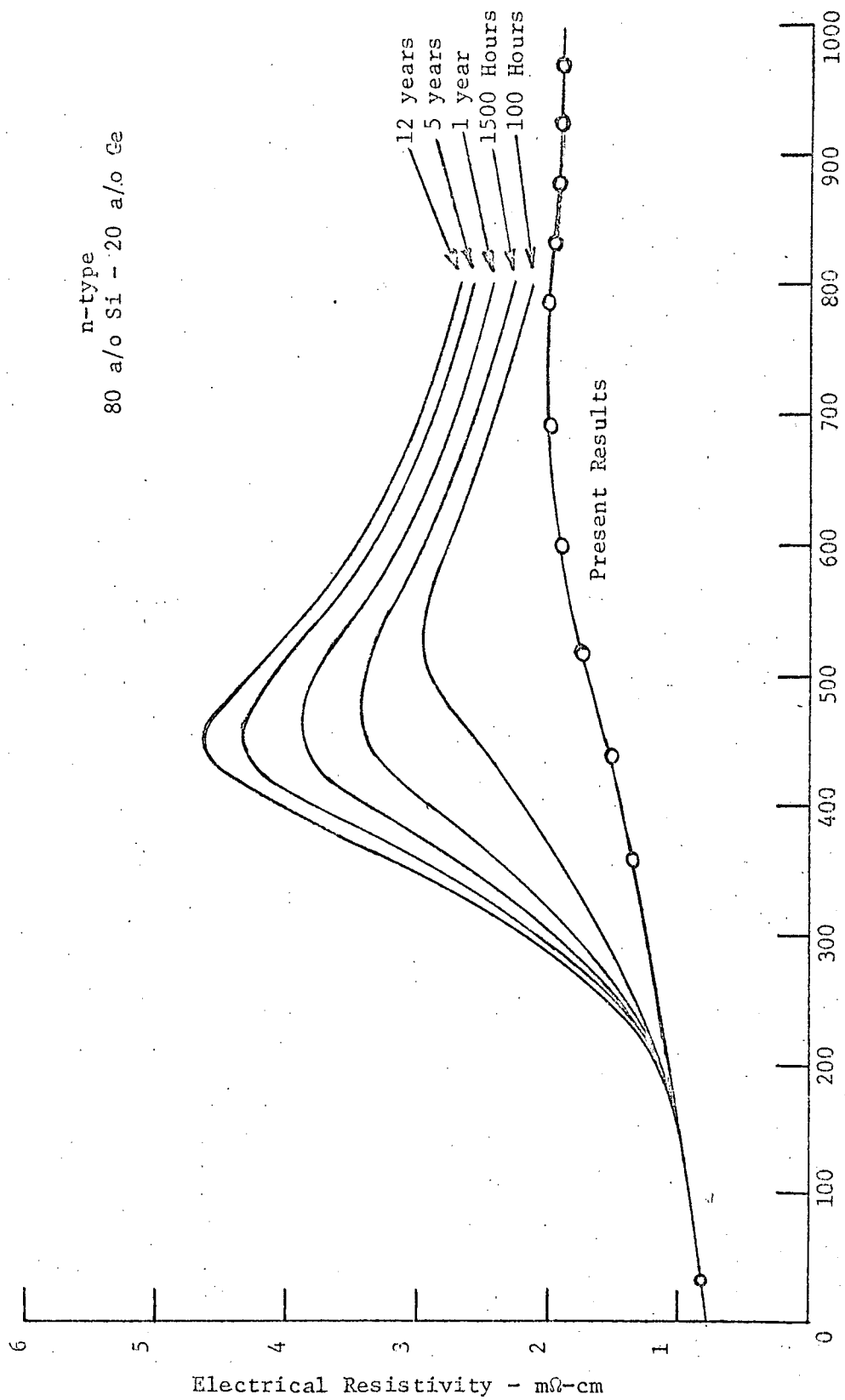
n-type
80 a/o Si – 20 a/o Ge

12 years
5 years
1 year
1500 Hours
100 Hours

Present Results

Electrical Resistivity – mΩ-cm

Temperature – °C

Figure 17

52.

On the assumption that all of the thermoelectric property curves for the n-type 80 a/o Si - 20 a/o Ge alloy converge at the temperature of 1000°C, the thermoelectric property curves of the alloy given above were modified by extrapolating the electrical resistivity curves to a common value of electrical resistivity at 1000°C. The common value of electrical resistivity is that obtained by extrapolating the initial resistivity curve from 970 to 1000°C. Seebeck coefficient values corresponding to those of the modified electrical resistivity curves were determined according to the previous procedure of using a known relationship between electrical resistivity and Seebeck coefficient for n-type silicon-germanium alloys. The thermal conductivity is assumed to be the same as that given in Memorandum #8. Having thus generated new thermoelectric properties for the n-type 80 a/o Si - 20 a/o Ge alloy, these properties have been used to replace those in the data file of computer programs used by Resalab and JPL in the performance of design analyses on silicon-germanium RTG's.

Because the thermoelectric property data projected to 1000°C for use in a computer data file are based on a number of assumptions and one set of experimental data, it is felt that a complete presentation of these data in the present report is premature. It is expected that with time new updates of the thermoelectric property data for the n-type 80 a/o Si - 20 a/o Ge alloy will be made; the isothermal annealing of the test samples discussed in this section is being continued beyond the end of the present contract and will form a part of a subsequent follow-on effort. Material property projections will be made upon the availability of additional test data.

Insufficient isothermal annealing data have been obtained on the p-type 80 a/o Si - 20 a/o Ge alloy to enable reasonable material property projections on the present contract. The isothermal annealing of p-type test specimens will

also be continued beyond the end of the present contract and it is expected that detailed thermoelectric property projections as a function of time and temperature will be made for the p-type alloy as a part of subsequent follow-on efforts.

C. In-Gradient Annealing Tests

In order to supplement the thermoelectric property data obtained on n-and p-type 80 a/o Si - 20 a/o Ge alloy samples undergoing isothermal annealing, it was planned, early in the program, to conduct concurrent in-gradient annealing tests on the same material. The sequence planned for in-gradient testing involved the operation of cylindrical silicon-germanium alloy test samples in a temperature gradient in a special test fixture. The test fixture was designed to operate between any two desired temperatures. In the present instance it was envisioned that all testing would be done between a hot side temperature of 1000°C and a cold side temperature of 300°C, thus simulating the temperatures envisioned for the operation of the MHW-RTG. While being tested, temperatures, electrical resistance and output voltage of the samples were to be continuously monitored. The data thus obtained were to be converted to integrated average values of electrical resistivity and Seebeck coefficient. These data were to serve as a check on the data obtained on electrical resistivity in the isothermal annealing test. They were to also serve as a check on the relationship used between electrical resistivity and Seebeck coefficient. The isothermal annealing test was to be periodically interrupted and the thermal conductivity of the samples measured in a comparative thermal conductivity measuring apparatus. This was to be accomplished by removing the in-gradient test samples from the in-gradient test fixture and installing them in the comparative thermal conductivity measuring equipment. Measurements of thermal conductivity as a function of temperature in the range of temperatures of 300 to 600°C were to yield the desired data.

All thermal conductivity measurements were to be performed with a temperature gradient of some 20 to 30°C across the test samples. Because the instrumentation of the in-gradient test samples was to include current lead wires and thermocouples, it was to be also possible to concurrently measure the electrical resistivity and Seebeck coefficient of the samples. As before, the latter data were to be useful in confirming the relationship between Seebeck coefficient and electrical resistivity and were to also permit the determination of the dependence of thermal conductivity on the other two thermoelectric properties. The main intent of the in-gradient test, of course, was to determine the thermal conductivity values of the 80 a/o Si - 20 a/o Ge alloy as a function of time and this was to be done by periodic measurement.

The measurements performed on the in-gradient test samples in the comparative thermal conductivity measuring equipment were to only cover the given range of temperatures of 300 to 600°C because it is at these temperatures that the greatest property changes were anticipated. The actual performance of the measurements were to be conducted relatively rapidly because it is important to minimize any perturbations of the properties as a result of the measurement process itself. Such perturbations would occur because of the temperature dependent solid solubility of dopant in silicon-germanium alloys and because the measurements were performed at temperatures other than those of the in-gradient test. Based on past experience, it is known that for total measurement times of the order of a few hours or less, any perturbation of material properties because of the solid solubility phenomenon are insignificant. If perturbations were to occur, they would be apparent when in-gradient test data prior to and after each thermal conductivity measurement sequence are compared.

Although in-gradient test equipment was finished fairly early during the contract, in-gradient testing of the 80 a/o Si - 20 a/o Ge alloy samples

was not started because suitable silicon-germanium alloy test samples were not available. The comparative thermal conductivity measuring equipment, planned to be used in conjunction with the in-gradient tests, requires cylindrical test samples of 5/8 inch diameter because the calibrated hot and cold side calorimeter sections are of that diameter. Hot pressed silicon-germanium alloys available from the RCA Corporation can be fabricated into samples having a maximum diameter of 1/2 inch, thereby appreciably less than the diameter required to match the calorimeter sections of the thermal conductivity measuring equipment. The start of the in-gradient test was delayed in anticipation of material that could be fabricated into test specimens with suitable overall diameters. Such material was expected to be made by a new hot press installed at RCA. Although the availability of material from the new hot press was imminent for a long time, it was decided, in a meeting with cognizant JPL project personnel, that delaying the start of the in-gradient test was not justified and that the then available material should be used in such a test. Although suitable material was available from other sources, the intent of the in-gradient test was to evaluate material used on the MHW-RTG program, thus material made by RCA.

In order to accomodate in-gradient silicon-germanium test samples of diameters less than 5/8 inch, it was necessary to modify the comparative thermal conductivity measuring equipment. The modification entailed the replacement of the 5/8 inch diameter hot and cold side calorimeter sections with one having a smaller diameter. It also entailed the recalibration of the comparative thermal conductivity measuring equipment against a standard having a known thermal conductivity. As in the past, the calorimeter sections and the standard used for calibration were made of Pyroceram because the thermal conductivity of Pyroceram reasonably matches that of silicon-germanium alloys. Suitable Pyroceram sections were obtained from Dynatech in Cambridge, Massachusetts.

In another subsequent meeting with cognizant JPL project personnel, it was decided to change the method of in-gradient testing prior to any testing having actually started. Whereas previously it was planned to periodically interrupt in-gradient testing in order to measure the thermal conductivity and other thermoelectric properties of the test samples, it was decided that only electrical measurements translatable to electrical resistivity and Seebeck coefficient should be determined on the in-gradient test samples. This enables in-gradient testing to continue uninterrupted after it is started. It was decided to also make changes in the in-gradient test fixture. Rather than being affixed to common hot and cold side heat sinks, it was decided to connect the test samples to individual hot heat sinks. The samples still make use of a common cold heat sink. Individual hot heat sinks enable the samples to be annealed at different hot side temperatures.

After all of the delays and modifications, the in-gradient annealing test was finally started in April of this year. The test involved two n-type and two p-type samples of zone levelled 80 a/o Si - 20 a/o Ge alloy. Each sample was made of two cylinders of 0.5 inch diameter and 0.75 inch length placed in an end-to-end configuration. Each test sample was contacted to a separate heater block but all four samples made use of a common water cooled heat sink. Thermocouples were placed on the heater blocks, the heat sink and along the lengths of each sample. Each sample possessed four tungsten/niobium thermocouples, with two thermocouples on each half of each test specimen. The heater blocks were spring loaded against the test specimens and a tungsten disk was used to separate two of the test specimens from the molybdenum heater blocks. The remaining two test specimens made use of graphite separators. As started, the in-gradient test samples operated at an approximate hot side temperature of 1000°C and a cold side temperature of about 50°C. Shortly after the start of

57.

the test, two of the four heaters failed. The test was nevertheless continued but after some 450 hours of test the remaining two heaters also failed and the test was interrupted.

It is not known why heater failure occurred because use was made of tungsten heaters that normally exhibit long life at these test temperatures. Oxidation of the tungsten is possible but unlikely because the background pressure in the vacuum bell jar of the test facility was of the order of 10^{-6} Torr throughout test. The in-gradient test will be restarted on a follow-on program and continued as soon as the heaters are replaced. It has been decided to dispense with the tungsten heaters and to rather use heaters similar to those of the four-couple test modules fabricated by Resalab for JPL. These heaters possess proven long-term life at test temperatures considerably higher than those of the in-gradient test. In fact, the four-couple test modules have been operated at temperatures as high as 1000°C. The new heaters for the in-gradient test were placed on order towards the end of the present contract with the vendor that supplies heaters for the four-couple test modules. The in-gradient test will be restarted and continued as soon as the heaters become available and the test facility can be modified to accomodate them.

Prior to the interruption of the in-gradient testing, some 450 hours of test time were attained on the longest life samples. The other samples were tested for shorter periods of time because of earlier heater failures. Preliminary analyses of the data obtained on the in-gradient test were conducted. Table III lists the results of the analyses for one n-type and one p-type 80 a/o Si - 20 a/o Ge alloy sample for operating times of 72 and 264 hours. The table lists the effective electrical resistivity and Seebeck coefficient values for these samples in terms of values calculated from the experimental and those calculated

TABLE III

RESULTS OF IN-GRADIENT ANNEALING OF N-AND P-TYPE
80 a/o SI – 20 a/o GE ALLOY TEST SAMPLES

Time 72 Hours

Sample Type	Hot or Cold Side	Resistivity-mΩ-cm		Seebeck Coeff.-μv/°C		S^2/ρ x 10^5 watt/°C^{2}cm	
		Measured	Calculated	Measured	Calculated	Measured	Calculated
n	Hot	2.33	2.03	269	268	3.11	3.54
	Cold	1.37	1.60	222	207	3.60	2.68
p	Hot	2.84	2.42	308	264	3.34	2.88
	Cold	1.56	1.55	206	199	2.72	2.55

Time 264 Hours

Sample Type	Hot or Cold Side	Resistivity-mΩ-cm		Seebeck Coeff.-μv/°C		S^2/ρ x 10^5 watt/°C^{2}cm	
		Measured	Calculated	Measured	Calculated	Measured	Calculated
n	Hot	1.71	2.12	255	269	3.80	3.41
	Cold	1.79	1.73	231	212	2.98	2.60
p	Hot	2.90	2.41	305	264	3.21	2.89
	Cold	1.54	1.56	207	200	2.78	2.56

Measured values are those obtained on present test; calculated values obtained from so-called "standard" thermoelectric property data.

59.

from the most recent so-called standard thermoelectric property data for the 80 a/o Si - 20 a/o Ge alloy. It should be noted that for each test time and for each sample, two values of electrical resistivity and Seebeck coefficient are given. These two values correspond to the hot end and the cold end of the test samples. For both sets of values, a temperature gradient of the order of 400 degrees existed between the thermocouples that were used to determine the Seebeck voltage and the electrical resistance of portions of the samples. The range of temperatures covered by the hot side thermocouples span approximately between 550 and 950°C; the range of temperatures covered by the cold side thermocouples was approximately 50 and 450°C. It is noted that although discrepancies do exist between measured and calculated values of electrical resistivity and Seebeck coefficient, the disagreement is not major and can be explained in terms of a possibly different thermal history of the samples in in-gradient test and those used to generate the so-called standard thermoelectric property data for the 80 a/o Si - 20 a/o Ge alloy. Namely, the Seebeck coefficient and the electrical resistivity in most cases follow each other, i.e., if for example, the measured resistivity is higher than that calculated then so is the Seebeck coefficient. If, in fact, the ratio S^2/ρ is the same for the calculated and measured data then all discrepancies are explainable on the basis of the dopant precipitation model and/or differing doping level between the samples currently on test and those used to generate the so-called standard property data. In the expression S^2/ρ, the S of course refers to the absolute Seebeck coefficient and the ρ is the electrical resistivity. The appropriate values of this parameter have been calculated for the data shown in Table III and are also listed. In the instances in Table III where a significant difference exists between the measured and so-called calculated values of S^2/ρ,

it is possible that either the present experimental results are uncertain or that the relationship between the Seebeck coefficient and the electrical resistivity used to obtain so-called calculated values of Seebeck coefficient is in error. Discrepancies of the order of ten to 15 percent in measured and calculated values of S^2/ρ are explainable in terms of experimental uncertainty because, for example, a three percent uncertainty in the electrical resistivity and the Seebeck coefficient would result in a nine percent uncertainty in the quantity S^2/ρ. It should, however, be observed that invariably the measured values of S^2/ρ are higher than those calculated. This indicates a systematic discrepancy that possibly is not explainable on the basis of random error; a systematic error appears to be indicated. Further work in this area, coupled with detailed thermoelectric property measurements in the thermal conductivity apparatus, will resolve the question inherent to the results.

D.   Thermal Conductivity Annealing Tests

When it was decided to separate the thermal conductivity and in-gradient testing of n-and p-type 80 a/o Si - 20 a/o Ge alloy test samples, a test plan was formulated for the thermal conductivity annealing tests. It was planned to anneal silicon-germanium alloy samples at different temperatures. Each sample was to undergo one week of annealing in a comparative thermal conductivity apparatus at a fixed test temperature. After this, the annealing was to be continued in a separate annealing furnace until the sample was to be replaced for annealing in the thermal conductivity apparatus. It was planned to thus cyclically anneal a number of silicon-germanium alloy test samples concurrently. During its periodic occupancy of the comparative thermal conductivity apparatus, the thermoelectric properties of each sample were to be continuously monitored; Measurements were to be performed on all three thermoelectric properties, electrical resistivity, Seebeck coefficient and thermal conductivity. Testing was

61.

planned to continue for a number of cycles such that each sample under evaluation would undergo measurement in the thermal conductivity apparatus on a number of separate occasions. This would enable all three thermoelectric properties of each sample to be determined as a function of time and any observed changes in one or more properties could be correlated to those of the other properties.

Because of the unavailability of silicon-germanium test samples this evaluation program was not started during the present contract. Effort was, however, devoted to the calibration of the thermal conductivity apparatus in its modified form by means of a Pyroceram standard. It was mentioned above that the thermal conductivity apparatus was modified to accomodate 1/2 inch diameter test samples. The calibration of the modified thermal conductivity apparatus was completed prior to the end of the contract and the final results indicate that agreement with reported National Bureau of Standards value is of the order of one or two percent up to temperatures of the order of 550°C. At higher temperatures the agreement of calibration results with those reported by NBS was not as good. For example, presently determined thermal conductivity values for Pyroceram are some eight percent higher than those reported by NBS. This finding is not unexpected because most direct methods of thermal conductivity are subject to errors because of radiation losses at higher temperatures. It is believed that results of thermal conductivity measurements on silicon-germanium alloys will be relatively accurate up to about 700°C as long as use is made of the presently established calibration curve; the presently established calibration curve takes into account losses characteristic of the present thermal conductivity measuring equipment. The results of the calibration of Pyroceram are shown in Figure 18. The thermal conductivity of Pyroceram reported by the National Bureau of Standards is superimposed in Figure 18 for convenience of comparison.

62.

Figure 18

Thermal Conductivity of Pyroceram

National Bureau of Standard

Experimental

Temperature – °C

Thermal Conductivity-watts/°C-cm

63.
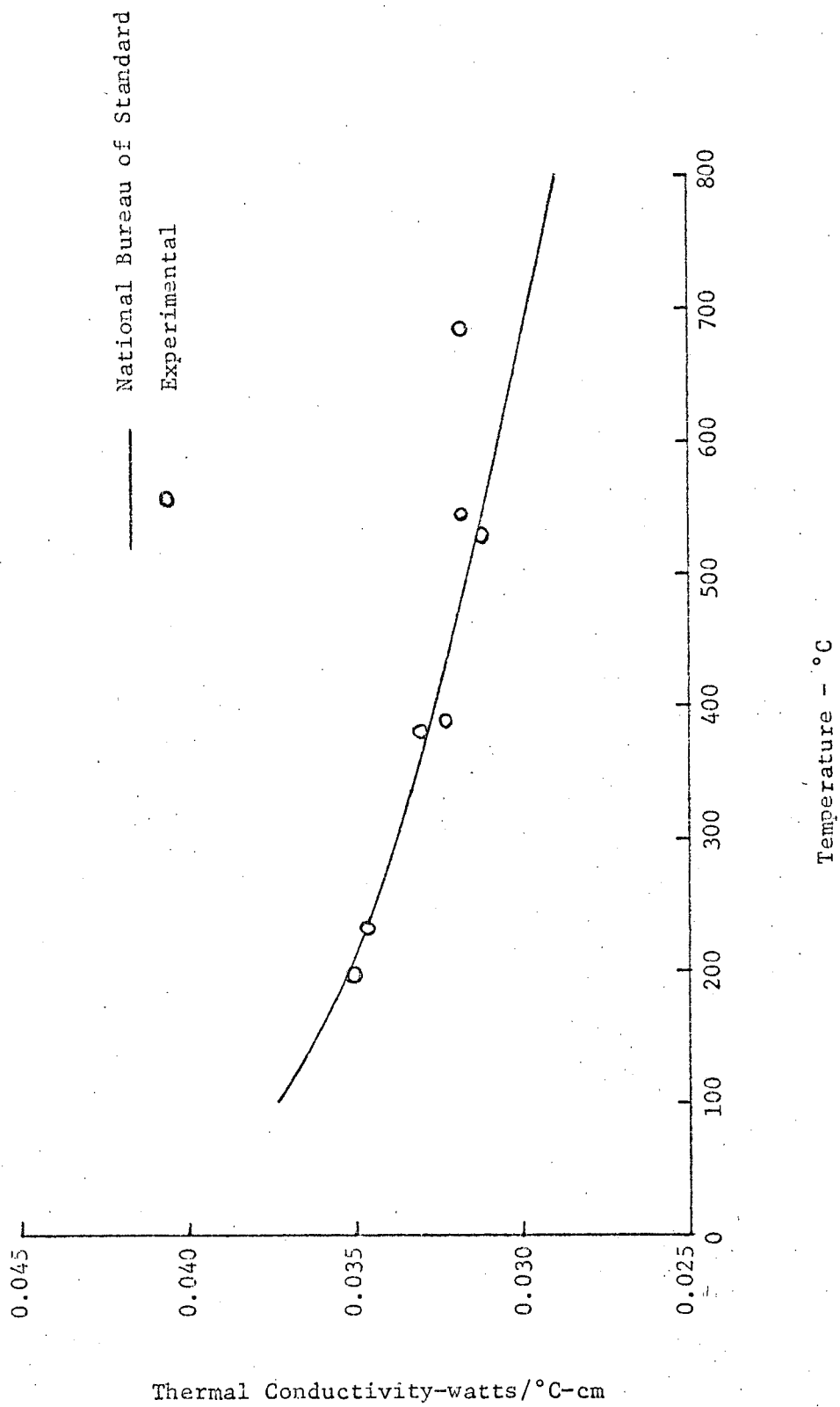
Although the clyclical measurement of n-and p-type 80 a/o Si - 20 a/o Ge alloy test specimens was not started on the present contract, everything is ready for such measurements when material becomes available from RCA. It is planned that the program will be continued on a subsequent study effort for JPL. In the meantime, additional calibration work on the thermal conductivity ap-- paratus may be conducted and attempts will be made to enhance the accuracy of the method and to extend it to temperatures higher than 700°C with reasonable accuracy.

IV.   SUBLIMATION OF SILICON-GERMANIUM ALLOYS

A.   Introduction

Work on the determination of the sublimation characteristics of silicon-germanium alloys was started on the present contract in February of 1971. Since that time this work has consisted essentially of two parts. The first part considered the experimental determination of the vapor pressures and evaporation rates of n-and p-type 80 a/o Si - 20 a/o Ge alloys. The bulk of the first part of this work was carried out in a mass spectrograph at Gulf General Atomics in San Diego, California. The second part of the task was performed totally at Resalab and involved the compatibility testing of coupons consisting of samples of various thermal insulations and silicon-germanium and silicon-molybdenum alloys as well as pure silicon. The thermal insulations used in the compatibility tests have involved silicon-dioxide based insulations such as Min K-2020, Astroquartz and dynaquartz as well as alumina. In some cases compatibility of silicon-germanium and silicon-molybdenum alloys and multi-foil insulation consisting of molybdenum foils and Astroquartz cloth has also been investigated. As a part of the task performed at Resalab, a number of test modules that simulate typical silicon-germanium RTG's were fabricated for test at JPL.

The results of the sublimation and compatibility studies were used to analytically predict the effects of sublimation on the performance of silicon-germanium RTG's such as the MHW-RTG. Efforts in some areas of compatibility testing are continuing and it is expected that they will be continued in subsequent follow-on efforts for JPL. Physical and analytical models depicting the effects of sublimation and interaction of RTG components are and will be updated in the future as additional experimental information becomes available.

B.   <u>Experimental Sublimation Studies</u>*

Much of the experimental work on the determination of sublimation characteristics of silicon-germanium alloys was performed in a mass spectrograph in which a Knudsen cell was used to supply species emanating from the 80 a/o Si - 20 a/o Ge alloy at different temperatures. Prior to the investigation of the evaporation characteristics of silicon-germanium alloys by means of a Knudsen cell, it was necessary to satisfy certain requirements. Because silicon and germanium are extremely reactive, it was important to control any reaction between test samples and the cell through the equilibration of all possible interactions. Although graphite and molybdenum were both considered initially as liner materials for the Knudsen cell, molybdenum was finally selected for this purpose because silicon-carbide, unlike molybdenum disilicide, has measurable volatility in the temperature range used in the present study. Knudsen cells made of molybdenum were accordingly used and in order to increase their life, the cells were lined on the inside with 0.003 inch molybdenum foil.

The system of Knudsen cell and mass spectrograph was pressure calibrated by making a plot of the product of signal intensity and absolute temperature as a function of reciprocal temperature for pure silicon and germanium. At the mid-temperature of the measurement range, the product of the signal intensity and absolute temperature was equated to the literature values of the vapor pressures of silicon and germanium. Results of experiments on cell reaction and the heats of vaporization measured for silicon and germanium during the pressure calibrations justified this procedure. The presently determined heats of vaporization determined for silicon and germanium are in excellent agreement with literature values.

The first silicon-germanium test specimens to be investigated were n-and p-type 80 a/o Si - 20 a/o Ge alloy that had been prepared by zone levelling at

---

* This work performed at Gulf General Atomics under sub-contract to Resalab

RCA. The species observed vaporizing from material of both polarity types were Ge^+, Ge_2^+ and Si^+. The n-type sample had an additional species in the form of P_2^+. The vapor pressures measured for silicon over zone levelled n-and p-type 80 a/o Si - 20 a/o Ge alloy, along with the vapor pressure of silicon over pure silicon are shown in Table IV. It is noted that a distinct difference in the vaporization of silicon from n-and p-type material exists and that both exhibit a behavior different from that of pure silicon.

Although initial vaporization studies were concerned with silicon-germanium alloys made by the zone levelling technique, subsequent investigations involved the use of material made by hot pressing because it is material of this type that is considered for use in the MHW-RTG. Prior to the start of the vapor-ization studies, the oxygen content of representative n-and p-type 80 a/o Si - 20 a/o Ge alloy samples was determined by neutron activation analysis. It was found that the material contains $\leq$ 10 ppm O_2. Samples of p-type silicon-ger-manium alloy were heated to 1000°C in a molybdenum Knudsen cell. It was noted that germanium vaporized as if from pure germanium for a period of approximately two hours. At this time, the temperature of the Knudsen cell was raised to 1175°C. In less than 45 minutes the germanium pressure decreased to a value equivalent to a germanium activity of 0.2, the value to be expected for an ideal solid solution containing 20 atomic percent germanium. The n-type hot pressed silicon-germanium alloy behaved similarly, except that the initial germanium pressure was not quite as large as it was for the p-type alloy. These results may be taken as indications that the hot pressed silicon-germanium alloy is very inhomogenous and that heat treatment enhances homogenity, at least as regards vaporization characteristics. It should be noted that the germanium vapor pressure above zone levelled n-and p-type 80 a/o Si - 20 a/o Ge alloy displayed a germanium activity of 0.2 upon initial heating.

TABLE IV

VAPOR PRESSURE IN ATMOSPHERE OF Si OVER ZONE-LEVELLED

n- AND p-TYPE 80 a/o Si – 20 a/o Ge

	n-Type	p-Type	Si	Expected Value for an 80 Atomic Percent Ideal Solution of Si
Temperature, °C	1234	1232	1231	1231
P (atm)	3.6×10^{-10}	2.2×10^{-9}	7.5×10^{-9}	6.0×10^{-9}
Reduction Factor in Si Partial Vapor Pressure from Ideal Solution	17	3		

The Si vapor pressure for the n-type is near the detection limit of the mass spectrograph and consequently could be somewhat inaccurate. Nevertheless, the partial pressure of silicon is clearly much smaller for the n-type alloy than for the p-type.

The species observed vaporizing from n-and p-type hot pressed 80 a/o Si - 20 a/o Ge alloy were Ge^+, Ge_2^+ and Si^+. The additional species of P_2^+ was also observed for the n-type alloy. The pressure of P_2^+ behaved in a manner similar to that observed for the zone levelled material in that it decreased with time to a constant value. Figures 19 and 20 show the present results on the vapor pressure of the hot pressed n-and p-type 80 a/o Si - 20 a/o Ge alloy. The germanium calibration curves used to calculate the pressures are also shown in Figures 19 and 20. The vapor pressure point shown for silicon was obtained at the lower limit of detection of the mass spectrograph.

The vapor pressure of Ge^+ and P_2^+ for n-and p-type zone levelled and hot pressed 80 a/o Si - 20 a/o Ge alloy are compared in Table V for a temperature of 1000°C. The value of P_2^+ partial pressure represents the fixed value observed after the initial decrease. The vapor pressure of germanium over all four materials is the same within the error of measurement. It was found that the average activity of germanium is 0.18 at 1000°C and thereby near the value expected for an ideal solid solution. Germanium activity increases slowly with temperature because the heat of vaporization of germanium from the silicon-germanium alloy is slightly higher than that from pure germanium. The vapor pressure of P_2^+ was found to be slightly higher above the hot pressed material than above zone levelled material. The temperature used in the present study exceeded the boiling temperature of phosphorus and therefore the activity of P_2^+ in the silicon-germanium alloy is quite small. Because data could not be obtained as a function of temperature, it was difficult to compare the vapor pressures of silicon for the zone levelled and hot pressed alloy. Figure 21 shows the vapor pressure points of silicon obtained for the two types of material, with a point given for each polarity type. The solid line in Figure 21
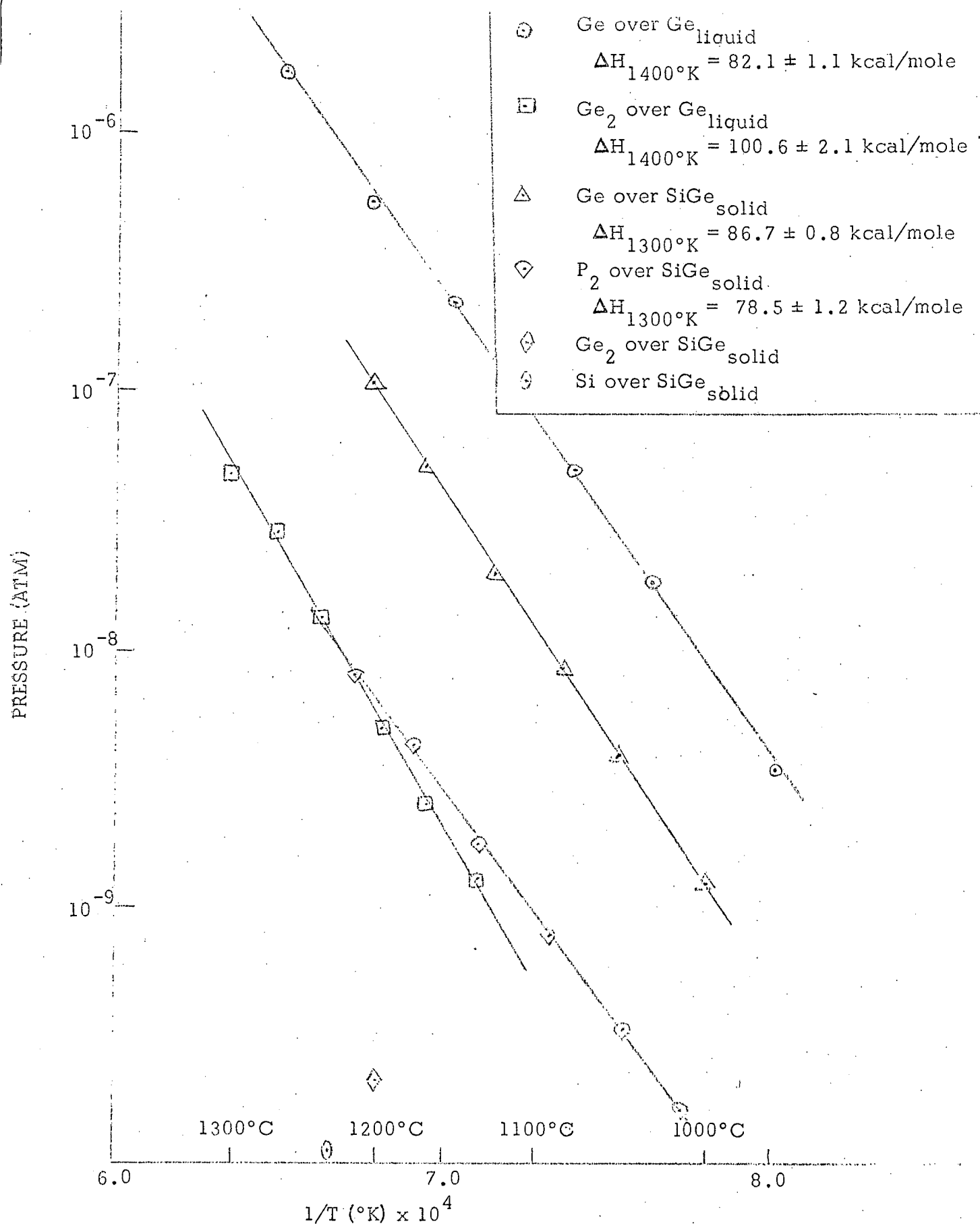
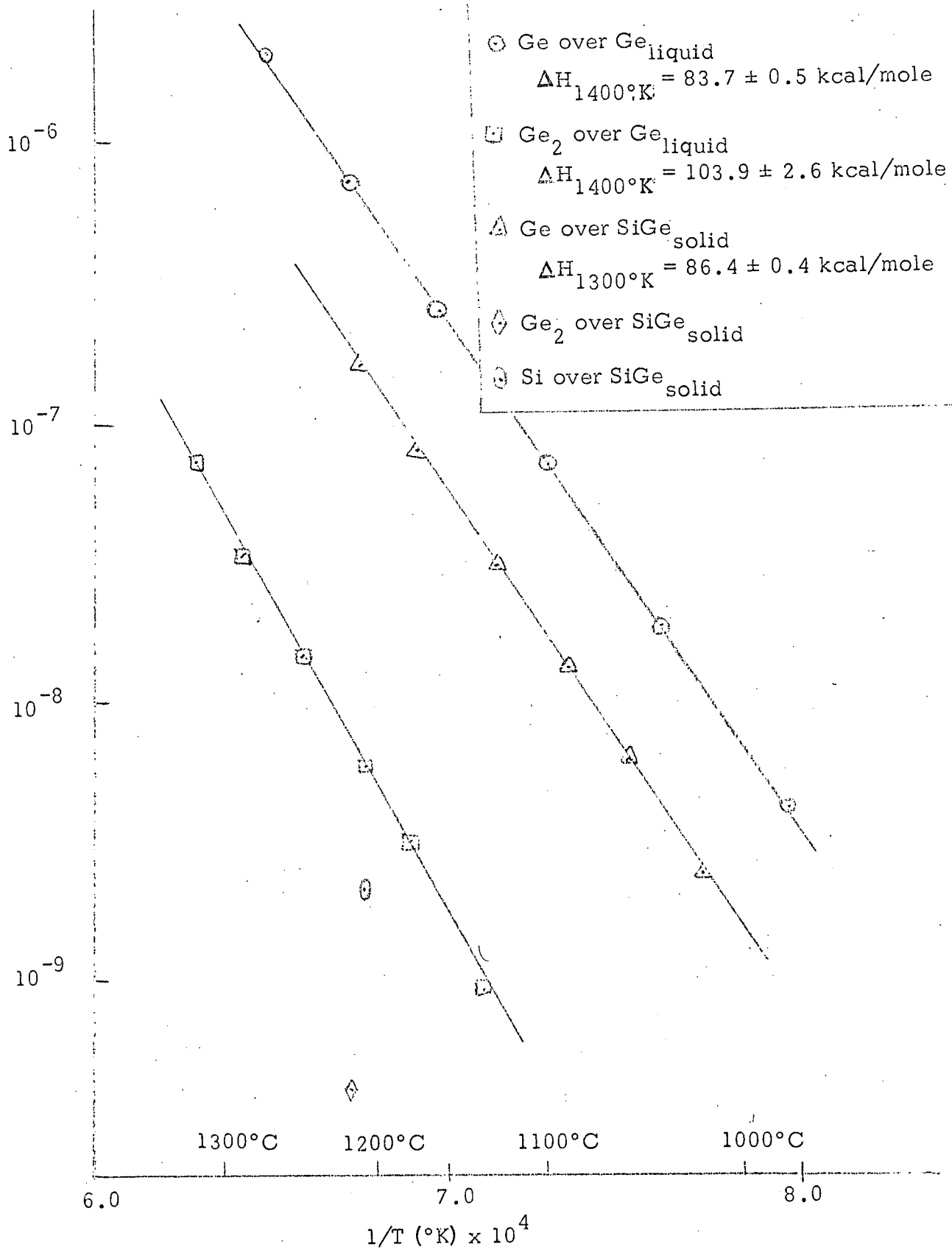Figure 19   Hot-Pressed n-type 80 a/o Si - 20 a/o Ge
alloy vapor species

70.

Figure 20 Hot-pressed p-type 80 a/o Si – 20 a/o Ge
alloy vapor species

71.

TABLE V

COMPARISON AT 1000°C OF Ge AND P_2 VAPOR PRESSURES AND HEATS OF VAPORIZATION

BETWEEN HOT-PRESSED AND ZONE-LEVELLED 80 a/o Si – 20 a/o Ge ALLOY

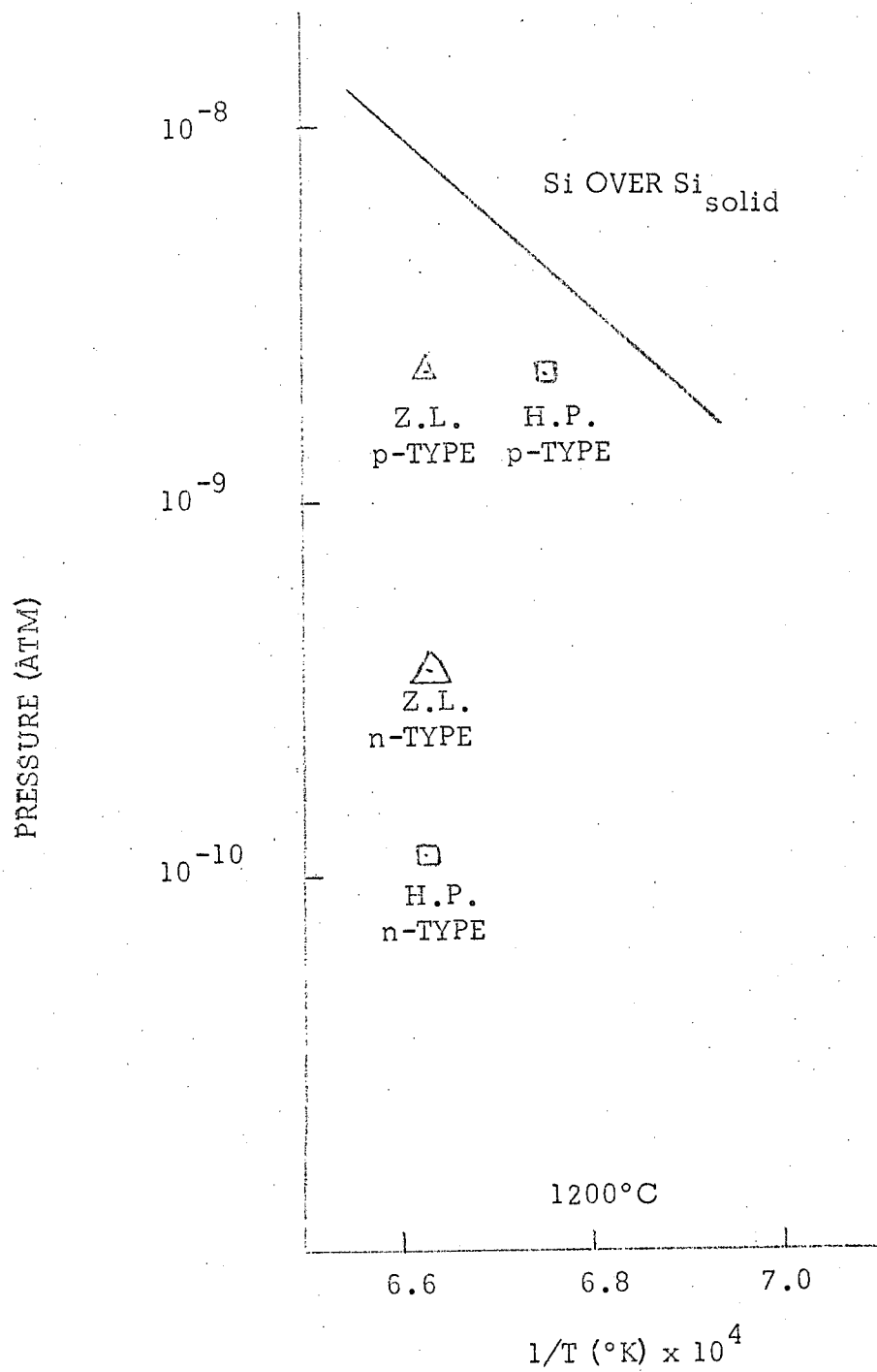|	Zone-Levelled		Hot Pressed		Pure Material	Expected Value for a 20 Atomic Percent Ideal Solution of Ge
	p-type	n-type	p-type	n-type		
Ge P(atm)	1.0×10^{-9}	1.5×10^{-9}	1.5×10^{-9}	1.0×10^{-9}	7.0×10^{-9}	1.4×10^{-9}
$\Delta H_{1300°K}$ (kcal/mole)	90.1	87.1	86.4	86.7	83.7, 82.1	---
P_2 P(atm)	---	6.0×10^{-11}	---	1.0×10^{-10}	---	---
$\Delta H_{1300°K}$ (kcal/mole)	---	75.1	---	78.5	---	---

Figure 21 Comparison of Si vapor pressures over
zone-levelled and hot-pressed 80 a/o
Si - 20 a/o Ge alloy

73.

shows the vapor pressure of silicon over pure silicon in the corresponding temperature range. The silicon vapor pressure over the p-type alloy is below the expected activity of 0.8. The silicon vapor pressure over the n-type alloy is significantly lower than that over the p-type alloy. It should be noted that the data points shown for the n-type alloy in Figure 21 are only approximate because they were obtained at the lower limit of detection of the mass spectrograph for silicon. No explanation is available for the observed anomolus partial pressure of silicon, especially in view of the nearly ideal behavior found for germanium.

In addition to the experimental determination of the vapor pressure and evaporation rate of n-and p-type 80 a/o Si - 20 a/o Ge alloy, a series of tests was also conducted on the compatibility of various oxide insulating materials and the silicon-germanium alloy. Compatibility tests between ZrO_2 and silicon-germanium alloy indicated that zirconia releases large quantities of SiO, GeO and Ge in the presence of the silicon-germanium alloy at 1200°C. Zirconia by itself at the same temperature releases only small quantities of the same species. The conclusion of these compatibility tests is that Zirconia and silicon-germanium alloys react to yield volatile species. The same test was repeated with silicon-germanium alloy and SiO_2. At 1200°C substantial amounts of SiO, GeO, Ge and Si were observed to be emitted. The reaction product SiO was the most prominent of all of these species. In the case of n-type silicon-germanium alloy and SiO_2, the additional species of P_2 was observed as well. The major difference between the compatibility of SiO_2 and n-type and p-type silicon-germanium alloys was the occurance of a lower silicon vapor pressure in the case of the n-type material. The lower silicon vapor pressure for the n-type silicon-germanium alloy is in the same direction that was previously

noted for the vapor pressure of silicon over hot pressed 80 a/o Si - 20 a/o Ge when heated without the presence of SiO_2.

C. Compatibility Tests

While the experimental sublimation studies were being conducted at GGA, in a meeting with cognizant JPL project personnel, it was decided to conduct a series of compatibility tests involving various thermal insulations and silicon-molybdenum and silicon-germanium alloys. The series of tests was to include a test in which samples of silicon-germanium and silicon-molybdenum alloys were placed in cavities inside sections of multi-foil insulation consisting of molybdenum foils and Astroquartz cloth spacers, another test in which silicon-germanium and silicon-molybdenum alloys would be in continuous contact with various thermal insulations, a test in which silicon is in the proximity of silicon-dioxide insulation without actually touching it and a test for the determination of the sublimation rate of bare silicon-germanium and silicon-molybdenum alloys. Information obtained from all of these tests was to be analyzed and used in the development of physical and mathematical models depicting the effects of sublimation from silicon-germanium Air-Vac thermocouples on the performance of RTG's such as the MHW-RTG. Results of all coupon tests were to be analyzed on the basis of weight and dimensional measurements and visual inspection. All coupon tests were to be conducted kinetically at a number of different temperatures in the range of temperatures of 1000 to 1200°C. The reason for the inclusion of a variety of thermal insulations in the coupon test is the fact that different insulations can be conceivably used in high temperature silicon-germanium RTG's, such as the MHW-RTG, for electrical and/ or thermal isolation of components. Both Astroquartz and dynaquartz thermal insulations are basically silicon-dioxide, an insulator that is planned for use as a spacer between refractory metal foils in a multi-foil insulation system.
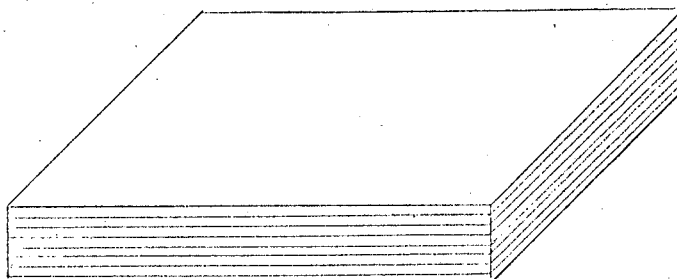
Alumina has been proposed for use as an electrical isolator between the multi-foil insulation and silicon-molybdenum hot shoes of silicon-germanium Air-Vac thermocouples.

The first compatibility test was intended to determine the compatibility of silicon-germanium and silicon-molybdenum alloys and multi-foil thermal insulation consisting of molybdenum foils and Astroquartz spacers. This test made use of coupons made of sections of multi-foil insulation with silicon-germanium and silicon-molybdenum alloys embedded in cavities inside the sections. A typical coupon configuration is illustrated in Figure 22. The coupons were isothermally annealed at a variety of temperatures in the range of 1000 to 1200°C. Originally it was planned that a coupon containing a silicon-germanium alloy test piece and one containing a silicon-molybdenum alloy test piece would be removed from test at each test temperature after 100, 500, 1000, 2000 and 5000 hours of test. During the actual testing, however, it was found that test sample weight loss proceeded much more rapidly than originally anticipated and therefore the whole test was terminated after 300 hours. Each coupon removed from test was analyzed for weight and volume change and a comparison with the initial state of the coupon enabled the determination of the rate of sublimation/reaction of the silicon-germanium and silicon-molybdenum alloys with the Astroquartz yarn and the multi-foil insulation surrounding them.

In order to reduce the test data, a mathematical model was formulated in terms of test sample surface area and weight as a function of time. Assuming parallelepipedal samples, with initial side lengths of S_{10}, S_{20} and S_{30} a cubic equation can be formulated for the average effective evaporation rate of material. This relationship can be written as

$$X^3 - \left(S_{10} + S_{20} + S_{30}\right)X^2 + \frac{1}{2}A_o\,X = \frac{M_{SO} - M_S}{\rho}\,, \tag{12}$$

8 layers
½ mil moly foil
separated by
J. P. Steven #594
Astroquartz cloth
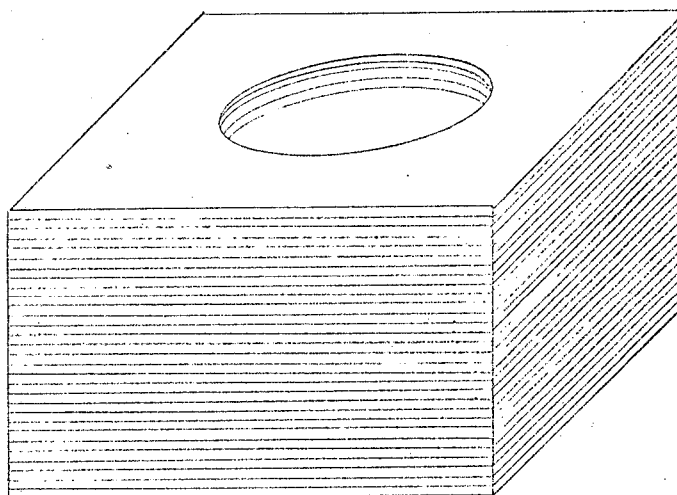
3/8" Dia. Hole

Insert Sample
(0.18" x 0.2" x 0.25")

Wrapped with two layers
of astroquartz braiding
yarn

34 layers
½ mil moly foil
separated by
#594
Astroquartz cloth

8 layers
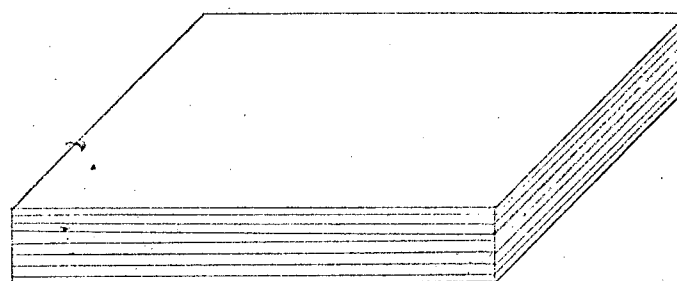½ mil moly foil
separated by
#594 Astroquartz
cloth

Figure 22 Compatibility Test Coupon Configuration

where

$$X = \frac{2kt}{\rho} \quad .$$ (13)

In the above relationship, A_o is the initial total surface area of the sample, M_{SO} is the initial mass of the sample, M_S is the mass of the sample at time t, ρ is the density of the sample and k is the evaporation rate of the sample. Insertion of actual measured sample weights at different times in the above relationship enables the solution of the cubic equation for sample evaporation rate. It should be noted that the above relationship assumes a constant stoichiometric evaporation rate; evaporation rates calculated by means of this relationship thereby represent effective time averaged values.

Applying the above model to the actual test data obtained from the coupon test, the evaporation rates were calculated for silicon-germanium and silicon-molybdenum alloys in the proximity and completely surrounded by Astroquartz/molybdenum foil thermal insulation. The results of the calculations are shown in Figures 23 and 24. Figure 23 shows the evaporation rate of p-type 80 a/o Si - 20 a/o Ge alloy as a function of inverse absolute temperature. The solid lines indicate curves calculated from Honig's vapor pressure data for pure silicon and germanium. The dashed line indicates the data obtained at Gulf General Atomic on n-type 80 a/o Si - 20 a/o Ge alloy under subcontract to Resalab. The circular data points are derived from present coupon tests and the triangles represent data reported by the General Electric Company for the initial sublimation rate of the 80 a/o Si - 20 a/o Ge alloy. It should be noted that the present results are somewhat higher than those reported by GE but that they do agree well with the GGA results. All sets of experimental data are somewhat higher than one would expect from a stoichiometric 80 a/o Si - 20 a/o Ge alloy as judged by the curves due to Honig. Figure 24 shows the evaporation rate of
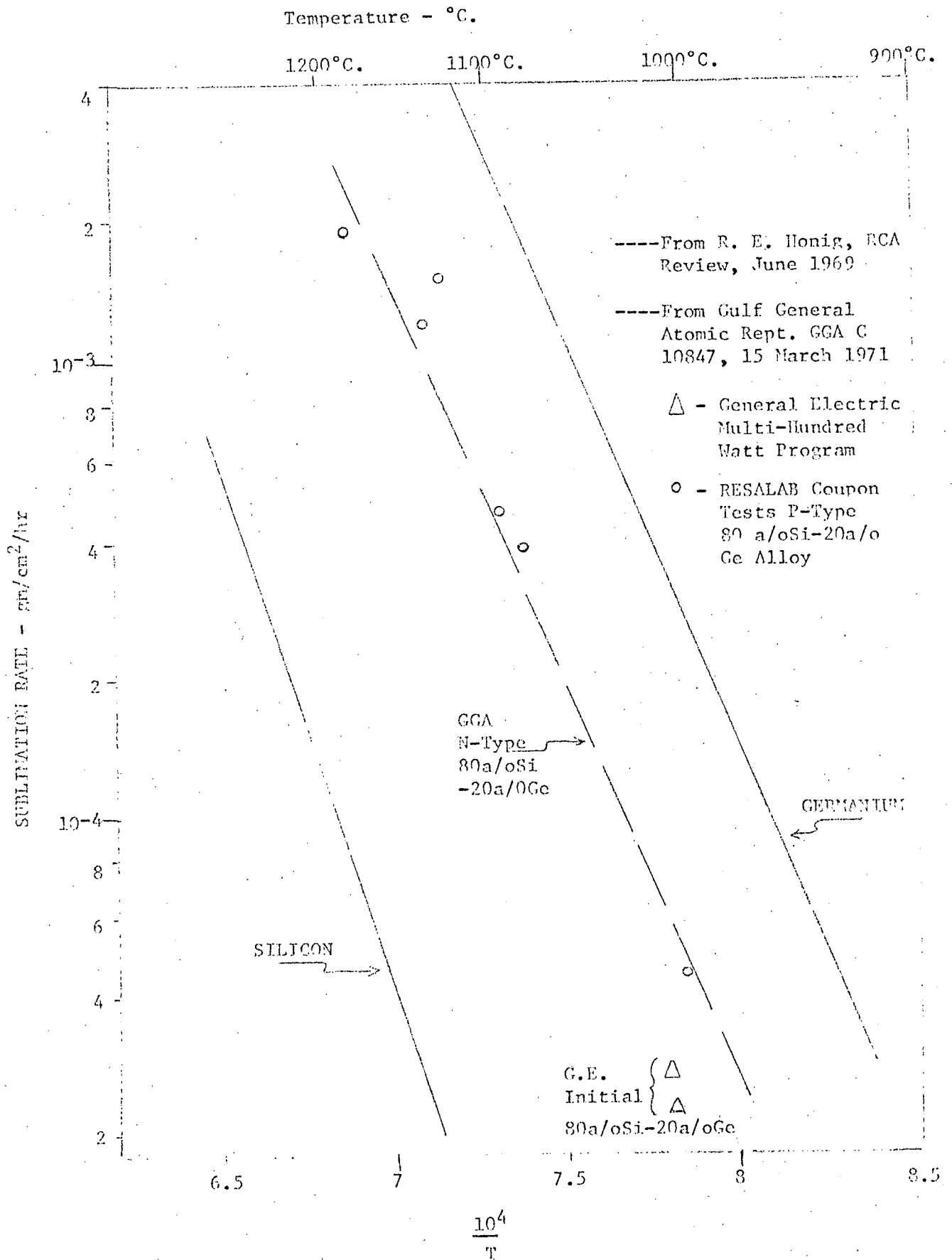
SUBLIMATION RATE OF 80 a/o Si - 20 a/o Ge ALLOY

Figure 23

Temperature – °C.

1200°C.   1100°C.   1000°C.   900°C.
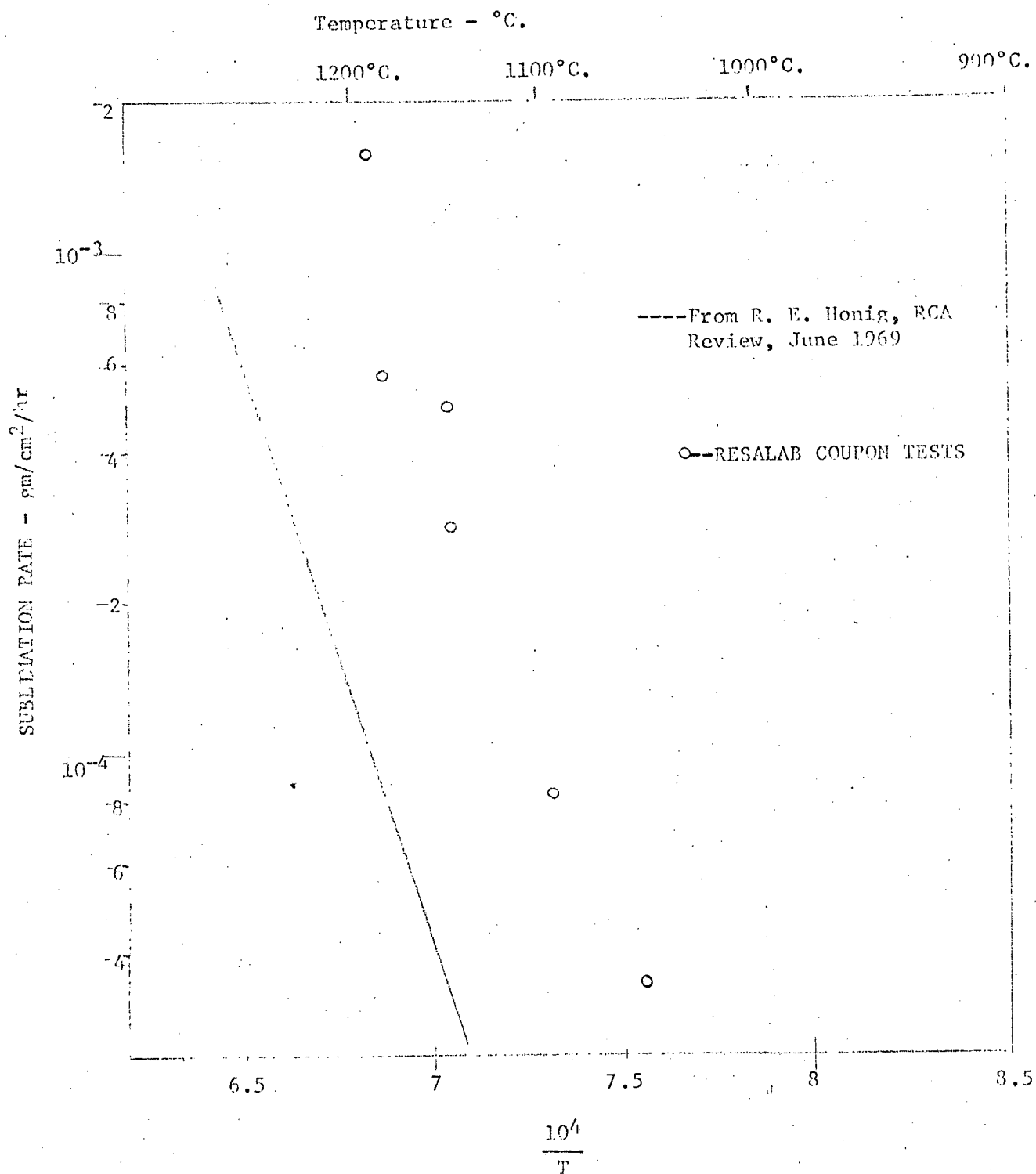
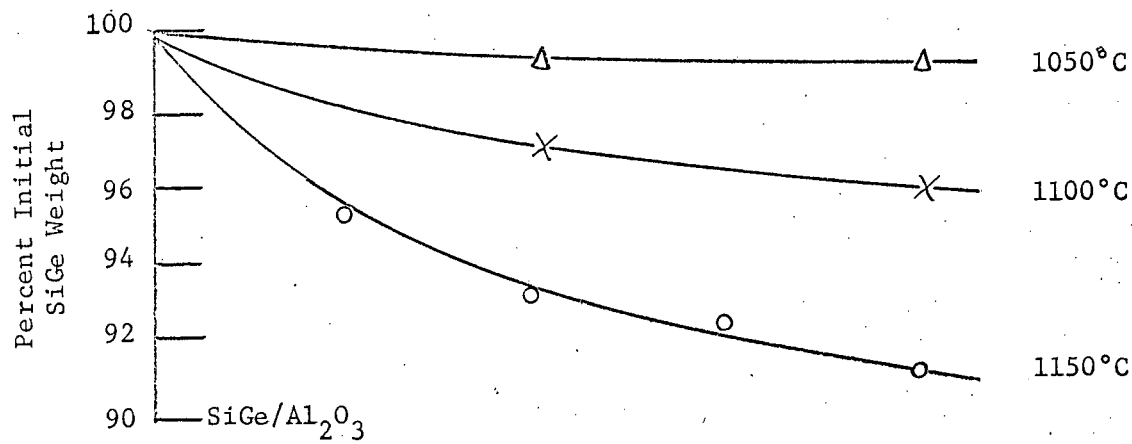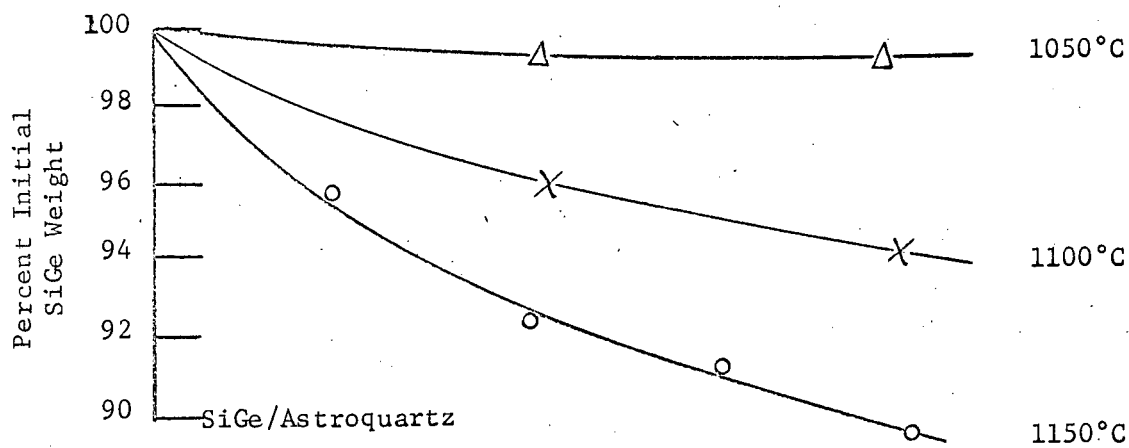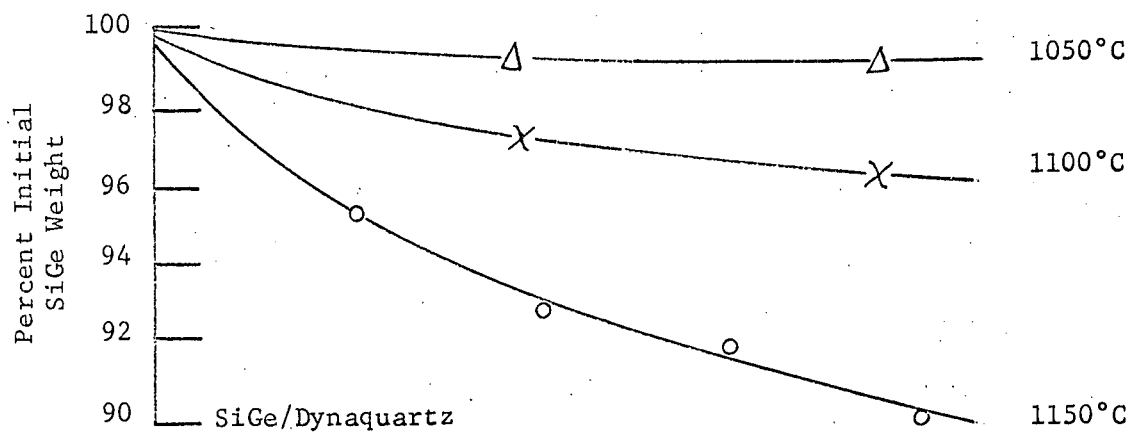SUBLIMATION RATE OF SILICON-MOLYBDENUM ALLOY

Figure 24

silicon-molybdenum alloy as a function of inverse absolute temperature. The data points indicate the results of the present coupon tests and the solid curve indicates the sublimation rate of pure silicon as calculated from Honig's vapor pressure data. As with Figure 23, it is noted that the presently determined evaporation rate for the silicon-molybdenum alloy is somewhat higher than that of pure silicon as determined from Honig's vapor pressure data. The reason for the higher than expected values of evaporation rate of silicon-germanium and silicon-molybdenum alloys is not, at present, known. Whether it is a real sublimation rate or the result of enhanced sublimation due to interaction with insulation and/or environment will have to be independently determined.

The second compatibility test made use of coupons in which silicon-germanium and silicon-molybdenum samples were in direct contact, but not surrounded by, samples of Astroquartz, dynaquartz and alumina. This compatibility test was conducted kinetically at test temperatures of 1050, 1100, 1150 and 1200°C for periods of time up to 100 hours. The silicon-germanium and silicon-molybdenum components of each coupon consisted of disks 0.1 inch thick and having approximate surface areas of two square centimeters, although variation did exist in the cross-sectional area of different samples. The insulation component of each coupon had as nearly as possible the same cross-sectional area as the silicon alloy components and a thickness of the same order. The coupons consisting of the silicon alloy disks placed on the thermal insulation samples were annealed in separate coupon test furnaces simultaneously at all test temperatures. Periodic weight measurements of each coupon, including the silicon alloy and the insulation component were performed every 25 or 50 hours; the latter test time was used for coupons being annealed at 1150 and 1200°C and the former test time was used for coupons being annealed at 1050 and 1100°C. The placement of the coupon with the silicon alloys directly on top of the insulation

sections assured continuous contact between the silicon alloys and the thermal insulations throughout the test time as a result of gravity feeding.
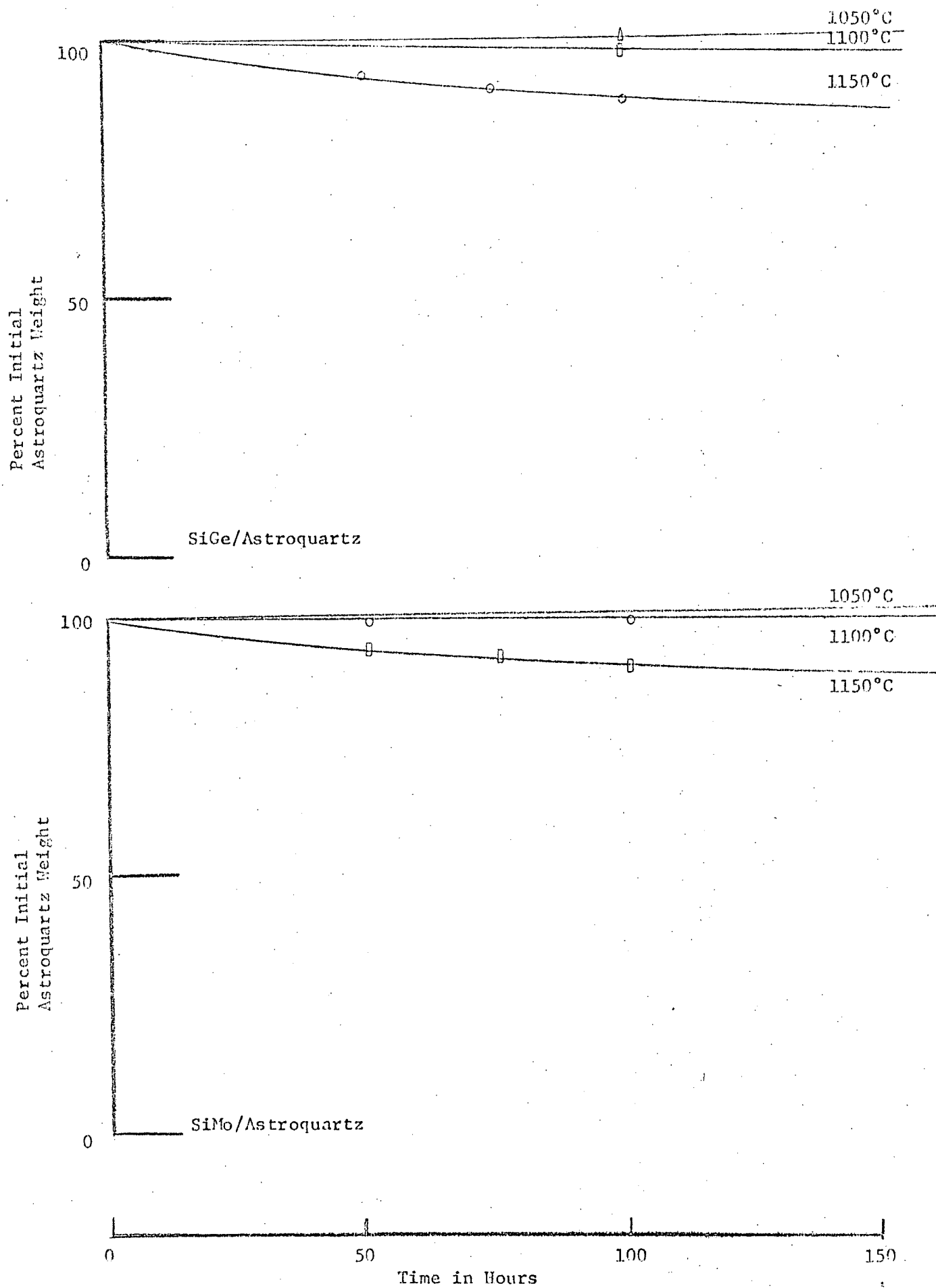
Figures 25 and 26 illustrate the results of the coupon test in terms of silicon-germanium and silicon-molybdenum alloy percent weight loss as a function of time at the test temperatures of 1050, 1100 and 1150°C. The results at 1200°C are not shown because, in most instances, the weight loss was so great that accurate results were not possible. Figure 25 shows the weight loss of p-type 80 a/o Si - 20 a/o Ge alloy in contact with dynaquartz, Astroquartz and alumina. The corresponding plot for the silicon-molybdenum alloy is shown in Figure 26. It is noted, in both cases, that no significant difference in the weight loss of the alloy exists for the different insulation coupons, although a slight but perceptible difference exists between the weight loss of silicon-germanium and silicon-molybdenum alloys; the silicon-germanium alloy, probably because of the presence of the relatively volatile germanium, exhibits a greater weight loss than does silicon-molybdenum.

The results of the coupon test in terms of weight loss of the insulation materials are illustrated in Figures 27 and 28. Figure 27 shows the percent weight loss of Astroquartz as a function of time at 1050, 1100 and 1150°C when in contact with silicon-germanium and silicon-molybdenum. The corresponding plot for weight loss of dynaquartz is shown in Figure 28. It is noted that a dramatic difference exists between the weight loss of Astroquartz and dynaquartz, the former loosing weight at a significantly lower rate than the latter. The results for the weight loss of alumina, when in contact with silicon-molybdenum and silicon-germanium alloys, is not shown because very little weight is lost from alumina even at the highest test temperature of 1200°C. Because of experimental uncertainties and the small amounts of weight lost, no perceptible difference in the weight loss of alumina appears to exist when alumina is in contact with silicon-germanium or silicon-molybdenum alloys.

Figure 25

Time in Hours

83.

Figure 26

Figure 27

85.

Figure 28

86.
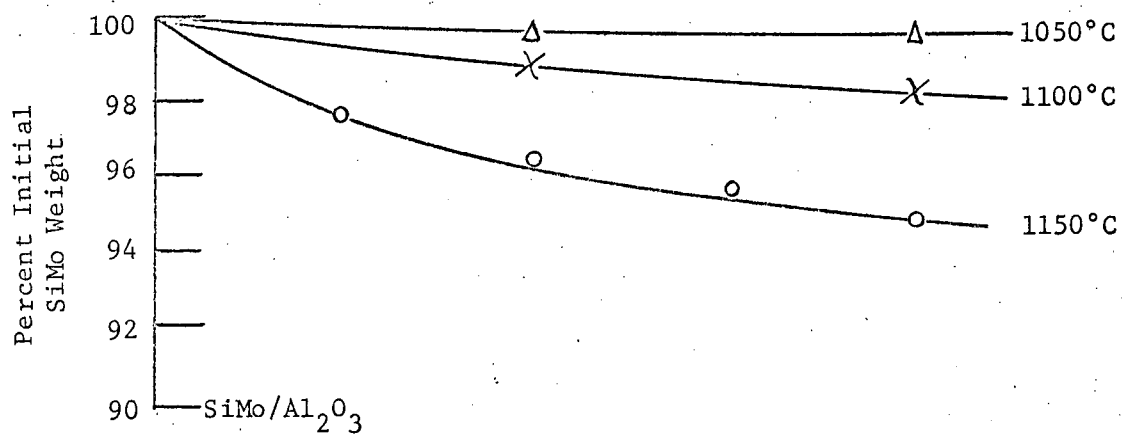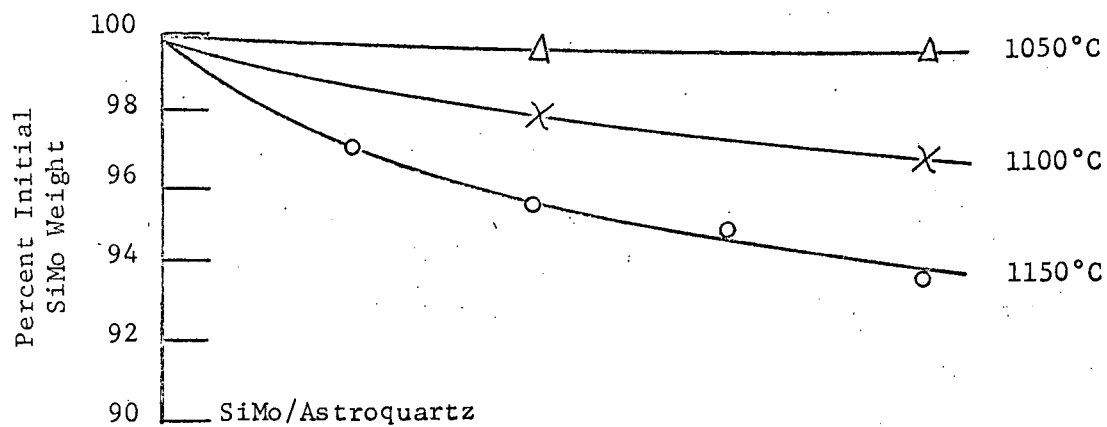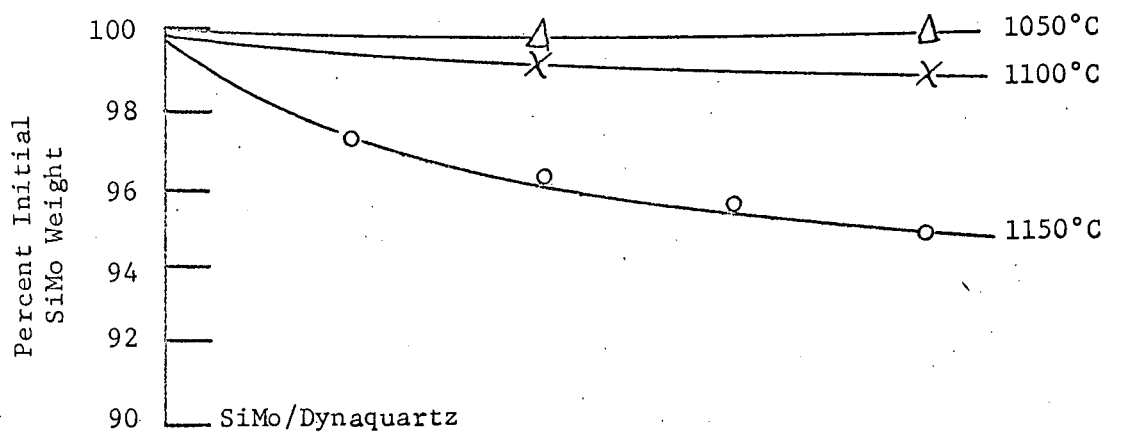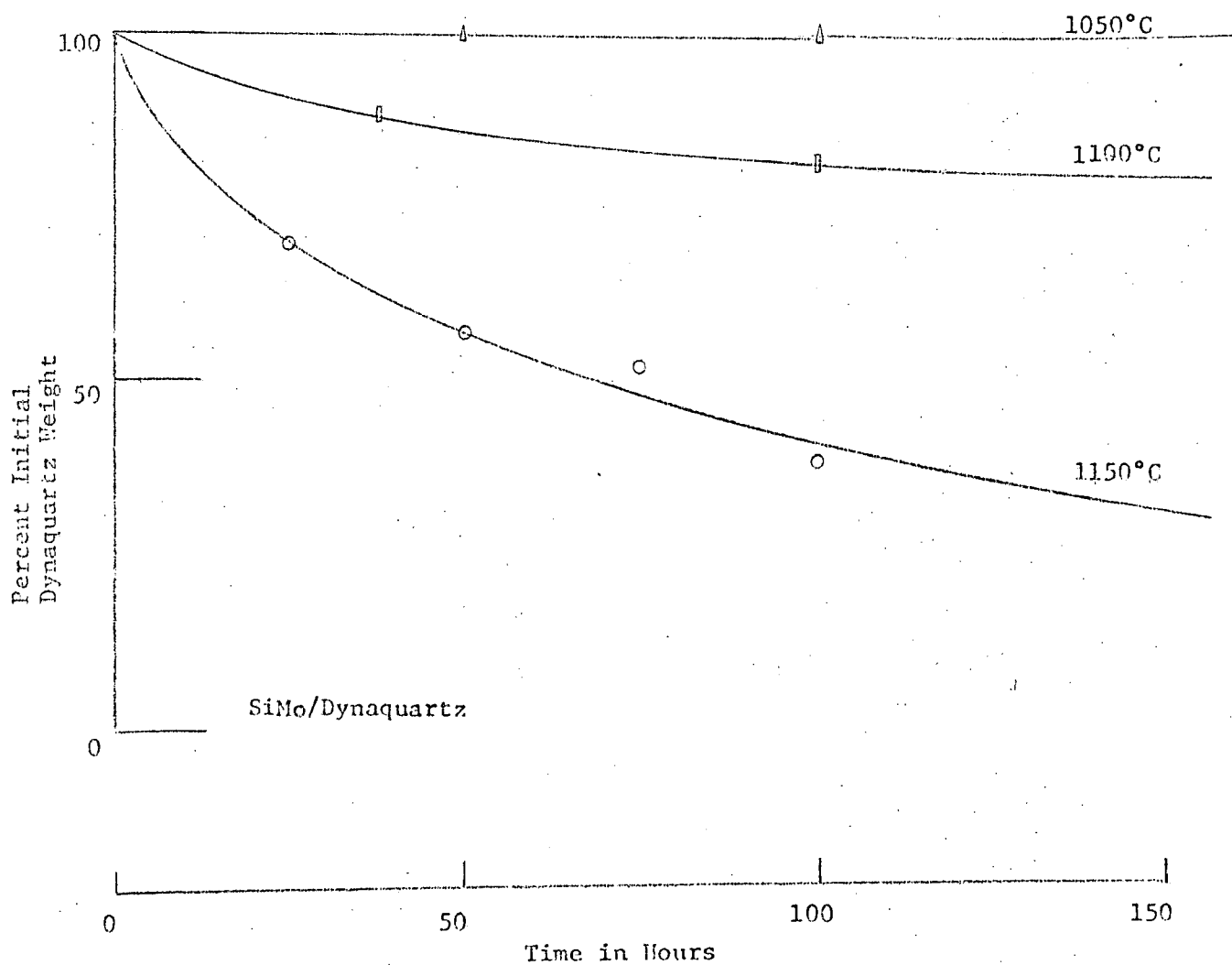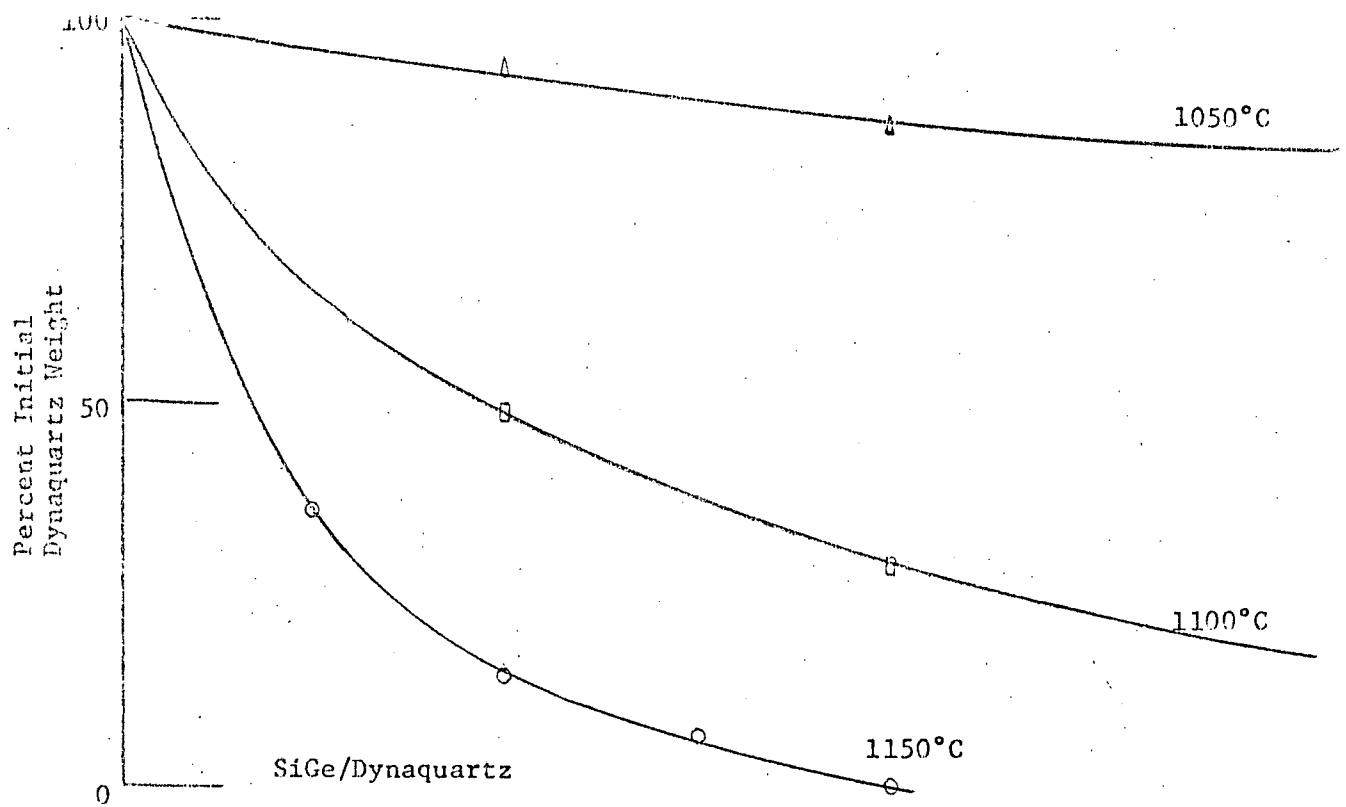
The silicon-germanium and silicon-molybdenum alloy weight loss illustrated in Figures 25 and 26 have been converted to effective values of sublimation/weight loss per unit area and unit time in order to determine how the results of this compatibility test compare to those obtained in the first test. The results of the comparison are shown in Figures 29 and 30 in terms of sublimation rate as a function of inverse temperature. The results of the second compatibility test are shown in Figure 29 as squares and represent the average values of all data obtained at each test temperature. The deviation of all data from the average is shown by the bars on each data point. It should be noted that no apparent difference exists between the sublimation rate of silicon-germanium between the three different types of coupons used in the present coupon test. It is noted that the present data indicate a sublimation rate that is lower than obtained with coupons in which the silicon-germanium alloy test specimens were completely surrounded by multi-foil thermal insulation. In addition to the present results showing a lower sublimation rate, it is also noted that the present results yield a somewhat higher heat of sublimation than previously found; the heat of sublimation is, of course, manifested by the slope of the curve in plots of the type shown in Figure 29.

The reason for the lower apparent sublimation rate of the 80 a/o Si - 20 a/o Ge alloy found in the second compatibility experiment is not obvious. It could be accounted for partly by the fact that the coupons underlying the present data did not consist of a form in which the silicon-germanium alloy test samples were completely surrounded by thermal insulation. If interaction with the thermal insulation enhances the sublimation rate of silicon-germanium, it is probable that the results of the present coupon test would yield a lower effective silicon-germanium sublimation rate than found previously. Another possible explanation for differences in the sublimation rates determined by the
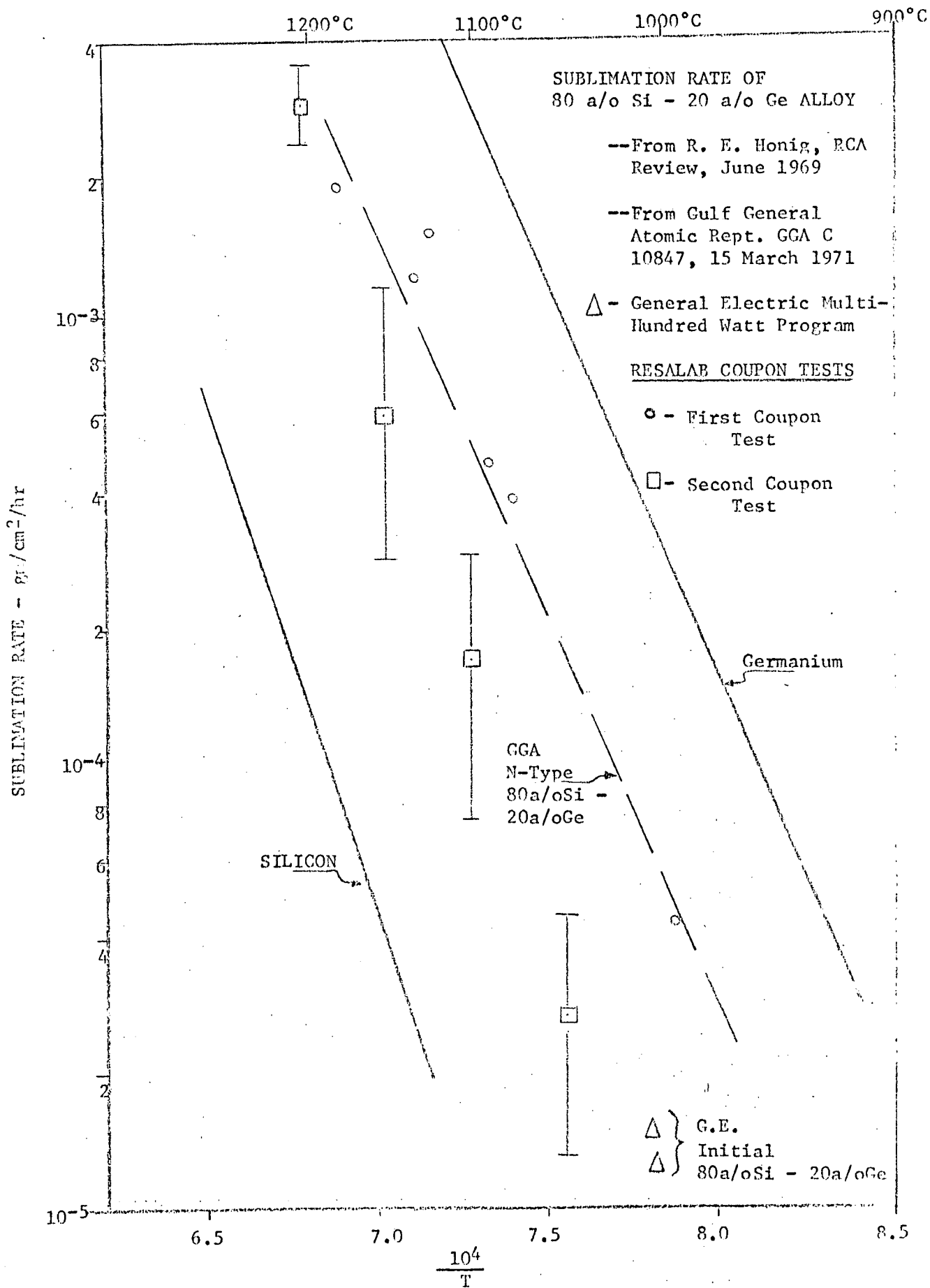
87.

Figure 29

88.

first and the second compatibility tests is that in each case some uncertainty exists in the surface area used to reduce raw weight loss data into a sublimation rate. The silicon-germanium alloy test samples were different in each case. In the former coupon test they were in the form of cubes that rested on insulation. Although the whole cube was completely surrounded by thermal insulation, effectively only 1/6 of the total surface area of the cube was in physical contact with the thermal insulation. The silicon-germanium alloy test samples of the second coupon experiment consisted of wafers that rested on thermal insulation. Nearly one half of the total surface area of each silicon-germanium test sample thus made contact to the thermal insulation. Percentage values of silicon-germanium surface area used to reduce the results of each coupon test thus very likely should be different. Because it is uncertain as to how the surface area should be treated or what value should be used, it has arbitrarily been decided to make use of the total surface area in the case of both coupon tests.

Data similar to those shown for the 80 a/o Si - 20 a/o Ge alloy in Figure 29 are shown for the silicon-molybdenum alloy in Figure 30. Figure 30 shows the sublimation rate as a function of inverse absolute temperature of the silicon-molybdenum test samples of the second compatibility experiment as squares. As before, the data represent the average values of all data at the different test temperatures. It is again noted that the present results yield a somewhat lower sublimation rate than that previously found. Whether this is real or due to the manner of data reduction is not certain and the discussion given on this in connection with Figure 29 also applies in the present instance. The overall conclusion to be drawn from Figures 29 and 30 is that the actual sublimation rate of both silicon-germanium as well as silicon-molybdenum alloys appears to be

SUBLIMATION RATE OF SILICON-
MOLYBDENUM ALLOY

—From R. E. Honig, RCA Review,
June 1969

RESALAB COUPON TESTS
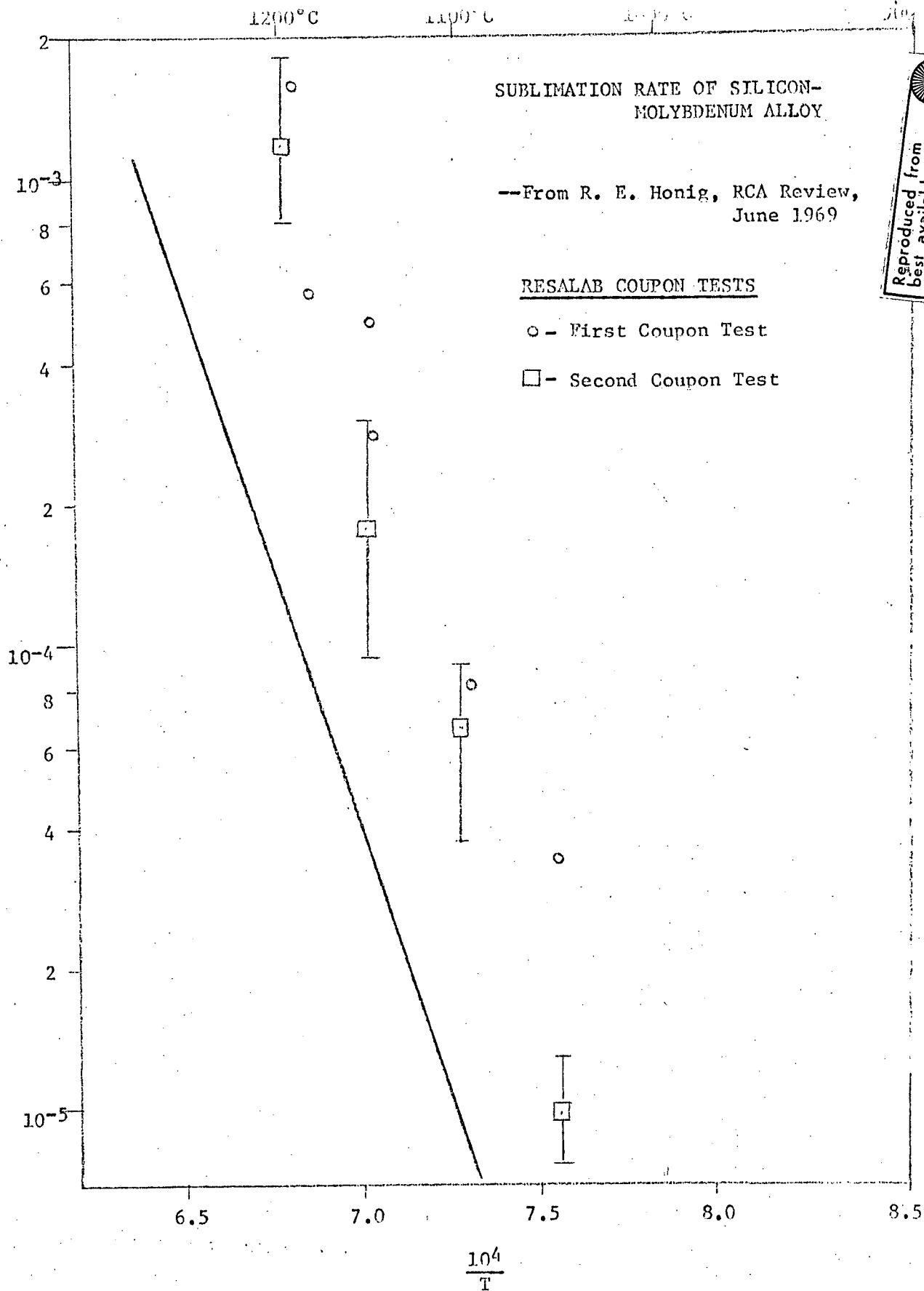
o – First Coupon Test

□ – Second Coupon Test

Figure 30

somewhat higher than would be predicted on the basis of the theory. Whether this is due to an actually higher sublimation rate or is due to interaction with thermal insulation or a result of the experimental technique is not known. It is hoped that additional tests will clarify this. In the meantime, the use of sublimation rate data approximately two to ten times higher than theoretical very likely yields realistic, and possibly worse case, estimates of the amount of sublimation to be expected from Air-Vac thermocouples.

The third compatibility test conducted on the present contract involved the determination of weight loss of silicon when in the proximity of silicon-dioxide thermal insulation without making physical contact with the insulation. The use of silicon rather than silicon-germanium and/or silicon-molybdenum alloys attempts to eliminate the confusion that sometimes results when interpreting the results of alloy sublimation. Moreover, it is felt that after an initial spurt of germanium, the bulk of sublimation that occurs from silicon-germanium alloys as a function of time is in the form of pure silicon because the activation energy of germanium diffusion is higher than is its heat of sublimation. The third compatibility test involved a sample of silicon inside an alumina crucible and supported by an alumina rod. One end of the crucible was open, but covered with three layers of finely woven Astroquartz cloth. The three layers of Astroquartz cloth assure that no direct line of sight path from the silicon sample was available to the outside of the crucible; any silicon emanating from the silicon sample could thus exit the crucible without contacting either the walls of the crucible or the Astroquartz cloth. Previously it had been seen that the reaction between alumina and silicon proceeds extremely slowly and therefore it was to be expected that the bulk of any reaction between silicon and its surroundings would occur between it and the Astroquartz

cloth which is primarily silicon-dioxide. Silicon-dioxide is known to react readily with silicon and/or germanium. The third coupon test was the first such test in which the silicon is not in physical contact with the thermal insulation; any interaction results from vapor transport and deposition. The test was conducted at a test sample temperature of 1100°C. Inasmuch as the alumina crucible was nearly isothermal, the Astroquartz cloth was at a temperature very close to 1100°C.

After six sets of data points it was decided to terminate the third compatibility test because of an observable weight change in the alumina crucible itself. Originally it had been thought, based on the results of an earlier coupon test, that very little interaction between silicon and alumina takes place up to 1200°C. Whereas the present results appear to belie that belief, it is to be concluded that the use of an alumina crucible is not proper when it is desired to study only the interaction of silicon and/or silicon-germanium alloys and silicon-dioxide. The results of the third compatibility test are given in Table VI in terms of the weight loss of the silicon sample, the Astroquartz cloth and the alumina crucible as a function of time. It should be noted that the lid of the alumina crucible, made also of alumina, did not exhibit any weight change during the test. This is explainable on the basis that the lid was completely shielded from the silicon sample by the Astroquartz cloth. Table IV also gives the calculated sublimation rate of silicon as a function of time. It is noted that the sublimation rate for later test times is reasonably close to the values calculable from Honig's vapor pressure data for silicon. The discrepancy at early test times quite likely is due to a systematic error in the weight measurements.

At the termination of the third compatibility test, a meeting was held with cognizant JPL project personnel and it was decided to discontinue the use

TABLE VI

Component	Initial Weight – gms	Initial Surface Area – cm^2	Weight Loss in mgms as a function of time in hours				
			24	88	127	168	207
Silicon	11.40	16.0	1.3	8.3	13.1	18.7	23.9
Astroquartz	0.8454	10.0	2.3	7.8	12.1	18.0	24.2
Al$_2$O$_3$ Crucible	92.9	138	1.5	10.2	14.8	31.8	26.0
Crucible Lid	12.4	21	0	0	0	0	0
Silicon sublimation rate – µg/cm^2/hr			3.4	6.8	7.7	8.5	8.3

93.

of the alumina crucible in this test series. A new test fixture was concieved
for the continuation of the tests. This fixture makes use of a molybdenum
holder that supports a silicon test sample and Astroquartz cloth such that the
two are in close proximity but not touching. In this fixture, the total area
of molybdenum visible to either the Astroquartz or the silicon is very small
compared to the total cross-sectional area of the two materials being tested.
In this way it is hoped to minimize the effect of molybdenum in the system.
Although it will not be possible to start the modified third compatibility test
during the present contract, work on the fabrication of the new test fixture
was started and it is expected to make use of it in subsequent follow-on efforts.
This is also true of the fourth test mentioned above, a test in which the weight
loss of bare samples of silicon-germanium and silicon-molybdenum alloys and
silicon are determined as a function of time and temperature. Although the
latter test was planned for completion on the present contract, the additional
effort incurred as a result of a number of test modifications did not make it
possible to do so.

D.   Compatibility Test Module

A compatibility test module containing four silicon-germanium Air-Vac
thermocouples was designed for use in evaluating the kinetics of sublimation/
interaction in representative RTG's of this type. The test module consists of
four major items: the outer case, the Air-Vac thermocouples, the electrical
heater and the thermal insulation. Details of each item are as follows:

1.   Outer Case

The outer case of the test module serves not only as a
container for all of the other components of the module but
also as the structural member for mounting the remainder of
the components. The outer surface of the outer case also

94.

serves as the radiator for heat rejection from the module.
All four sides and the top and the bottom plates of the
test module are machined from Type 304 stainless steel.
The exterior surfaces of the outer case are polished to
reduce the emissivity of the radiating surfaces. An Air-
Vac thermocouple is mounted on each of the four sides of
the outer case by a threaded fastener such that thermo-
couple electrical connectors are exposed at the outside
of the test module. The electrical connectors of each
thermocouple are inter-connected at the outside of the
test module. The electrical heater leads penetrate the
top plate of the test module and are insulated from it by
alumina sleeves. The ends of the heater leads are con-
nected to a power source by means of copper fasteners that
extend through a bracket on top of the test module.

The hot shoe temperature of each Air-Vac thermo-
couple is individually monitored by means of a tungsten/
niobium thermocouple inserted into a small hole in each
thermocouple hot shoe. The tungsten/niobium thermocouple
lead wires are routed through the thermal insulation of
the test module and out of the openings in the outer case
through which the Air-Vac thermocouple electrical connectors
exit. The tungsten/niobium thermocouple lead wires are in-
sulated by means of Refrasil tubing. Additional tungsten/
niobium thermocouples are installed between the Air-Vac
thermocouples and the inner surfaces of the outer case
for the purpose of monitoring Air-Vac thermocouple cold

junction temperatures. As with the hot junction thermocouples, the cold junction thermocouple lead wires exit through the Air-Vac thermocouple electrical connector penetrations in the outer case of the test module.

2.   Thermocouples

Four silicon-germanium Air-Vac thermocouples of the MHW-RTG type are used in each test module. The thermocouples have segmented legs of n-and p-type 80 a/o Si - 20 a/o Ge. The n-type thermoelements are doped with phosphorus and the p-type with boron. Thermocouple hot shoes are made of a silicon-molybdenum alloy; one half of the hot shoe is doped with phosphorus and the other half with boron. The hot shoe of the Air-Vac thermocouple serves as a receptor for the heat from the heat source and funnels the heat to the thermoelements. The hot shoe also serves as an electrical connector between the n-and p-type thermoelements at their hot sides. Electrical connectors are located at the cold sides of the Air-Vac thermocouples for their inter-connection. An electrical insulator isolates the electrical connectors and thermoelements from thermocouple support members. Thermocouple support members include a threaded fastener along with a mating nut. Various compensator disks provide thermal expansion matching between the low expansion thermoelements and the high expansion threaded fastener.

3.   Heater

The heater of the test module is a conventional tungsten filament cathode heater. The heater is enclosed

in a cylindrical molybdenum shell with a diameter and height of 0.75 inch. The heater filament leads are made of rhenium and are heliarc welded to the porous tungsten filament. The filament is a helical coil which has been machined from an isostatically pressed and sintered tungsten powder ingot. The heater filament is impregnated with an oxide composite and fired in a hydrogen atmosphere and is potted in the molybdenum outer shell of the heater. The heater is installed in the test module in the space between the hot shoes of the four Air-Vac thermocouples. The input leads to the heater are clamped in a copper connecting bracket and the heater is supported on its bottom side by three prongs that penetrate the thermal insulation on the bottom of the test module. After the fabrication and final assembly of the first two test modules with heaters as described above, it was decided to modify the heater design to better simulate the operating environment of the MHW-RTG. Consequently, the remaining test modules fabricated and assembled during the present contract contained heaters with hafnia coated Iridium sleeves.

4. Thermal Insulation

The first test module fabricated and assembled during the present contract was thermally insulated with dynaquartz fibrous insulation. Because considerable reaction occurred between the silicon-germanium Air-Vac thermocouples and the dynaquartz insulation during the

97.

test of the first test module, subsequent modules, with the exception of one which used Min K-2020, were assembled with Astroquartz/molybdenum foil thermal insulation. In the case of all test modules, Astroquartz yarn was wound around the thermoelements of each Air-Vac thermocouple, The use of the Astroquartz yarn and the Astroquartz/molybdenum foil thermal insulation simulates the internal environment of the MHW-RTG. The thermal insulation is installed in the test modules between the hot shoes of the Air-Vac thermo- couples and the inside wall of the outer case such that it completely fills the volume and minimizes extraneous heat losses.
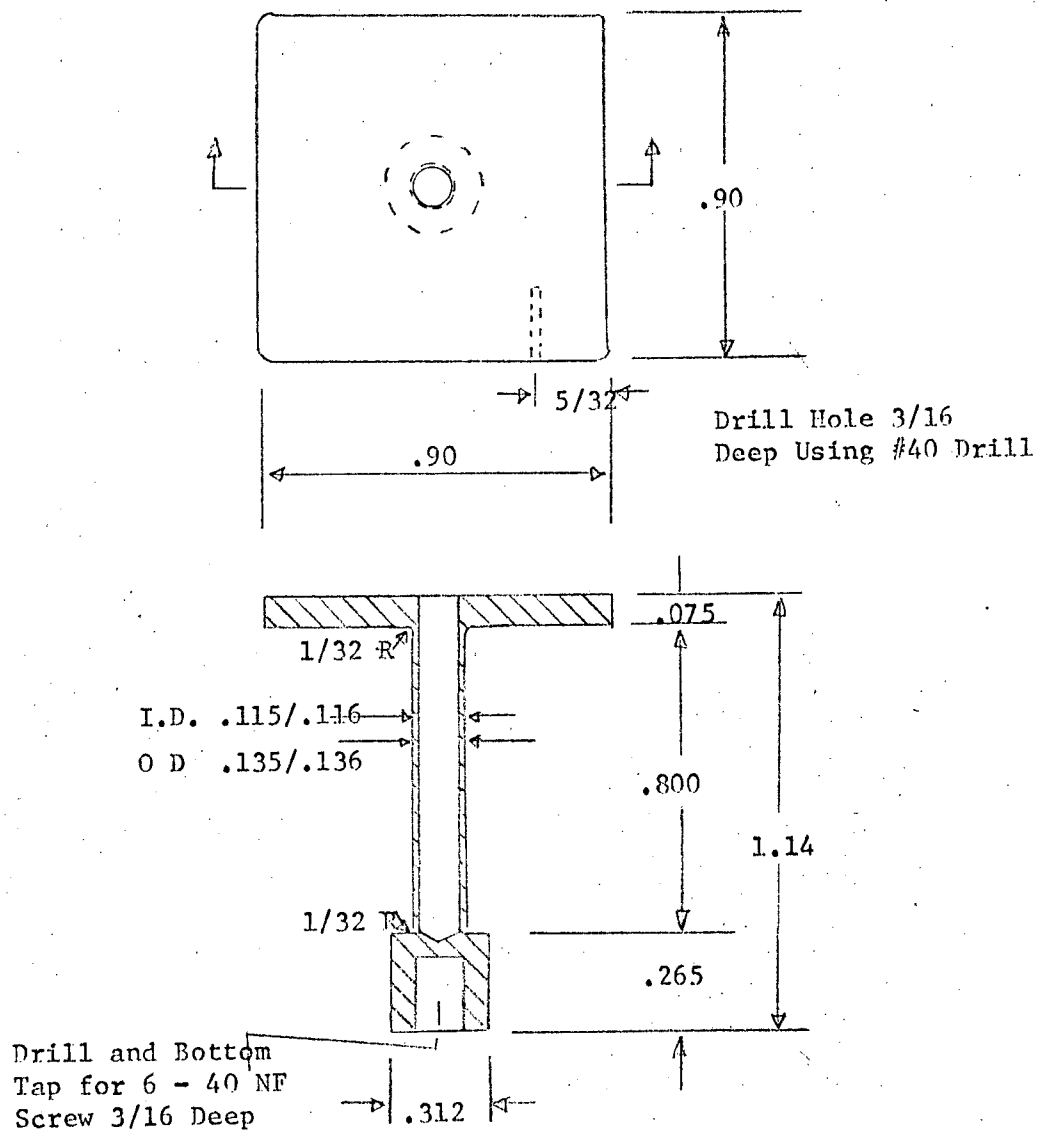
Seven test modules were fabricated and final assembled during the present contract. All modules were delivered to JPL for test purposes. Of the seven test modules, one was insulated with dynaquartz thermal insulation, five were insulated with Astroquartz/molybdenum foil thermal insulation and one with Min K-2020. The dynaquartz insulated test module was tested at an average hot shoe temperature of 1200°C at JPL. The five Astroquartz/molybdenum foil insulated test modules were tested at average thermocouple hot shoe temperatures of 1000, 1050, 1100, 1150 and 1200°C. The test module insulated with Min K-2020 thermal insulation was tested at an average thermocouple hot shoe temperature of 1000°C.

An additional test module that uses dummy thermocouples was designed and fabricated for test at JPL. The module was delivered to JPL towards the end of the present contract. The intent of the dummy module is to thermally mock-up an actual four-couple test module but to eliminate any and all effects due to silicon-germanium and silicon-molybdenum alloy sublimation/interaction with the thermal insulation. To this end, a thermocouple design was formulated with

98.

molybdenum hot shoes and a thermoelement consisting of silica insulation completely enclosed by a 0.003 inch thick molybdenum foil. A mocked-up thermoelement of this type results in a structure with a thermal conductance exactly the same as that of a MHW-RTG type silicon-germanium Air-Vac thermocouple operating between hot and cold side temperatures of 1000 and 300°C.

An investigation of the fabricability of a thermocouple of the given description indicated that such a structure is not especially practicable, even though it does dimensionally and thermally simulate an actual Air-Vac thermocouple. A new thermocouple design was formulated for the dummy thermocouples. This design still makes use of a molybdenum hot shoe but replaces the parallelepipedal molybdenum encased silica thermoelement with a hollow molybdenum configuration, except for the hot shoe, does not mock-up a MHW-RTG type Air-Vac thermocouple; the thermal conductance of this structure, however, is the same as that of an Air-Vac thermocouple.

Figure 31 shows a schematic diagram of the dummy thermocouple used in the mocked-up four-couple test module. It is noted that the simulated thermocouple has a nominal wall thickness of 0.020 inch and an equivalent height of 0.800 inch, the same as the height of the thermoelements in a MHW-RTG type Air-Vac thermocouple. The whole dummy thermocouple is machined from one piece of molybdenum. Its bottom has a threaded receptacle 3/16 inch deep and the cavity inside the simulated thermoelement has an opening at the top of the hot shoe. The silica fluff is stuffed into the cavity to eliminate direct radiation heat transfer from the test module heater to the cold side of the module. The hot shoe has a thickness of 0.075 inch and because molybdenum possesses a thermal conductivity significantly higher than that of the silicon-molybdenum alloy, the temperature drop across the simulated hot shoe is substantially smaller than across an actual hot shoe. Because this drop in an actual hot shoe is only of the order

.90

.90

→| 5/32 |←

Drill Hole 3/16
Deep Using #40 Drill

.075

1/32 R

I.D. .115/.116

O D .135/.136

.800

1.14

1/32 R

.265

Drill and Bottom
Tap for 6 - 40 NF
Screw 3/16 Deep

→| .312 |←

SIMULATED MHW RTG THERMOCOUPLE MADE OF MOLYBDENUM

Figure 31

of 30 to 40°C and because the temperature differential across the thermocouple
is some 700°C, it is believed that the difference in the hot shoe temperature
drop is not especially important. The dummy thermocouples are attached to the
insides of the test module outer case by means of a screw attachment that makes
use of the threaded receptacle at the thermocouple cold sides. A hole is
drilled 3/16 inch into the edge of the hot shoe for the placement of an instru-
mentation thermocouple. The hole corresponds to one obtained by using a #40
drill.

Four dummy thermocouples of the configuration and dimensions of that
shown in Figure 31 were fabricated. The components of a standard test module,
including the molybdenum-foil/Astroquartz insulation, the heater and the outer
case were also fabricated and a test module using these parts was assembled.
The module was delivered to JPL.

V. SPECIAL STUDIES

A. Introduction

The work under the Special Studies task of this contract has included a number of topics related to thermoelectric power conversion that Resalab has conducted at JPL's request. Each special study has been an entity onto itself and has been summarized by the issuance of a report or memorandum. All memoranda that Resalab has prepared for JPL are numbered sequentially, even those that were issued prior to the start of the present contract. The memoranda issued under the present contract can be listed as follows:

Memorandum #6 - Thermoelectric Properties of 80 a/o Si - 20 a/o Ge Alloy as a Function of Time and Temperature.

Memorandum #7 - Characterization of RTG Performance in Both Air and Vacuum.

Memorandum #8 - Thermoelectric Properties of Silicon-Germanium Alloys as a Function of Time and Temperature.

Memorandum #9 - Effects of Sublimation on Silicon-Germanium RTG Performance.

Memorandum #10 - Performance of MHW-RTG in the Martian Environment.

Memorandum #11 - Thermophysical Properties of RTG Insulation Components.

Memorandum #12 - Performance of the MHW-RTG in the Temperature Range 900 to 1000°C and Lower Bounds on Gains Obtainable From the Use of Radiation Fins.

Memorandum #13 - Performance of a Cascaded Thermoelectric Generator.

Memorandum #14 - Mathematical Model and Computer Program for the Design and Analysis of Silicon-Germanium Air-Vac RTG's.

A brief summary of each documented special study listed is given below.

B.   Memorandum #6

This special study, titled Thermoelectric Properties of 80 a/o Si –
20 a/o Ge Alloy as a Function of Time and Temperature, concerned itself with the
projection of the thermoelectric properties of n–and p–type 80 a/o Si – 20 a/o
Ge alloy to operating times of 12 years. Available information on the short
term behavior of the thermoelectric properties of this alloy were used to calcu-
late the unknown temperature dependent constants in the equation, due to Lifshitz
and Slyozov, this describes dopant precipitation from solid solutions. The use
of these constants in the equation enabled the projection of the electrical re-
sistivity of the n–type alloy to any desired operating time. The corresponding
Seebeck coefficient values were derived from a known relationship between elec-
trical resistivity and Seebeck coefficient for n–type silicon–germanium alloys
in the range of alloy compositions of 60 a/o Si – 40 a/o Ge to 80 a/o Si – 20
a/o Ge. The thermal conductivity of the n–type alloy was assumed to be that
determined for zone levelled specimens on a previous study conducted for NASA[8].

The properties of the p–type 80 a/o Si – 20 a/o Ge alloy were assumed
to stay constant with time and were assumed to be the same as those given in
the just referenced report[8]. Even though, at the writing of Memorandum #6, it
was known that p–type silicon–germanium alloys do exhibit dopant precipitation
much as the n–type alloy, not sufficient information was available at that time
to make long-term property projections for the material. In fact, the property
projections of the n–type alloy very likely have limited accuracy because the
experimental basis used to calculate the constants in the Lifshitz and Slyozov
relationship were of limited extent, covering a relatively short time period of
the order of 1000 to 1500 hours. In issuing Memorandum #6 it was therefore
realized by Resalab that the memorandum would very likely have to be updated
upon the availability of more extensive experimental data in the future. In

the meantime, the property data presented in this memorandum served a useful

purpose in enabling the calculation of the approximate expected performance of

silicon-germanium RTG's in long-term operation.

No detailed data contained in Memorandum #6 will be given here because

some six months after its issuance Memorandum #6 was superseded by Memorandum

#8. The latter memorandum contained more detailed and extensive information on

the long-term properties of n-and p-type 63 a/o Si - 37 a/o Ge and 80 a/o Si -

20 a/o Ge alloys. The results presented in Memorandum #8 will be given in Part

D of this section.

C.   Memorandum #7

This special study summarized in Memorandum #7, titled <u>Characterization</u>

<u>of RTG Performance in Both Air and Vacuum</u>, concerned itself with the analytical

prediction of the performance of unsealed silicon-germanium RTG's, such as the

MHW-RTG, in various ambient environments. The specific intent of Memorandum #7

was to determine the performance of the MHW-RTG analytically in both air and

vacuum. In order to determine RTG performance in various ambient environments

a calculational model was developed and data therefrom applied to existing gen-

erators whose performance had already been established in the laboratory. After

demonstrating the capability of the model to calculate generator performance in

both air (nitrogen) and vacuum, the calculations were extended to include the

MHW-RTG operating in different inert gases, air and vacuum. A brief summary of

the calculational model as well as some of the more important results obtained

in this study are presented below.

Of prime importance in the development of the calculational model was

the heat transfer process which occurs at the heat rejection surface (radiator)

and within the RTG. In air operation, the radiator surface temperature may be

expected to decrease due to the addition of convective cooling; whereas heat

transfer within the generator could be modified according to the particular geometry selected. Both an "open" and "enclosed" configuration were considered. The possibility of including inert gases in the enclosed system was an added consideration. For both thermoelement lengths the effects of the gas were balanced by an appropriate adjustment of the insulation thermal conductivity.

The heat rejected from the radiator must be equal to the total heat input less that converted to electrical energy and mounting support losses. Assuming the rejection process is a combination of radiative as well as convective heat transfer, rejection can be expressed with the following equation:

$$Q_{Rej} = Q_{in} (1-\eta-\alpha) = A_R \sigma \epsilon_r \eta_f F \left(T_R^4 - T_{amb}^4 \right) + K A_C \left(T_R - T_{amb} \right)^\beta \quad , \quad (14)$$

where η is the conversion efficiency, α is the fraction of conductive heat loss, A_R is the radiative area, σ is the Stefan-Boltzman constant, ϵ_r is radiator emissivity, η_f is radiator fin efficiency, F is radiator view factor, T_R is radiator temperature, T_{amb} is ambient temperature, K is the convective heat transfer coefficient, A_C is convective area, and β is an exponent. The convective heat transfer coefficient, K and the exponent, β, depend upon the particular mode of convective heat transfer applicable to a given situation. In the case of natural convection, the numerical values of K and β depend upon whether turbulent or laminar heat flow exist in the boundary layer between the radiator surface and the adjacent environment. In all the cases studied, both K and β were determined prior to using the equation in the calculational model. As it stands, the above equation contains two unknowns. First, the radiator temperature, T_R, and secondly the generator efficiency, η. Additional equations required to affect a solution on the pertinent RTG temperatures are provided by the heat balance at the hot junction of the thermocouple:

$$\lambda Q_{in} = K_T \Delta T + \frac{\Gamma \Delta T}{(1+m)^2} \left[T_H (1+2m) + T_C \right] \tag{15}$$

and by the simple conductive identity:

$$T_C = T_R + \Delta T_C \tag{16}$$

λ is fraction of total heat input that traverses the generator in the radial direction, K_T is the total radial thermal conductance, Γ is a numerical quantity which depends upon the number and thermophysical properties of the individual thermocouples, T_H and T_C define the hot and cold junction temperatures respectively, ΔT_C is the conductive temperature drop across the cold stack, m is the load factor, and $\Delta T = T_H - T_C$.

An iterative solution of the above equations is obtained by employing the Newton-Raphson technique in combination with the RTG performance equations. Thus, with load voltage, power output, and load current additionally given, the performance characteristics of the generator are completely defined.

In order to test the validity of the mathematical model discussed above and in order to calculate the thermal conductivities of selected thermal insulations, the performance of several thermoelectric converters tested by RCA were calculated. These thermoelectric converters are designated C-2, C-3 and C-3Z[9,10]. The thermoelectric material used by all of these converters is a silicon-germanium alloy of composition 63 a/o Si - 37 a/o Ge in the conventional "Air-Vac" configuration with silicon-molybdenum alloy hot shoes. Both the n-and p-type thermoelements have a 0.0889 cm^2 cross-sectional area with an active length of 2.155 cm in all three converters. All converters employ eighteen thermocouples arranged electrically in series and have a hexagonal overall geometry. The thermal insulation in each converter has an effective area of 171 cm^2.

The effective thermal conductivity values calculated for multi-foil, Min K and Zircar thermal insulations are shown in Figure 32. The thermal insulation conductivity values were obtained by adapting the above calculational model to measured generator performance data. The insulation thermal conductivity was adjusted until calculated performance agreed with the experimental values. The thermal conductivity data shown in Figure 32 therefore represent the effective thermal conductivities of the given insulations in an actual thermoelectric generator structure.

In evaluating the performance of the MHW-RTG several distinct cases were considered. The calculations included performance evaluation of an RTG employing a multi-foil, Zircar and Min-K 2020 thermal insulation. The first case (Case I) utilized generator geometry designed to optimize a RTG employing foil insulation which required a thermoelement length of 0.8 inch. The generator was initially considered "open", thus allowing direct exposure of the internal components when operated in air. In the second case (Case II), the generator had an approximate 18 percent increase in the thermoelement ℓ/A ratio to permit RTG performance optimization with fibrous insulation. Again the generator was initially considered "open". The calculated performance was then established for both air and vacuum conditions.

For each of the above thermoelement lengths, the MHW-RTG was then considered hermetically sealed such that an inert gas could be contained within the generator during the air-operation phase. This was noted to eliminate many of the problems associated with generator operation in air. Although the generator exterior operated in air, the temperatures were found low enough to avoid most problems associated with chemical reaction, etc. By selecting a low thermal conductivity gas, such as Xenon, the generator could deliver a significant amount
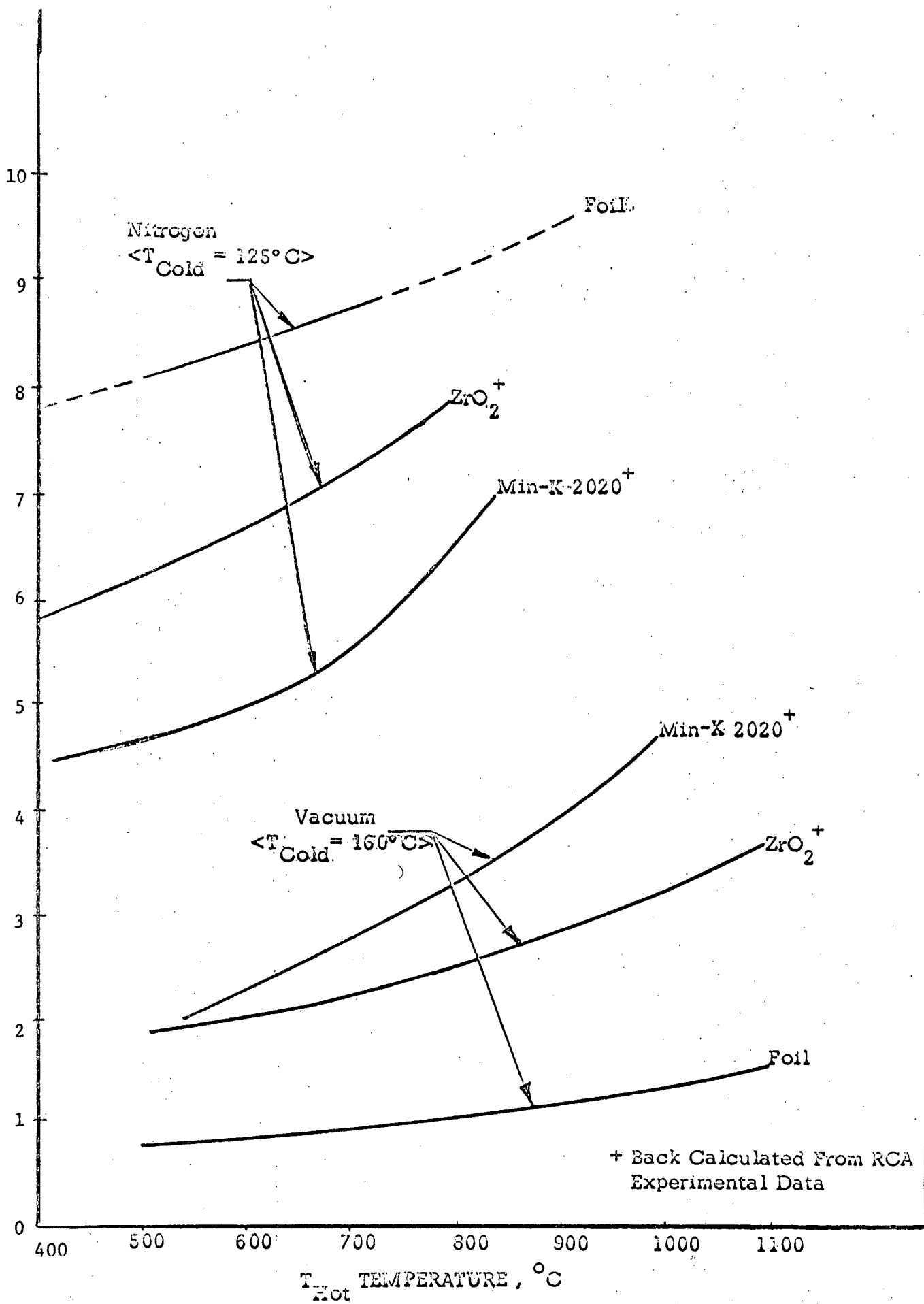
Effective Thermal Conductivity in Vacuum and Nitrogen – Figure 32

108.

of power in the "pre-launch" condition. After reaching the eventual vacuum en-

vironment of space, the generator could be vented to allow its performance

level to be re-established to that corresponding with vacuum operation.

The inert gases that were tested included argon, helium, krypton and

xenon. The effects of these gases on the thermal conductivity of the insula-

tion were established and the MHW-RTG performance was re-examined. To include

gas conductance effects, the insulation thermal conductivity was described by:

$$K = k_v + Ak_g \quad , \tag{17}$$

where k_v was the effective vacuum conductivity, A an empirical constant and k_g

the conductivity of the particular gas being analyzed. The empirical constant,

A, as well as k_v, were determined from Figure 32 and the gas conductivity calcu-

lated from the Sutherland formula using the relationship $k/(\mu C)$ = Constant.

Where k is the conductivity, C is the specific heat and μ is the viscosity of

the gas.

The final results of the calculation of MHW-RTG performance in both of

the gases mentioned are presented in Tables VII and VIII. In these tables, the

maximum power output and the power output at 30 volts are shown for three dif-

ferent thermal insulations, foil, Zircar and Min-K. The hot and cold junction

temperatures are also given at the maximum power output point.

In short, the object of the study was the development of a model to de-

termine gas and vacuum performance of thermoelectric generators. The validity

of the model was verified by its applications to several existing generators that

have been tested in both vacuum and air (actually nitrogen) environments. The

model was also used to back-calculate the thermal conductivities of selected

thermal insulations that are being considered for use in high temperature

TABLE VII

MHW-RTG Performance in Vacuum and Gas Environments
for Thermoelement Length of 0.8 in.

FOIL INSULATION						
GAS	VAC	HELIUM	AIR	ARGON	KRYPTON	XENON
$P_{Max,}$ Watt	138	17	69	84	106	118
$P_{30V,}$ Watt	137	-	56	80	105	117
$T_{H,}$ °C *	1065	543	810	872	939	972
$T_{C,}$ °C *	321	282	279	278	276	275
ZIRCAR INSULATION						
$P_{Max,}$ Watt	124	24	73	88	103	111
$P_{30V,}$ Watt	123	-	61	85	101	109
$T_{H,}$ °C *	1012	591	844	885	929	950
$T_{C,}$ °C *	323	282	279	278	277	276
MIN-K 2020 INSULATION						
$P_{Max,}$ Watt	116	35	84	94	103	108
$P_{30V,}$ Watt	115	-	77	91	101	106
$T_{H,}$ °C *	986	652	860	903	929	941
$T_{C,}$ °C *	323	281	279	278	277	277

* Temperatures are for maximum power points

TABLE VIII

MHW-RTG Performance in Vacuum and Gas Environments for Thermoelement Length of 1.2 in.

GAS	VAC	HELIUM	AIR	ARGON	KRYPTON	XENON
FOIL INSULATION						
$P_{Max,}$ Watt	161	28	92	114	135	145
$P_{30V,}$ Watt	155	-	91	114	132	140
$T_{H,}$ °C *	1195	641	934	1016	1070	1100
$T_{C,}$ °C *	320	282	277	276	274	273
ZIRCAR INSULATION						
$P_{Max,}$ Watt	135	37	101	110	123	130
$P_{30V,}$ Watt	134	8	101	110	122	128
$T_{H,}$ °C *	1125	700	970	1002	1039	1057
$T_{C,}$ °C *	321	281	277	276	275	275
MIN-K 2020 INSULATION						
$P_{Max,}$ Watt	123	51	110	105	112	115
$P_{30V,}$ Watt	122	32	110	105	112	114
$T_{H,}$ °C *	1102	774	1004	987	1006	1015
$T_{C,}$ °C *	322	280	276	276	276	276

* Temperatures are for maximum power points

111.

silicon-germanium RTG's. Finally the model was applied to the MHW-RTG generator, with two different thermoelement lengths, to determine its performance under various environmental conditions. The initial characterization was performed in vacuum and then the effects of various inert gases upon the insulation conductivity were included, the results of which established generator operability for air/vacuum pre-launch periods.

D.   Memorandum #8

The special study summarized in Memorandum #8, titled Thermoelectric Properties of Silicon-Germanium Alloys as a Function of Time and Temperature, concerned itself with the development of long-term thermoelectric property data for the two silicon-germanium alloys most commonly used in power generation applications: the 63 a/o Si - 37 a/o Ge and the 80 a/o Si - 20 a/o Ge alloys. Most of the effort pertained to the generation of property data for alloys having an n-type polarity. Because of a lack of sufficient experimental data, the properties of the p-type alloys were not projected. The p-type alloy properties given in Memorandum #8 were as earlier presented in an above referenced report[8]. The projected thermoelectric properties of the n-type alloys given in Memorandum #8 are based on short term experimental data, of the order of 1000 to 1500 hours obtained on past programs. As such, these data cannot be considered final and will have to be periodically updated. Nevertheless, they do fill a gap in the interim as regards silicon-germanium alloy properties for generator design and performance analyses.

The rate and extent to which the thermoelectric properties of n-type silicon-germanium alloys change with time is obviously temperature dependent. At the temperatures of maximum solid solubility of phosphorus, the material is in equilibrium and thus little change takes place. At temperatures exceeding

112.

those of maximum dopant solid solubility, the precipitation process goes to completion extremely fast because of the high temperatures in question. It is at temperatures below those of maximum dopant solid solubility that observable long-term changes in the electrical properties of n-type silicon-germanium alloys occur. Because the solid solubility of phosphorus decreases with temperature at temperatures below the solid solubility maximum, the "driving force" for precipitation increases with decreasing temperatures. The diffusion rate of phosphorus in the silicon-germanium matrix, diffusion preceding precipitation at a nucleation site, however decreases with decreasing temperatures. The net result of the opposing temperature dependences of these two mechanisms is that it is at intermediate temperatures in the range of 300 to 700°C that the biggest changes occur in the electrical properties of n-type silicon-germanium alloys as a result of dopant precipitation. At very low temperatures, such as room temperature, precipitation proceeds so slowly as to be practically unobservable.

Although no all-encompassing model exists for quantitatively describing the precipitation of phosphorus in silicon-germanium alloys for all times, Ekstrom and Dismukes[4] have suggested that a model due to Lifshitz and Slyozov[11] reasonably accounts for at least a part of the process. In this model the precipitate phase consists of particles of nearly continuously varying radii. The surface energy of the particle-solution interface determines this critical radius. Particles having radii smaller than the critical value tend to redissolve in the matrix whereas particles with radii exceeding the critical radius tend to grow as the precipitation proceeds. The two competing processes initially decrease the precipitation rate to values less than expected from a diffusion limited precipitation process by itself. At long times, after complete dissolution of the small particles, the precipitation rate in silicon

germanium alloys approaches that solely due to a diffusion limited precipitation process. The initial distribution of precipitated particles with nearly continuously varying radii is introduced into the alloys during crystal growth and related high temperature treatments. It should be noted that in materials that exhibit a retrograde dopant solid solubility, nearly invariably there coexist a precipitate phase and a solute phase, even when the overall doping level is purposely kept below the maximum dopant solid solubility level.

According to the model of Lifshitz and Slyozov[11], a diffusion limited precipitation process which accounts for the resolution of small precipitate particles due to surface energy may be represented by

$$\left[\frac{C_i - C_e}{C_t - C_e}\right]^3 = \left[\frac{4}{9}\left(\frac{C_e}{C_p}\right)\left(\frac{C_i - C_e}{C_e}\right)^3 \frac{D}{\beta^2}\right]t + B, \qquad (18)$$

where B is a constant and β is defined as

$$\beta = \frac{2M\sigma}{\delta RT} \cdot \qquad (19)$$

In the above equations, C_i is the initial solute concentration, C_t is the solute concentration at time t, C_p is the concentration of solute in the precipitate phase and C_e is the equilibrium dopant solid solubility, D is the dopant diffusion coefficient at temperature T, M is the mean atomic weight of the matrix, σ is the interphase surface energy, δ is the density of the matrix, and R is the gas constant. It may appear that the constant B should assume the value of unity. Ekstrom and Dismukes[4], however, point out that B=1 is not physically meaningful if the characteristic precipitate particle size distribution is not present at the start of the precipitation process. The model represented by the preceding equation reasonably accounts for the precipitation of phosphorus in silicon-germanium alloys after the first few hours of the precipitation process. The

processes extant during the first few hours appear to be closely related to the previous thermal history of the alloys; it is not uncommon for the carrier concentration to remain constant or even increase initially. Although Ekstrom and Dismukes[4] obtained good agreement between theory and experiment for precipitation times exceeding a few hours, most of their work involved only the first 1000 hours of the precipitation process. It is therefore not precisely known how good the agreement between theory and experiment is at much longer precipitation times.

Although most of the work on phosphorus precipitation in silicon-germanium alloys reported by Ekstrom and Dismukes[4] pertains to alloys with a silicon content of 70 a/o, they did extend it in a preliminary manner also to alloys with silicon contents of 80 a/o and 85 a/o. Most of this latter work, however, remains unreported. It has been necessary, therefore, to reapply the theory to the 80 a/o Si - 20 a/o Ge and 63 a/o Si - 37 a/o Ge phosphorus doped alloys in an effort to determine the long-term behavior of their thermoelectric properties.

Underlying the application of the precipitation model in Memorandum #8 are experimental data on the time dependence of the electrical resistivity of phosphorus doped silicon-germanium alloys in the temperature range 400 to 800°C for operating times up to 1500 hours. Some of these experimental data have been reported earlier. The application of the model to the experimental data has enabled the evaluation of constants in the equation. Maintaining the constants at fixed values, it was possible to calculate the time dependence of the carrier concentration in the phosphorus doped silicon-germanium alloys. The carrier concentration values thus derived were converted to electrical resistivity through the inclusion of electronic charge and carrier mobility, the dependence of the latter on carrier concentration being taken into account. Known relationships

between electrical resistivity and Seebeck coefficient for n-type silicon-germanium alloys were used to determine the time dependence of the Seebeck coefficient from the electrical resistivity data. The thermal conductivities of the alloys were assumed to remain constant with time; experimental findings give validity to this assumption for carrier concentration changes of several tens of percent. The effect of much greater changes in carrier concentration may, however, be observable and must be experimentally determined.

The thermoelectric property data for the phosphorus doped 80 a/o Si - 20 a/o Ge alloy are shown as a function of time and temperature in Figures 33 to 36. Figure 33 shows the electrical resistivity as a function of temperature for operating times in the range of zero hours to 12 years. Figure 34 shows plots of the Seebeck coefficient of the phosphorus doped 80 a/o Si - 20 a/o Ge alloy as a function of time and temperature. The thermal conductivity of the alloy is shown in Figure 35. Only one set of data is given for the thermal conductivity. The figure-of-merit is shown in Figure 36.

The thermal conductivity data of the n-type 80 a/o Si - 20 a/o Ge alloy in Figure 35 are average data based on a fairly large number of samples independently measured at several laboratories. These data, although derived from thermal diffusivity measurements, at least approximately account for uncertainties in calculated specific heat values and thus should be fairly accurate. It should be noted that the thermoelectric property data given here for the n-type 80 a/o Si - 20 a/o Ge alloy are data mutually agreed upon by a number of groups interested in this alloy[*] and will be used by these groups until additional information warrants the updating of the data. The data given in Memorandum #8 for the long-term thermoelectric properties of the n-type 80 a/o Si - 20 a/o Ge alloy are similar, but not identical, to those earlier

---

[*] Meeting between representatives of JPL, Resalab, AEC, Sandia, GE and RCA, Harrison, New Jersey on August 19, 1970.
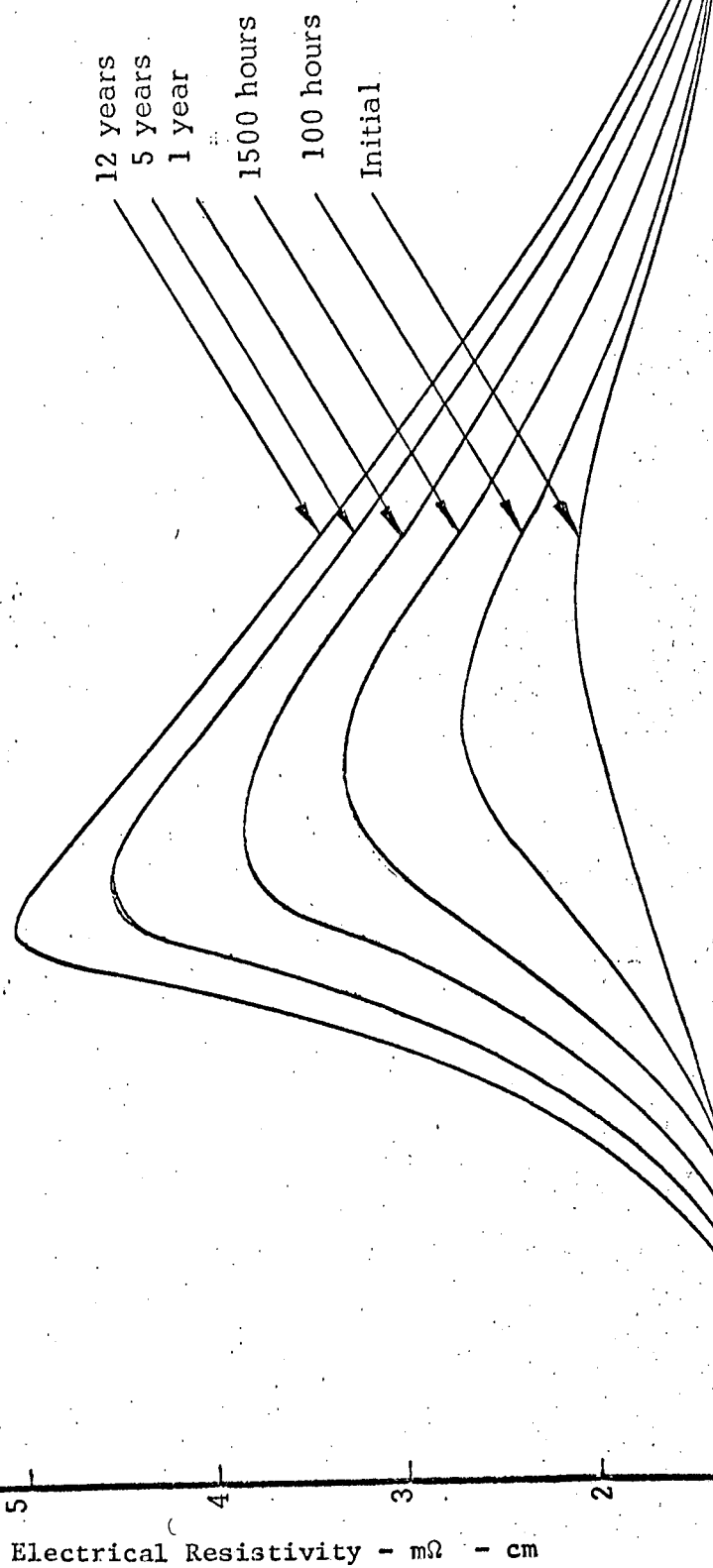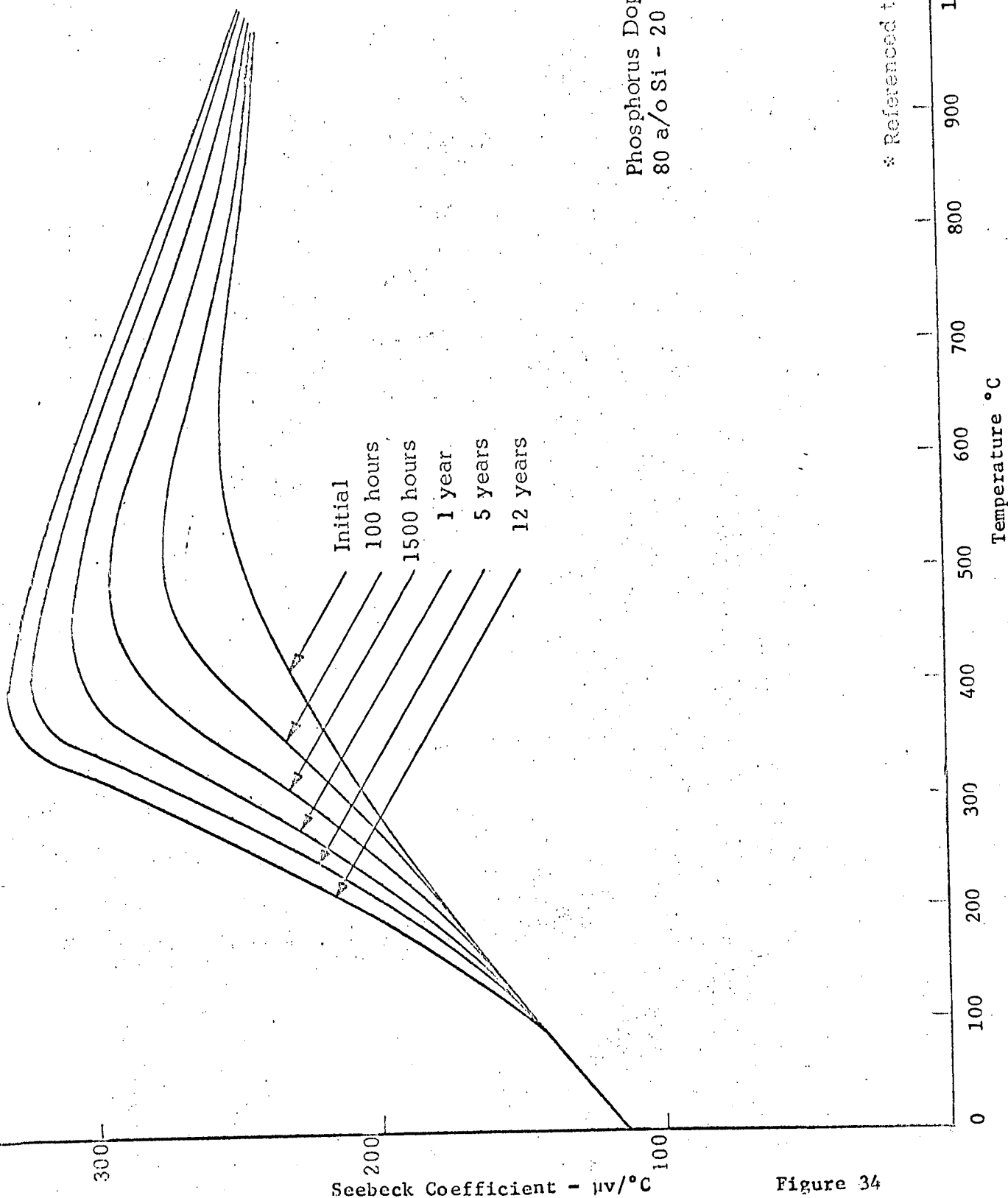
Phosphorus Doped
80 a/o Si - 20 a/o Ge

12 years
5 years
1 year
1500 hours
100 hours
Initial

Electrical Resistivity - mΩ - cm

Temperature - °C

Figure 33

117.

Initial
100 hours
1500 hours
1 year
5 years
12 years

Phosphorus Doped
80 a/o Si - 20 a/o Ge

* Referenced to absolute

Temperature °C

Seebeck Coefficient - μv/°C

300
200
100

0   100   200   300   400   500   600   700   800   900   1000   1100   1200

Figure 34

118.

PHOSPHORUS DOPED
80 a/o Si – 20 a/o Ge

TEMPERATURE – °C

Thermal Conductivity – Watt/°C – cm

119.

Figure 35

PHOSPHORUS DOPED
80 a/o Si – 20 a/o Ge

Initial
100 Hours
1500 Hours
1 Year
5 Years
12 Years

TEMPERATURE – °C

Figure-of-Merit x 10^3 – /°C

120.
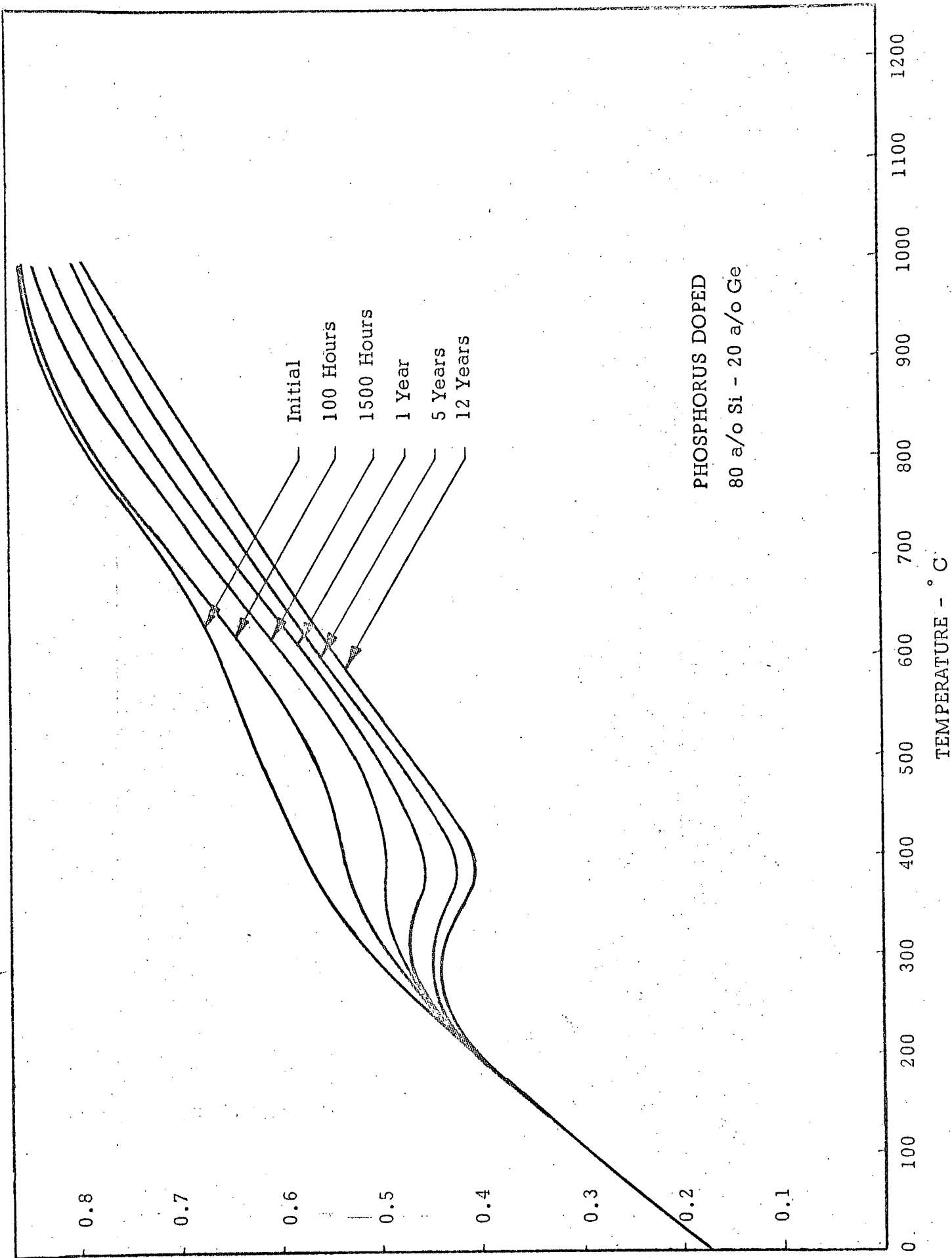
Figure 36

reported in Memorandum #6. As mentioned above, the thermal conductivity data presented in Memorandum #6 were those obtained in an earlier study[8]; the thermal conductivity data given in Memorandum #8 are average data based on a large number of independent measurements.

E. Memorandum #9

The special study summarized in Memorandum #9, titled <u>Effects of Sublimation on Silicon-Germanium RTG Performance</u>, concerned itself with the investigation of the effects of Air-Vac thermocouple sublimation on the performance of the MHW-RTG. A general result of sublimation is an overall reduction in effective thermoelement cross-sectional areas and a consequent increase in thermocouple hot junction temperature – an often disastrous combination that can exist in well insulated generators without any special effort at baffling.

The sublimation study focused on the MHW-RTG with its beginning-of-life thermocouple hot junction temperature of 1100°C and the required operating life of 12 years. The use of an effective thermoelement operating temperature enabled the calculation of the net sublimation rate from each thermoelement at the beginning-of-life operating temperatures. This effective thermoelement operating temperature is given by

$$
T_{eff} = \frac{\int_{T_C}^{T_H} T f(T) \, dT}{\int_{T_C}^{T_H} f(T) \, dT} \quad , \tag{20}
$$

where T is absolute temperature, T_H and T_C are the thermoelement hot and cold junction temperatures respectively and T_{eff} is the effective sublimation temperature of each thermoelement. The distribution function $f(T)$ is the sublimation rate of the

thermoelement material and for the 80 a/o Si - 20 a/o Ge alloy has been determined by interpolation from Figure 37 to be given by

$$f(T) = 5 \times 10^{11} e^{-\frac{51,000}{T}} . \tag{21}$$

It should be noted that because of the exponential character of the distribution function $f(T)$, the effective sublimation temperature T_{eff} depends heavily on thermocouple hot junction temperature, T_H, and only very little on the cold junction temperature, T_C. In the present study the effective sublimation temperature, T_{eff}, was calculated to be only some 20°C below thermocouple hot junction temperature, T_H, at any given time.

Using the calculational model just discussed, the effects of sublimation on the performance of the MHW-RTG generator were assessed. Figure 38 shows how the hot junction temperature of the generator varies with time and sublimation rate. The temperatures shown account for both the effects of silicon-germanium sublimation and isotope fuel decay with time. It should be noted that at the beginning-of-life MHW-RTG design operating temperature of 1100°C the hot junction temperature increases extremely rapidly and in a short time will lead to catastrophic generator failure. Although it takes longer for this to happen at beginning-of-life operating temperatures of 1050 and 1000°C, it nevertheless happens in times relatively short compared to the required 12 year RTG operating time.

The results shown in Figure 38 presuppose free sublimation of the silicon-germanium thermoelements. In an actual generator structure, however, the thermoelements are usually enclosed in insulation and the sublimed species in all liklihood is not removed as fast as it is formed. The effect of the resultant baffling is to reduce the sublimation rate of the material. Inasmuch
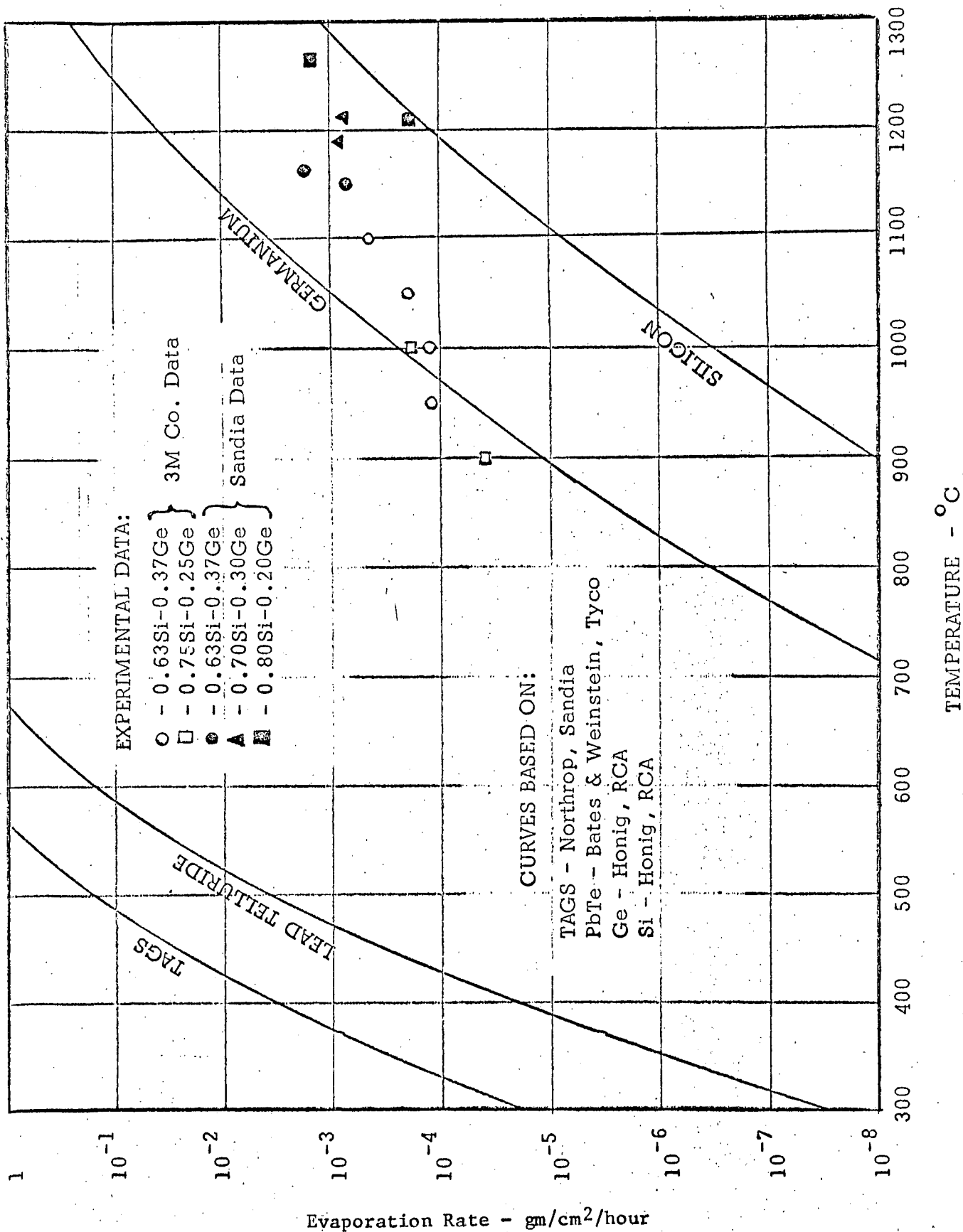
Evaporation Rate – gm/cm²/hour

Figure 37

123.

Multi-Hundred Watt RTG
Hot Junction Temperature
as a Function of Time
R = Sublimation Rate
R_o = Free Sublimation Rate
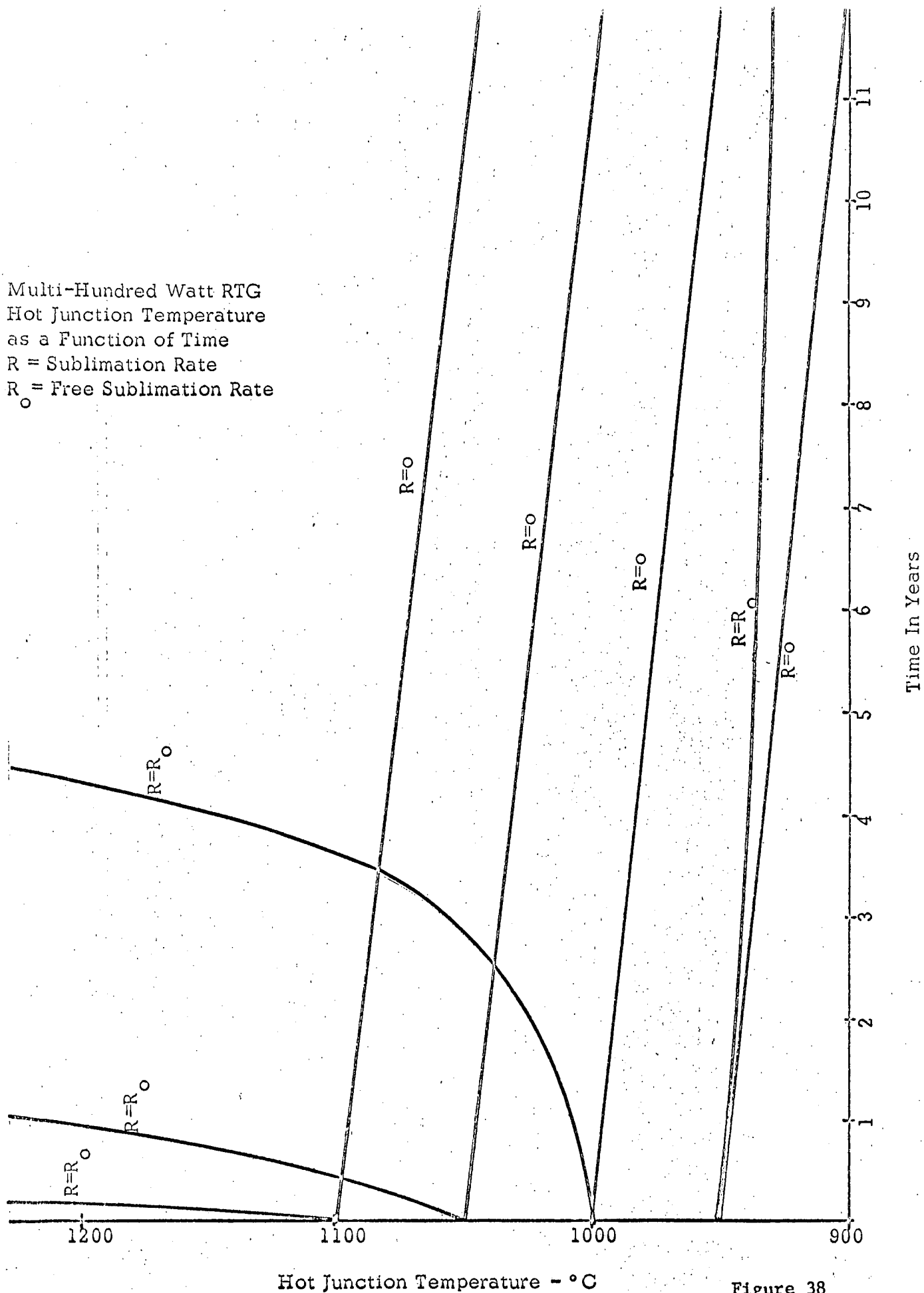
Hot Junction Temperature – °C

Time In Years

Figure 38

as it is nearly impossible to analytically predict the reduction of effective
sublimation rates of an actual generator structure, the calculations underlying
Figure 38 have been repeated for assumed sublimation rates of one and two orders
of magnitude below those shown in Figure 37 and used to calculate the MHW-RTG
hot side operating temperatures shown in Figures 39 and 40. Figure 39 shows the
results for a sublimation rate one order of magnitude lower than that used in
Figure 38. It should be noted that although the 1100 and 1050°C beginning-of-
life operating temperatures still lead to catastrophic generator failure within
the 12 year operating time, it is now possible to operate the RTG at a beginning-
of-life temperature of 1000°C without the undue effects of sublimation. The
corresponding results for silicon-germanium sublimation rates two orders of
magnitude lower than the maximum rates shown in Figure 37 are given in Figure 40.
It should be noted that although noticeable sublimation effects still occur at
most of the beginning-of-life operating temperatures shown, effects are rela-
tively small, even at the 1100°C beginning-of-life operating temperature. In
view of the results obtained in this study it was concluded:

     1.   Operation of silicon-germanium RTG's and specifically
    the MHW-RTG at beginning-of-life temperatures of 1100°C is
    advisable only if the effective sublimation rate of silicon-
    germanium alloys can be reliably reduced by some two orders
    of magnitude below the free sublimation rate. In view of
    stringent reliability requirements of most RTG applications
    it is questionable whether this can satisfactorily be
    accomplished.

     2.   Assuming the worst case of free sublimation of
    silicon-germanium, silicon-germanium RTG's should be de-
    signed for beginning-of-life operating temperatures at or
    below 1000°C.

Multi-Hundred Watt RTG
Hot Junction Temperature
as a Function of Time
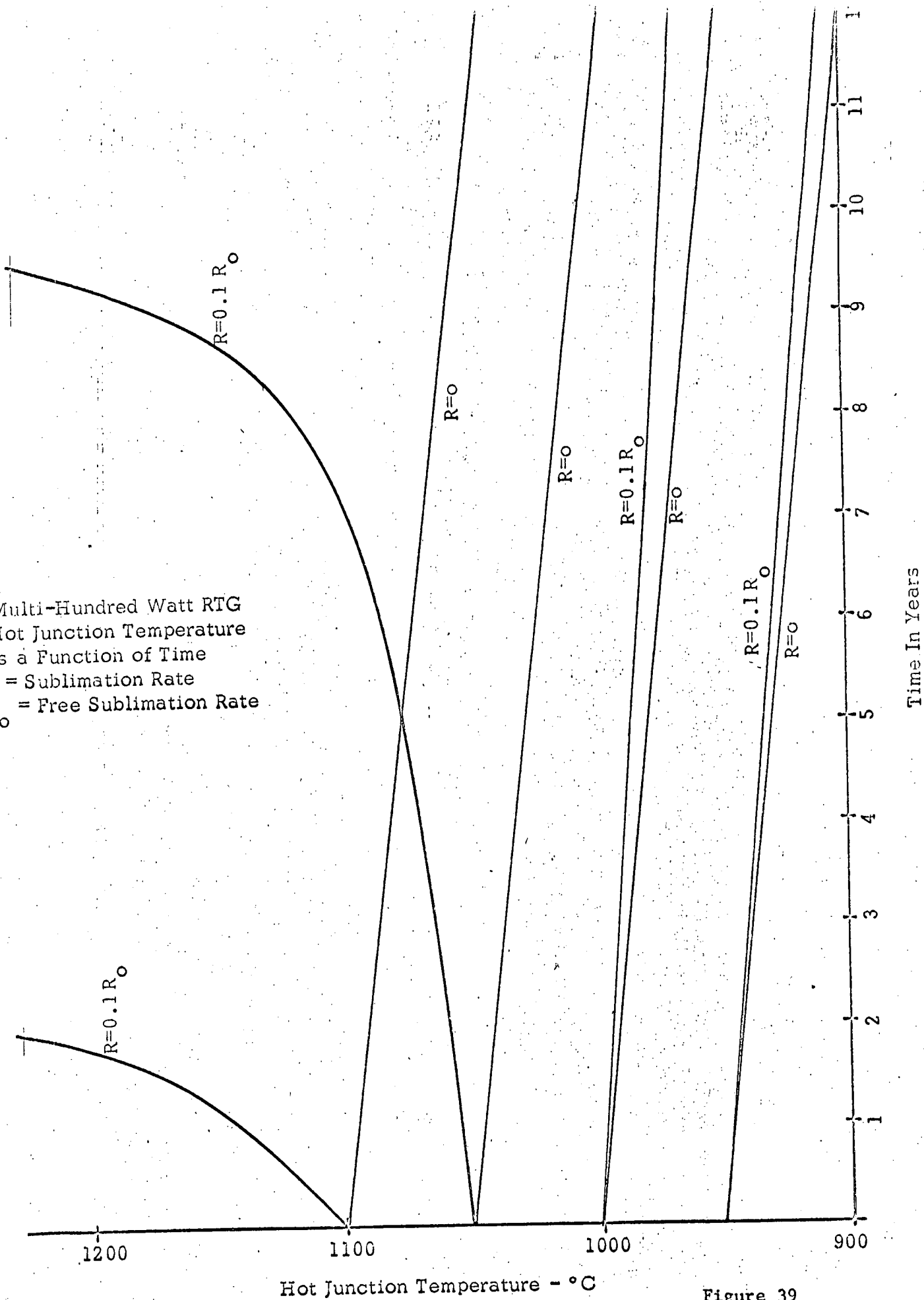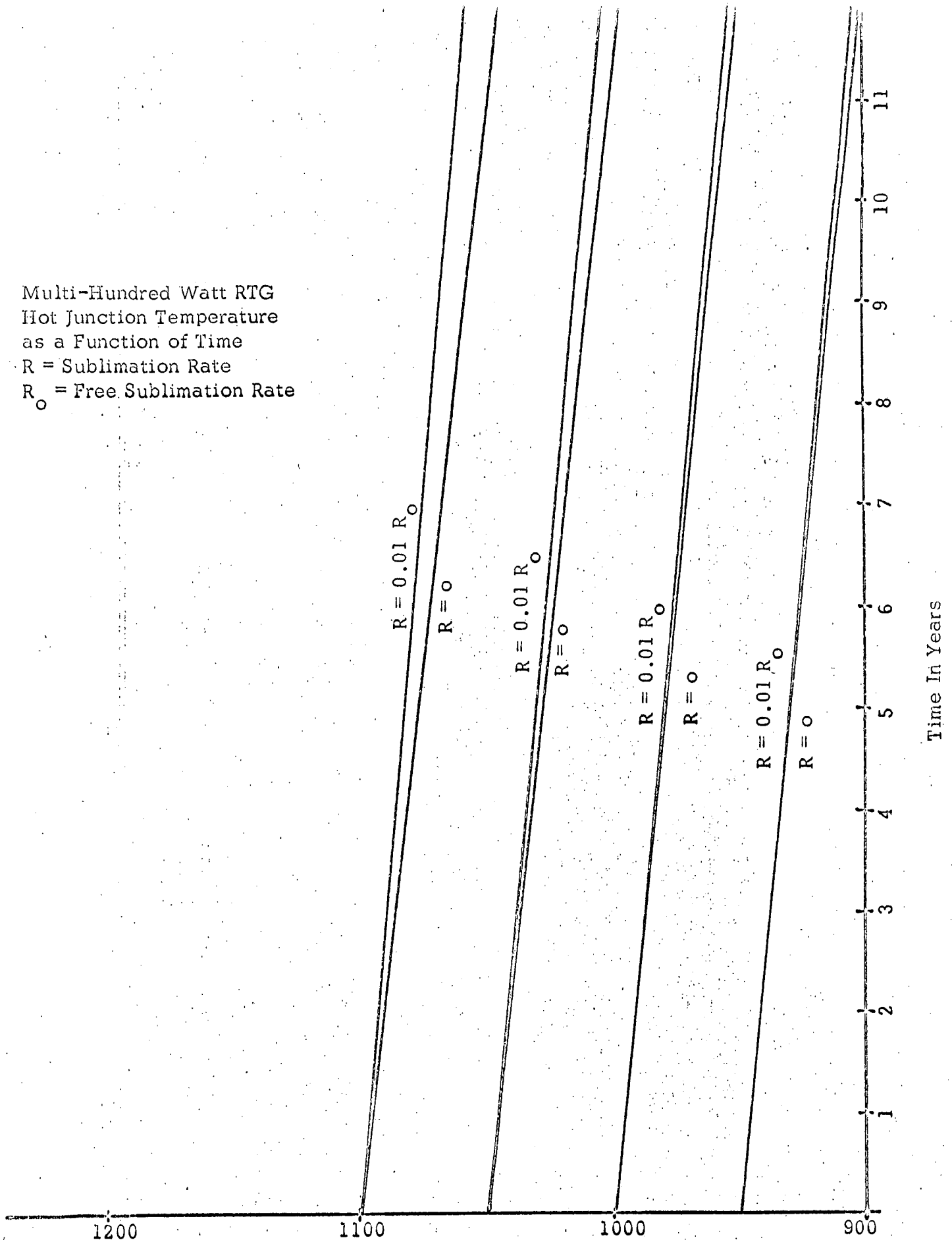R = Sublimation Rate
R_o = Free Sublimation Rate

Figure 39

126.

Multi-Hundred Watt RTG
Hot Junction Temperature
as a Function of Time
R = Sublimation Rate
R_O = Free Sublimation Rate

Hot Junction Temperature - °C

Time In Years

Figure 40

127.

3.   Because silicon-germanium couples and generators are
frequently tested under fixed temperature conditions, it is
possible that the mechanisms leading to catastrophic thermo-
couple failure are not uncovered in such tests of even fairly
long duration at temperatures in excess of 1000°C. The
maintenance of fixed operating temperatures does not ac-
curately depict the fixed heat input type operation that
thermocouples experience in an actual RTG.

4.   Relative sublimation effects can be reduced, but not
eliminated, by the use of relatively large silicon-germanium
thermocouples; therefore very small thermocouples should be
avoided if possible. Because it is the thermocouple length
to cross-sectional area ratio that has the first order
bearing on the thermocouple performance, it may be sug-
gested that the larger the thermocouple, for any given value
of ℓ/A, the less are the effects of sublimation.

F.   Memorandum #10

The special study summarized in Memorandum #10, titled Performance of
MHW-RTG in the Martian Environment, concerned itself with the determination of
the performance of the MHW-RTG on or near the planet Mars. Obviously the environ-
ment in which the RTG operates will affect the external heat rejection character-
istics of the RTG not only because heat rejection is a function of environmental
temperatures but because it depends upon the presence or absence of surrounding
gases, the type of gas and the thermal characteristics of the gas. In addition,
the external environment affects the internal operation of an unsealed RTG.

Nominally the RTG is designed as a sealed device and perhaps back-filled
with an inert gas prior to launch in order to exclude air from internal parts

128.

sensitive to the damaging effects of oxygen. However, operation of the RTG in a gaseous environment impairs the performance and therefore it is desirable to vent any gases from the RTG once it becomes isolated from planetary influences. If the RTG then reenters a gaseous environment, the internal structure would be exposed to the gas as well as the external of the RTG. Thus to assess the influence of environment upon RTG operation the internal effect as well as the external effect must be considered and in the case at hand, the internal effect is the most severe.

The accuracy that can be achieved in predicting the performance of the RTG on Mars will depend directly upon the accuracy to which the Mars environment can be described. The uncertainty about an atmospheric model of Mars can only be resolved by direct measurement. Lacking direct measurements, use is made of models of the Martian atmosphere which have been advanced.[12,13,14] The models are based upon evidence accumulated over the years from Earth observation, specifically data taken during the 1965 opposition, and from the Mariner IV occultation experiment in July, 1965 and Mariner probes of August, 1969.

Of primary concern to the performance of the RTG is the composition of the Martian atmosphere and the range of temperatures expected to be encountered. The atmosphere of Mars is strongly indicated to be 80 percent CO_2. The balance is assumed to be optically undetectable gases such as nitrogen or argon. For purposes of this analysis, the composition is assumed to be 80% CO_2 - 20% N_2. The mean surface temperature of Mars is estimated to be in the range of 225 to 300°K. The surface can be assumed to be an equivalent black body at 220°K[3] for purposes of heat transfer analysis. In addition, the atmospheric pressure at the surface of Mars is estimated to be between 3.5 and 8.5 Torr. A mean value of 6 Torr has been used in this analysis.

There are two primary areas of concern relative to the effect of the environment upon RTG performance. The first of these is the effect of the environment upon the external heat rejection rate of the RTG. The second is the effect of the environment upon the heat transfer and temperature distribution within the RTG.

As the MHW-RTG is designed for operation in a vacuum environment, the principal means of heat transfer from the exterior of the RTG is by radiation. If a gaseous environment surrounds the RTG then heat can be dissipated by conduction to the gas and if, in addition, a gravitational field exists, heat transfer by convection can occur. Thus, on Mars, heat rejection from the RTG could occur not only by radiation, but by conduction and convection as well.

Though the MHW-RTG will be operated until shortly after launch with an internal inert gas atmosphere, it is assumed that for a Mars mission, as for outer planet missions, this inert gas will be vented and the RTG will, in subsequent phases of operation, be exposed internally to its external environment. To determine the effect of the Martian environment upon the effective conductivity of the RTG insulation, the pertinent properties (primarily the thermal conductivity) of the environment must be determined. There is a large amount of data[15,16,17] available for the thermal conductivity of CO_2 and N_2 at pressures ranging from about 50 Torr to about five atmospheres. The conductivity in this region is predicted fairly accurately by the kinetic theory of gases[18] and is essentially independent of pressure.

Figure 41 shows the conductivity of N_2 and CO_2 as a function of temperature for the pressure insensitive range. Also shown is the conductivity of the mixture 80% CO_2 - 20% N_2. At pressures above and below the range of 50 Torr to five atmospheres the conductivity varies with pressure as well as temperature.
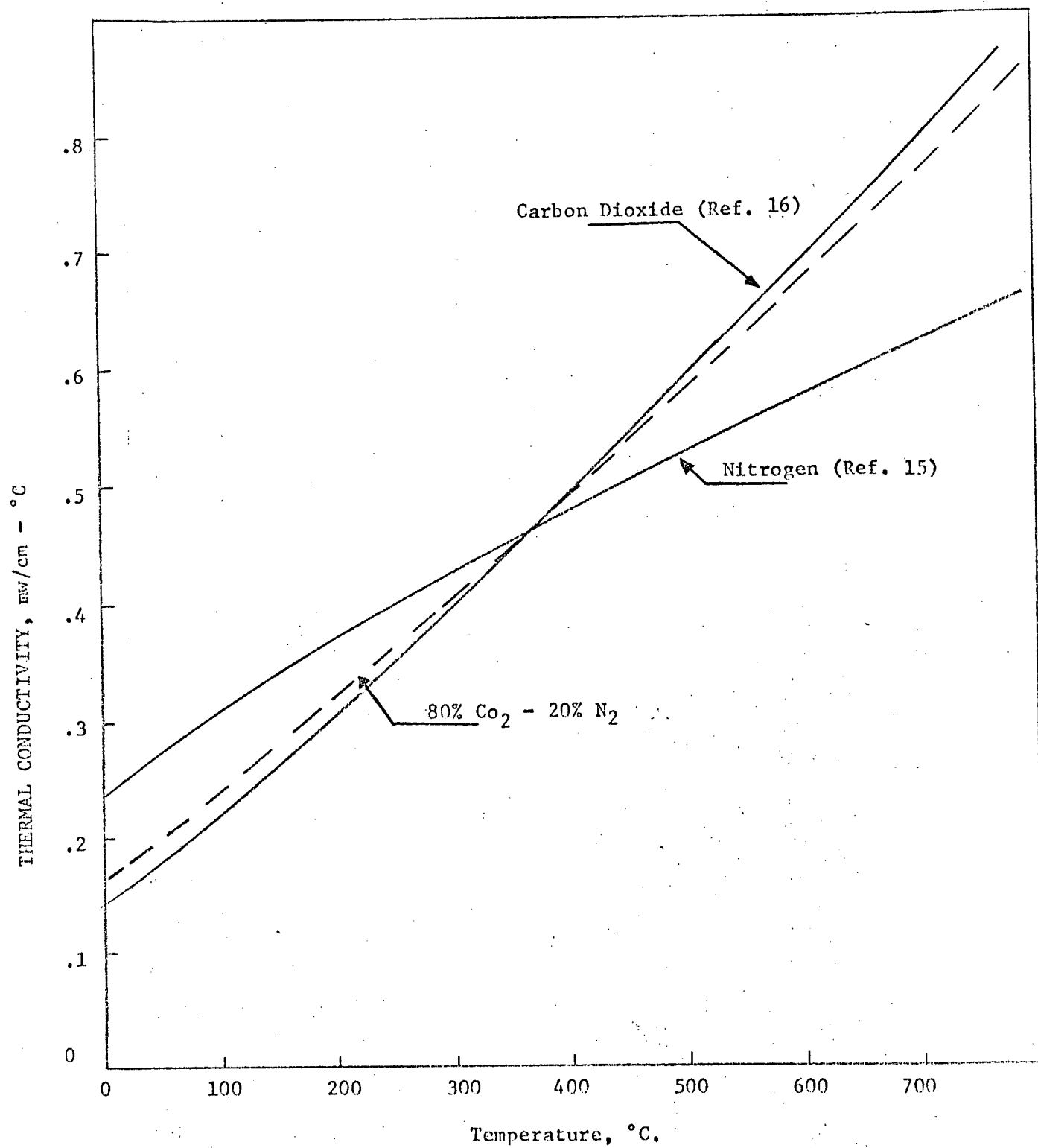
Figure 41 - GAS THERMAL CONDUCTIVITY

In a dilute gas the conductivity varies with the viscosity and the specific heat in the following manner

$$K = f\mu c_v \quad ,$$ (22)

where f is nearly independent of temperature. Thus the conductivity can be computed from the viscosity and specific heat. A similar calculation for CO_2 and the mixture of CO_2 and N_2 was made and the results are plotted in Figure 42 as a function of pressure for a temperature of 500°C. Note that the conductivity does not begin to decrease until the pressure has dropped to about 30 Torr. At 6 Torr the conductivity has decreased by about 15 percent from its one atmosphere value.

Three types of insulation are being considered for the MHW-RTG. These are multi-foil, Zircar and Min-K. The latter two are fibrous and have an irregular internal geometry. The density of the fibrous types can vary considerably with the mechanical loading applied and the methods used during assembly and installation. The conductivity of an insulation can be expressed[19] as

$$K = k_v + Mk_g \quad ,$$ (23)

where k_v is the conductivity of insulation in a vacuum, k_g is the conductivity of gas and M is an empirical constant.

A study[20] was made to assess the effects of a nitrogen atmosphere versus a vacuum atmosphere on the conductivity of insulation. In that study it was found that the value of M for Min-K was about .65, for Zircar about 1.0 and for multi-foil about 1.6. Thus this study indicates that the multi-foils are very sensitive to gas conductivity while Min-K is not as sensitive. Using the data of Reference 20 for vacuum thermal conductivity, the values of M discussed above, the CO_2 - N_2 gas conductivity shown in Figure 41 and taking into account the pressure effect
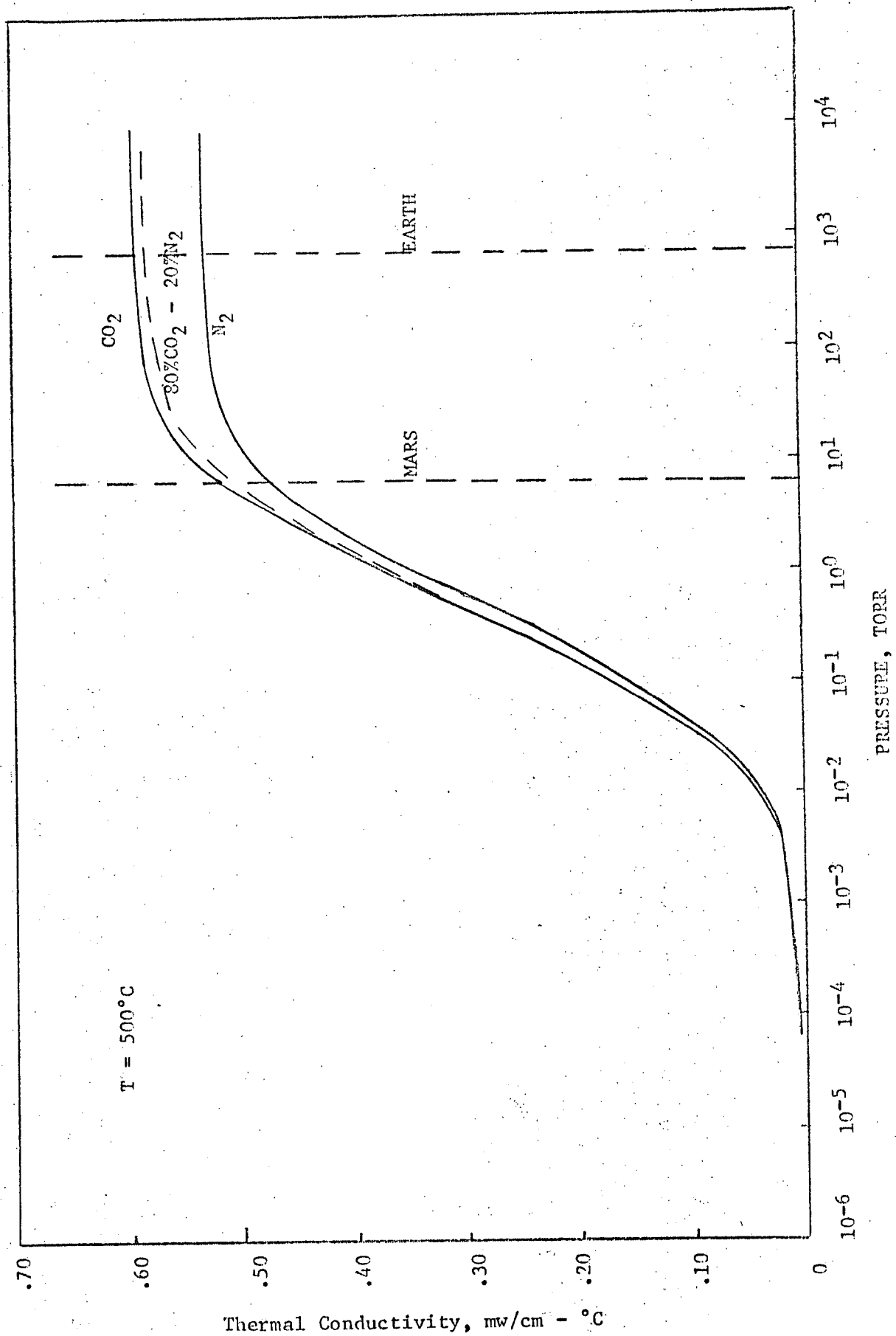
132.

FIGURE 42 – EFFECT OF PRESSURE ON GAS CONDUCTIVITY

133.

shown in Figure 42, the conductivity of the three types of insulation in a Mars environment were calculated and are shown in Figure 43 as a function of temperature. Also shown in Figure 43 is the conductivity of Min-K corrected for pressure by using the Johns-Manville pressure relationship to nitrogen. Thus the difference between the Johns-Manville curve and the other Min-K curve is due to two effects: 1) a different gas pressure effect, and 2) no allowance for penetration and edge effects being shown in the Johns-Manville curve.

The performance of the cylindrical MHW-RTG was calculated as a function of insulation conductivity for mission times of 1500 hours, five years and 12 years. The beginning-of-mission heat input for all cases was 2200 watts. The load voltage was held at 30 volts. The results are plotted in Figure 44. Using this figure and Figure 43, the power output of the MHW-RTG in a Martian environment was calculated and the results are shown in Table IX for the three types of insulation and for mission times up to 12 years. For Min-K a range of performance is shown to account for the possible range of effective conductivity for that material. The lower end of the range represents the power output using conductivity values calculated by neglecting the effect of mean free path while the upper end of the range results from conductivity values based on the manufacturer's information.

The performance of the MHW-RTG was found to be significantly poorer in a Mars environment than in a vacuum environment. In general, the power output of the RTG will only be 30 to 40 percent of the power output when operated in a vacuum environment. The primary reason for the reduced output is the fact that all of the insulation types proposed for the RTG suffer a significant increase in thermal conductivity when operated in a gaseous environment. Since less than five percent of the RTG area is occupied by thermoelements and the balance is filled
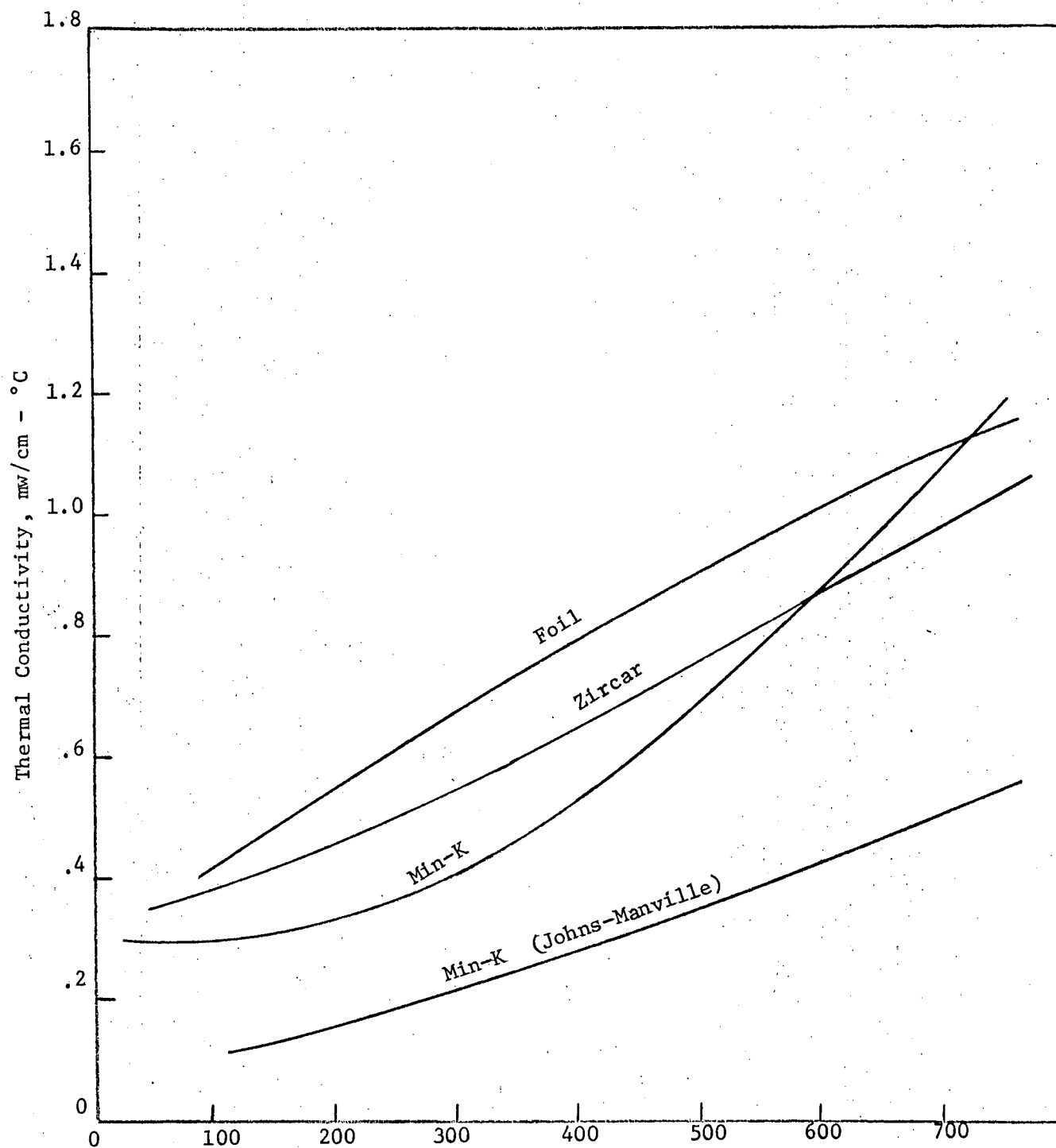
Figure 43   INSULATION CONDUCTIVITY IN
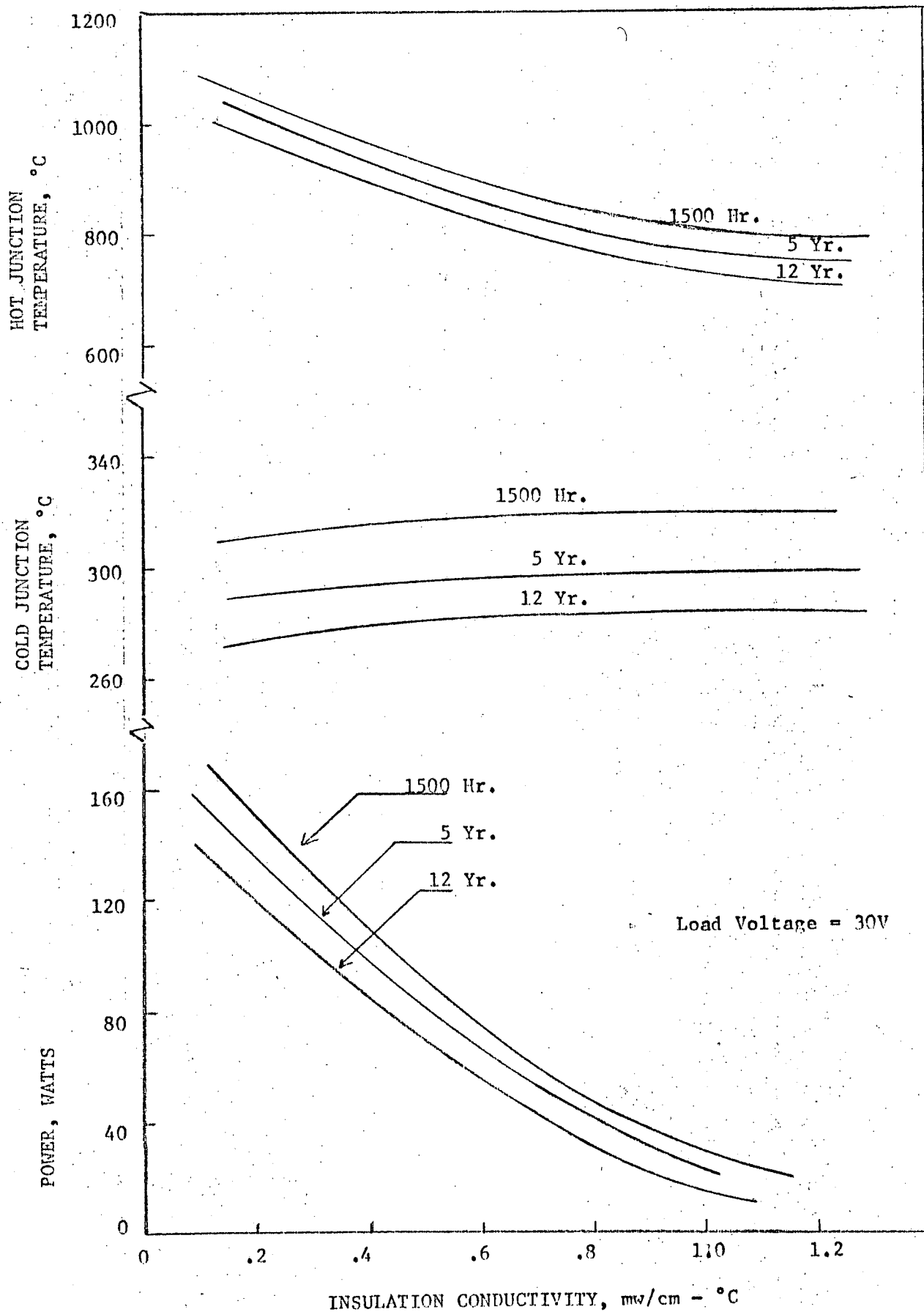80% CO_2 – 20% N_2 MIXTURE AT 6 TORR

135.

Figure 44 — EFFECT OF INSULATION CONDUCTIVITY ON MHW-RTG PERFORMANCE

136.

TABLE IX.

MHW RTG POWER OUTPUT IN MARTIAN ENVIRONMENT
LOAD VOLTAGE = 30V
POWER IN WATTS

Mission Time	INSULATION		
	Min-K	Zircar	Foil
1500 Hours	43-99	41	30
5 Years	42-94	38	26
12 Years	38-84	33	20

with insulation, any changes in the conductivity of the insulation are very significant and drastically affect the temperature drop which can be maintained across the thermoelements. The following conclusions can be drawn:

1. The performance of the MHW-RTG in a Martian environment will definitely be poorer than in a vacuum, the power output will be some 50 to 70 percent lower depending on the insulation type and density.

2. The conductivity of some types of insulation is more sensitive to the type of gas and its pressure than others; of the fibrous types, the more dense the insulation, the less sensitive it is.

3. A great deal of information is known about the conductivity of the insulation in gases at one atmosphere and at pressures less than 10^{-4} Torr. In between, very little is known.

4. At pressures below about 50 Torr very little is known about the conductivity of gases. In the low pressure region (less than 50 Torr) the conductivity becomes system dependent, i.e., in the case of insulations, the conductivity of the gas depends on the pore size of the insulation.

5. Experimental work needs to be carried out to verify the conductivity of insulations in the gas pressure range of 10^{-2} to 50 Torr.

G. Memorandum #11

The special study summarized in Memorandum #11, titled Thermophysical Properties of RTG Insulation Components, concerned itself with an attempt to

summarize the most important data on high temperature thermal insulations and to present the results in a form that is readily usable to the thermoelectric generator designer. Much of the high temperature thermal insulation data has been obtained as a by-product of thermoelectric generator testing and is, therefore, difficult to apply to different generator geometries. The data presented in this study pertain to bulk quantities and as such must be appropriately modified to account for a specific application. Effects such as penetration losses, compression, and gas conduction must be satisfactorily taken into account in thermoelectric generator analysis if realistic results are to be obtained. The following material properties were included in the scope of the study.

1. Chemical composition

2. Density

3. Dimensional stability

4. Useful temperature range

5. Thermal conductivity

6. Specific heat

Candidate insulation materials were divided into two major categories: fibrous and multi-foil types. Fibrous insulations are as varied as the applications in which they are used. Their low thermal conductivity and low density makes them especially attractive in a wide range of applications. The ability to mold this type of insulation to irregular geometries and still provide adequate structural integrity is an important asset. However, the characteristics which make fibrous insulations widely used also cause a wide disparity in their reported performance and their ability to effectively insulate. The large number of parameters which affect the thermal conductivity of these insulations and the wide range over which they vary contribute to the variation in thermal characteristics noted in the literature. Among such important parameters are

density, pore size, the presence or absence of gases and their pressures, composition, heat treatment and geometry.

The thermal conductivity of a fibrous material is a complex property, since all three mechanisms of heat transfer play a role. Some heat is conducted through solid material and some through gas in the pores. Convection can also occur in any gas pockets large enough to support circulation currents in a gravity field. Finally, radiation can travel from one surface to another and some radiation may travel through the solid if it is partially transparent to infrared. It can be deduced from this that thermal conductivity is not strictly a proper term but since most of the available data are given in terms of thermal conductivity, this term will be used to mean apparent or effective thermal conductivity. Since a fibrous material possesses a complex geometry, no single theory will describe the heat transfer through it. The method of analysis used is generally adapted to the particular case being considered, with, depending upon the accuracy desired, certain less important factors being neglected compared to the dominant ones.

Fibrous materials are generally assumed to have a random distribution of fibers. The fibers will consequently, on the average, have equal components projected on three axes. Conduction heat transfer is generally made up of solid conduction and gaseous conduction by taking appropriate account of the void fraction. The conduction portion of the heat transfer is thus dependent only on the insulation density and will increase with increasing density. Convection depends not only upon the density (pore volume) but upon the pore size as well. In a gravitational field, the gas circulation increases as the cell size increases. The convection occuring within an insulation can thus be reduced without any change in density by reducing the pore size. Radiation transfer within a

fibrous insulation depends primarily upon the temperatures involved since radiation varies with temperature to the fourth power. However, it is also dependent upon the number of pores through which heat passes. Radiation heat transfer varies generally inversely with the number of pores in a line parallel to the direction of heat flow.

When the relative values of all three modes of heat transfer are considered, it is generally found that the radiation and convection modes are most significant in fibrous materials. At high temperatures, however, radiation is usually the larger of these two modes of heat transfer. Solid conduction is usually negligibly small; gaseous conduction can be significant. Whether gas conduction is significant or not depends upon several factors. Obviously, if no gas is present, it will not be significant. However, if it is present the pore size and gas pressure are important. At very low pressures, where the mean free path of the gas molecules becomes comparable to pore size, kinetic theory does not hold. Analysis shows that at extremely low pressures, below about 0.5 Torr, gas thermal conductivity is linearly proportional to pressure, approaching zero conductivity at zero density. Only in insulations which have pores of comparable size to the mean free path of gas molecules is the effect of low gas pressure reflected in a reduced thermal conductivity of the insulation.

As previously mentioned, various analytical techniques have been advanced to predict the conductivity of fibrous insulations. However, as these techniques are usually tailored to fit a certain type of fibrous material, they are not of general applicability. Thus the thermoelectric designer must usually depend upon experimental data obtained from tests carried out in situations that agree with the intended use of the insulation.

Foil type insulations have received a significant amount of analytical and developmental effort during the past ten years due to the increasing demand

for insulations having low thermal conductivity at high temperatures where the predominant mode of heat transfer is radiation. Most of the development work on high temperature foil insulations has been done by Linde and TEECO. Linde multi-foil systems differ from those of TEECO primarily in that Linde uses a thin layer of low conductivity material, generally of a fibrous type, such as Astroquartz to separate individual foils, whereas TEECO achieves foil separation by spraying a thin coat of oxide on the foil.

The effective thermal conductivity of a multi-foil system can generally be expressed as

$$k_{eff} = \frac{a}{2}\left(T_1 + T_2\right) + \frac{b}{4}\left(T_1^2 + T_2^2\right)\left(T_1 + T_2\right) . \qquad (24)$$

where a is a factor describing the amount of solid conduction between adjacent foil layers, T_1 and T_2 are insulation hot and cold side temperatures and

$$b = \frac{2\sigma\varepsilon}{\eta}$$

where σ is the Stefan-Boltzmann constant, η is the foil layer density and ε is the foil emissivity. The factors $\frac{a}{2}$ and $\frac{b}{4}$ have been determined experimentally for several foil systems and are shown in Table X. The factor $\frac{b}{4}$ can be adjusted for different emissivities or different layer densities.

In addition to the thermal conductivity, there are several other factors which significantly affect the choice of a multi-foil insulation for a particular application. One of the most significant points to be considered is the effect of temperature changes on differential expansion. In applications where large temperature gradients occur across the multi-foil insulation it is obvious that the layers on the hotter side will expand more than those on the cooler side. As a result, buckling and/or gaps can occur at joints and corners of the insulation. These penetrations may result in large heat losses.

Table X

FOIL INSULATION FACTORS

Foil Spacer	$\frac{a}{2}$ watt/cm-K^2 x 10^9	$\frac{b}{4}$ watt/cm-K^4 x 10^{14}	η cm^{-1}	ε	Valid Temperature Range °C
Ni – Astroquartz cloth	9.66	1.48	45	.24	40 to 1100
Ni – Refrasil quartz fiber paper	6.24	1.24	36	.163	40 to 1100
Cu – Refrasil quartz fiber paper	2.97	0.52	31	.059	40 to 700
Cu – Copper flake opacified Refrasil quartz fiber	10.08	0.84	27	.081	40 to 700
Al – Glass fiber paper	1.65	0.52	45	.086	40 to 500
Ta – Astroquartz cloth	0.93	1.61	53	.306	40 to 1000
Al – Al-flake opacified glass paper	0.31	0.67	57	.137	40 to 500

143.

In many high temperature applications the use of some metals, which are ideal in applications at lower temperature, are obviously ruled out due to sublimation and melting problems. For example, aluminum is limited to temperatures below 500°C. Refractory metals are the only foil candidate for materials for many high temperature applications. Severe oxidation problems may, however, occur at elevated temperatures. This problem is somewhat alleviated by using a "graded" foil system, i.e., a different foil material is chosen for each specific range of temperatures. As a result, such a system may include two or more different types of metal foils.

The emissivity of foils is important because the primary method of heat transfer reduction through multi-foils is the suppression of radiant heat transfer. Not only is foil emissivity important at time of manufacture but the stability of emissivity with time in the operating environment is equally important. Oxidation and sublimation affect emissivity and therefore these factors have to be carefully analyzed. Possible oxygen sources have to be eliminated and the multi-foil itself requires careful outgassing prior to operation at temperatures at which oxidation will occur. In addition to sublimation of the foil material, sublimation of nearby materials has to be ascertained as the deposition of sublimed species from foreign surfaces can be just as detrimental as the sublimation of the foil itself. In addition to affecting the emissivity of the foils, outgassing can adversely affect the heat transfer between foils by conduction through the gaseous interface. In fact, the conductivity of a multi-foil system in air is essentially equal to the conductivity of air itself.

Obviously there is a large number of possibilities for the types of multi-foil insulations. Aluminum, copper, nickel, tantalum, platinum, molybdenum and tungsten are all used. Opacified and unopacified glass, quartz paper, quartz, Astroquartz and Refrasil cloth and other materials including sprayed oxide coatings

are used for the foil spacer materials. Table XI lists common materials used in multi-foils and their temperature limitations. The weight of various materials for specified thicknesses is included for convenience of multi-foil weight computations. Figure 45 shows the effective thermal conductivity of selected types of multi-foil insulations. The data pertain to vacuum operation.
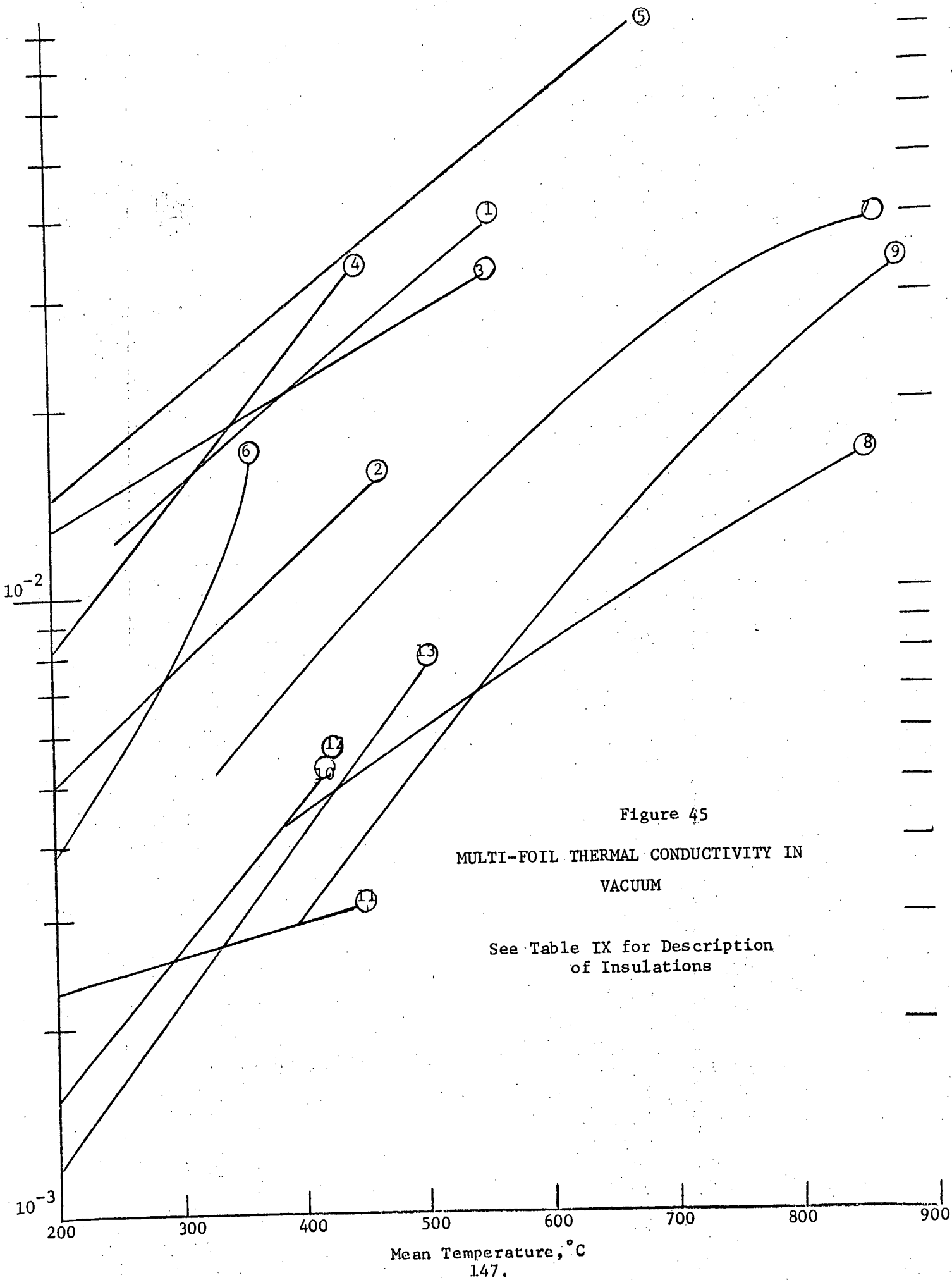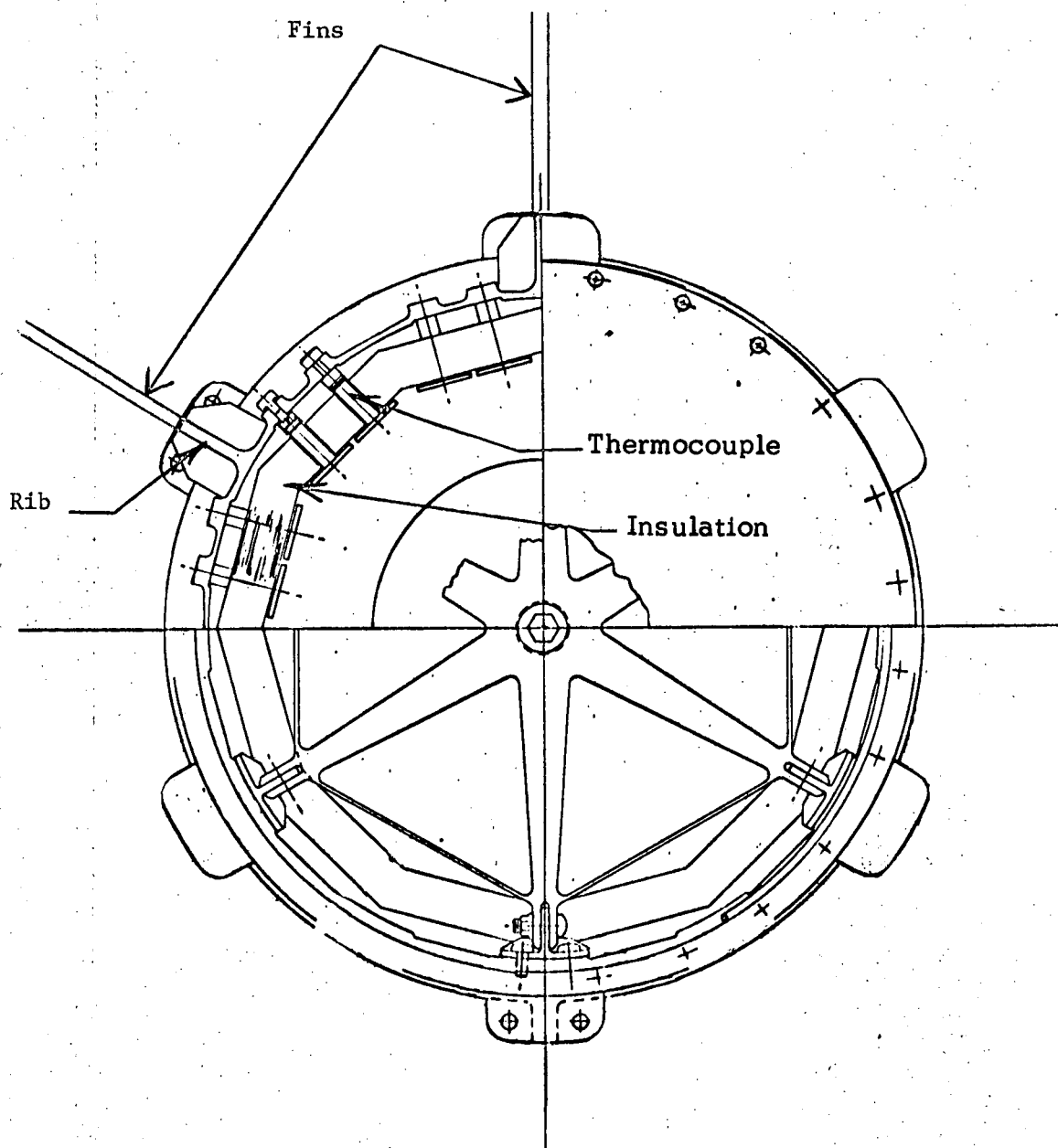
H.   Memorandum #12

The special study summarized in Memorandum #12, titled <u>Performance of the MHW-RTG in the Temperature Range 900 to 1000°C and Lower Bounds on Gains Obtainable From the Use of Radiation Fins</u>, concerned itself with the extent to which the performance of the 1000°C BOL design of the MHW-RTG can be enhanced by optimization. This study determined the optimum performance of the MHW-RTG at BOL hot side temperatures in the range 900 to 1000°C. Although the present MHW-RTG design does not specifically include radiation fins, the investigation considered the use of such fins because their applicability generally increases with decreasing RTG hot side operating temperatures.

The design code, RATEG, was used to do all MHW-RTG performance calculations in this study. The RTG model used was based on the MHW-RTG reference sealed cylindrical design. A cross-section of the RTG is schematically shown in Figure 46. Also illustrated in Figure 46 is the manner in which fins were added to the outer case of the RTG in this study. The fin parameters that were varied were fin length, L_f; fin base thickness, t_b; fin tip to fin base thickness ratio, X; and total number of fins, N_f. The effective radiating area was calculated using the taut band perimeter. The fin effectiveness of the radiation fins and of the RTG outer case were calculated independently; the effect of temperature variations in the outer case and radiation fins on RTG performance was thus taken into account in the analysis. A heat sink temperature of 77°C was used; the outer case and

145.

TABLE XI

MULTIFOIL MATERIALS

Material	Thk. Mils	Weight gms/ft^2	Temperature Limit °C
Astroquartz cloth	5	10.4	1300
Refrasil Quartz Fiber Paper	5	2.4	1100
Copper Flake Opacified Refrasil	10	5.5	1100
Glass Fiber Paper	3	2.1	650
Aluminum	1	6.6	500
Copper	1	21	800
Nickel	1	21	1000
Tantalum	1	39	2800
Platinum	1	51	1125
Molybdenum	1	24	2200
Tungsten	1	44	3000
Titanium	1	10.6	1250

Figure 45

MULTI-FOIL THERMAL CONDUCTIVITY IN
VACUUM

See Table IX for Description
of Insulations

Mean Temperature, °C

147.

Fins

Rib

Thermocouple

Insulation

MHW-RTG CROSS-SECTION

Figure 46

had an emissivity of 0.8. The assumed heat sink temperatures represented the anticipated pre-launch/launch environmental temperatures.

The generator was assumed to be insulated with multi-foil insulation of thermal conductivity of 0.13 milliwatt/cm – °C. RTG thermal end losses were calculated by assuming the ends to be insulated with multi-foil insulation having a thickness equal to thermoelement length. Extraneous internal electrical resistance of the RTG was maintained at ten percent of the thermoelement resistance.

The procedure used in the analysis was to vary the four fin parameters to find the optimum fin geometry for maximum specific power at a given hot junction temperature. Thermoelement dimensions, length and cross-sectional area were varied independently as a part of a total RTG performance optimization. The weight of the generator was calculated by adding fin weight and heat source weight to the base generator weight. Heat source thermal power was varied by varying heat source length as necessary to maintain thermocouple hot junction temperatures at any specified value for different radiator fin geometries. Regardless of RTG power output, heat source weight was calculated from an assumed heat source specific power of 55 watts/lb. The base weight of the remainder of the generator was assumed to be 32.4 pounds.

The dependence of RTG specific power on the four fin parameters is illustrated in Figures 47 and 48 for a BOL thermocouple hot junction temperature of 1000°C. It is noted that optimum fin base thickness is slightly below 0.15 cm. The minimum usable fin thickness is probably about 0.152 cm (60 mils) due to fabrication difficulties with smaller thicknesses. Thus, for the remainder of the fin parameter optimization the fin base thickness was fixed at 0.152 cm. Maximum specific power occurs with a fin height of about 9 cm. Optimum fin height varies slightly with hot junction temperature.
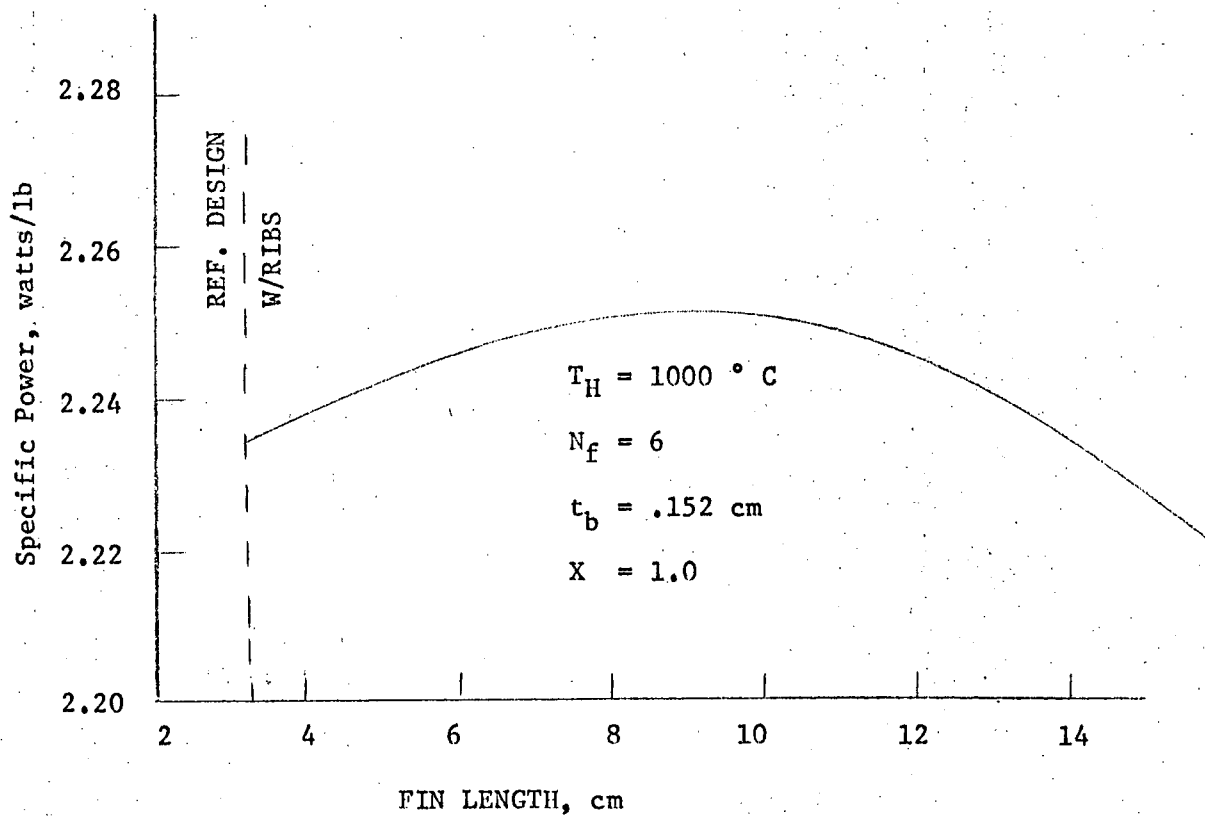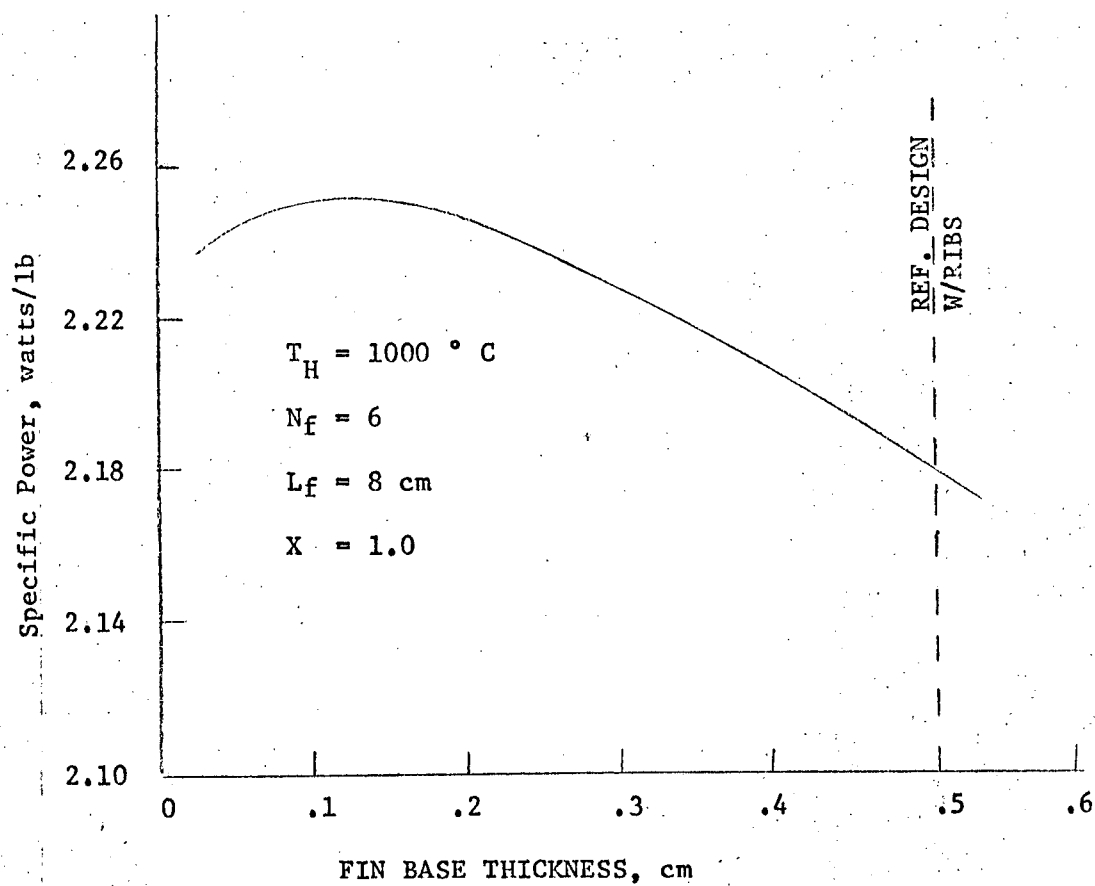
FIGURE 47 EFFECT OF FIN BASE THICKNESS AND FIN LENGTH ON
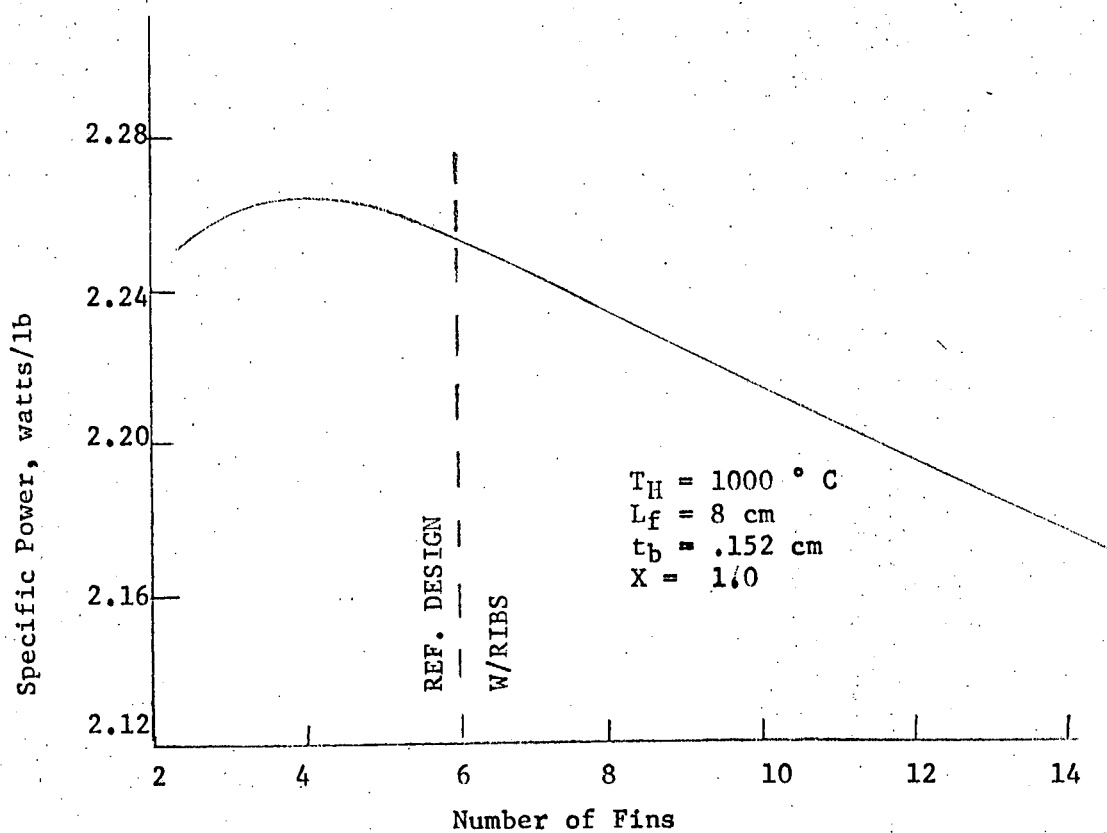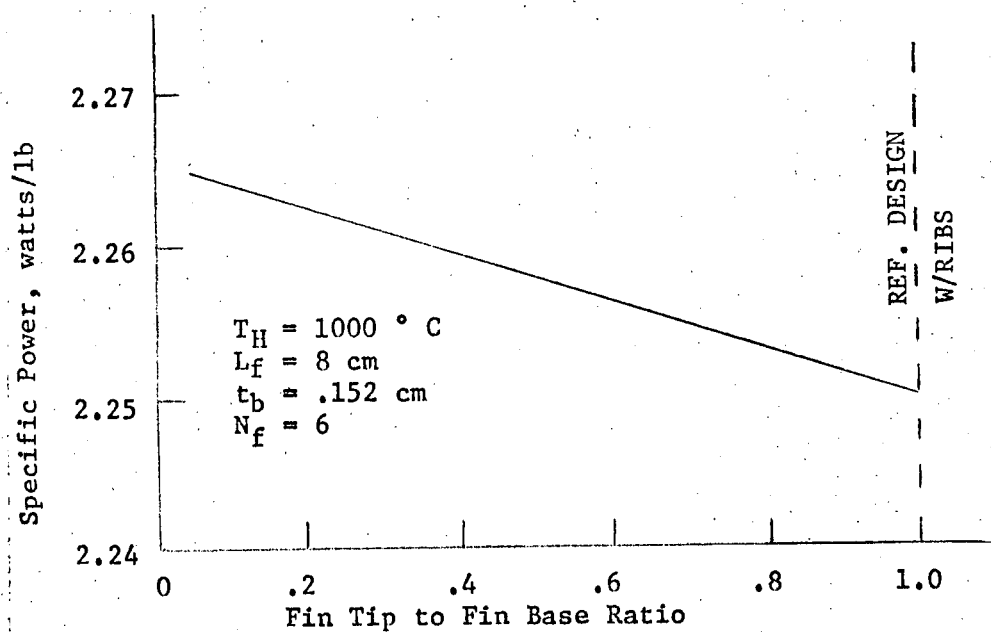SPECIFIC POWER

150.

FIGURE 48 EFFECT OF FIN TIP TO FIN BASE RATIO AND NUMBER OF
FINS ON SPECIFIC POWER

Figure 48 shows the effect of fin top to fin base thickness ratio on RTG specific power. A thickness ratio of one represents a rectangular fin while a thickness ratio of zero represents a triangular fin. As the fin base thickness was set at the minimum usable fin thickness, a thickness ratio of less than one would probably result in fins of questionable structural characteristics. Thus, even though a reduction in thickness ratio below one automatically results in a higher RTG specific power, such a thickness ratio is not practical. As with fin height, an optimum number of fins exists and this occurs at about four.

Figure 49 shows the effect of thermocouple hot junction temperature on RTG specific power for several generator designs. Optimization of the MHW-RTG results in greater improvement in specific power than just the addition of fins to the reference design generator. The use of radiation fins with optimum design generators enables a gain of about one percent in specific power at a BOL thermocouple hot junction temperature of 1000°C and some 3.6 percent at a BOL thermocouple hot junction temperature of 900°C. Based on these findings, it is suggested that a true design optimization that includes radiation fins will lead to even more significant performance gains/weight reduction for the MHW-RTG in the range of BOL thermocouple hot junction temperatures of 900 to 1000°C.

The optimum design performance curve in Figure 49 was based on an analysis reported earlier. In that analysis the total number of thermocouples, the area of the n-and p-type thermoelements, thermoelement length and radiator area were varied independently to achieve minimum RTG weight for given end-of-mission electrical power. That analysis made use of the same heat source specific power of 55 watts/lb as used here; five percent of the total thermal input power was assumed for RTG end losses. The BOL thermocouple hot junction temperature was varied from 700 to 1100°C. It was found that optimum thermoelement length

152.

1000° C REF. DESIGN (GE)

E_b = 30V
$Au = Ap + 0.1755$ cm^2

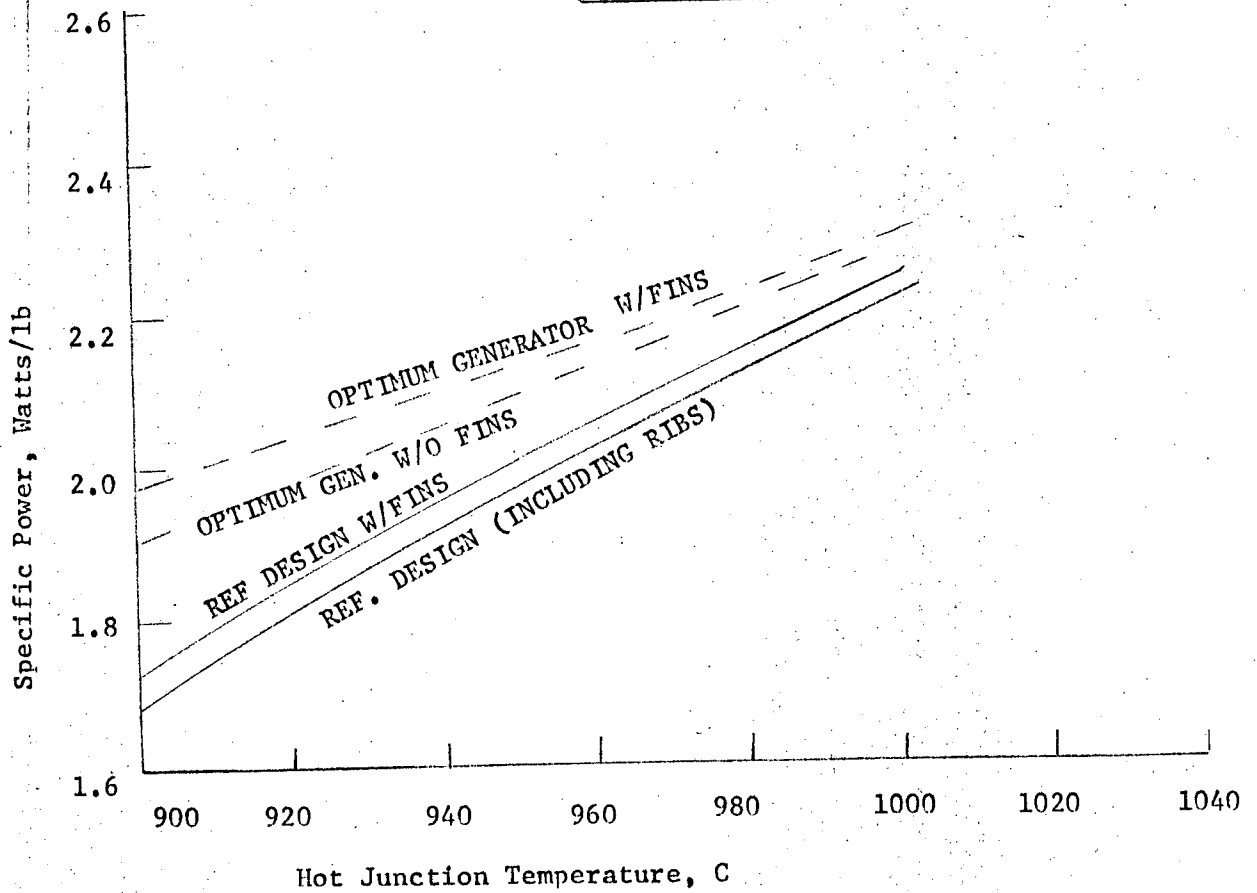|	Ref. Design	With Fins
N_f	6 (ribs)	6 (on ribs)
L_f	3.175 cm	Variable
t_b	.508 cm	.152 cm
X	1	1

FIGURE 49 MHW-RTG SPECIFIC POWER

decreases and optimum thermoelement area, total number of thermocouples and radiator area increase with decreasing hot junction temperature.

The effect of hot junction on generator power output for the reference design and the optimized fin design is shown in Figure 50. Power output decreases rapidly with decreasing hot junction temperature in both cases.

In conclusion, the study showed that an optimization of MHW-RTG design results in a RTG weight reduction of about five percent at a BOL thermocouple hot junction temperature of 1000°C; greater weight reductions are possible at lower BOL hot side operating temperatures. It may therefore be concluded that for operation at BOL hot side temperatures of 1000°C or lower, the design of the MHW-RTG should be optimized. The importance of design optimization, including the use of radiation fins, increases with decreasing BOL hot side operating temperatures.

I. Memorandum #13

The special study summarized in Memorandum #13, titled Performance of a Cascaded Thermoelectric Generator, concerned itself with the performance of a cascaded thermoelectric power converter that utilizes silicon-germanium alloys for the active thermoelectric material in the hot stage and lead telluride for the material in the cold stage. The two stages are thermally interconnected by a heat pipe. The cold stage of the cascaded generator was designed and fabricated by Westinghouse Astronuclear Laboratory and designated as a TEM-10 type thermoelectric module. It consisted of a tubular arrangement of PbTe washers arranged as shown in Figure 51. The p-type material of the module was 3M Company's TEGS-2P and the n-type material was General Electric's GE-2N material. The PbTe washers were insulated from each other by thin mica washers. A serpentine electrical path was created within the module by alternately connecting the n-and p-type washers at the inner and outer diameter by iron rings. The thermopile
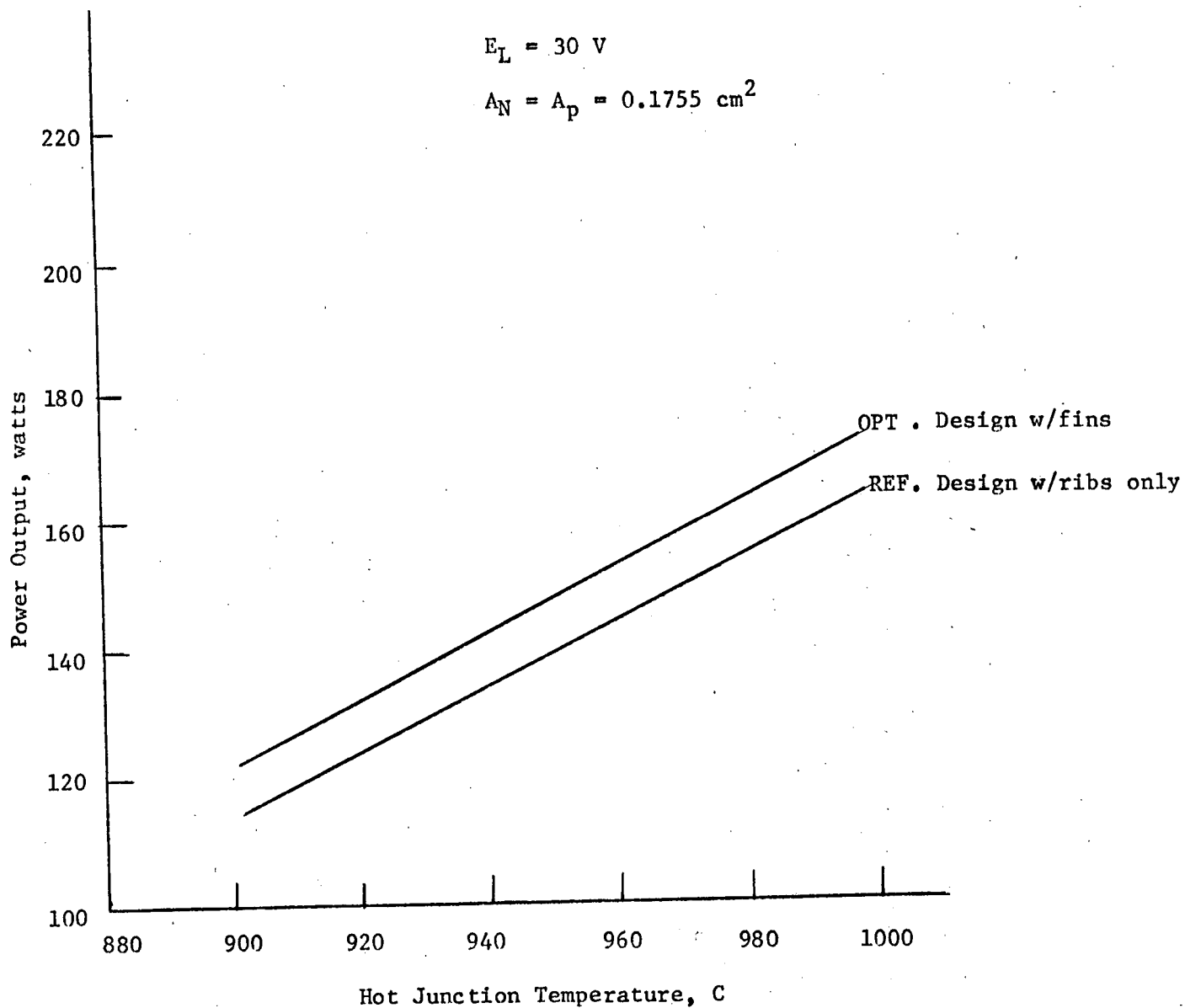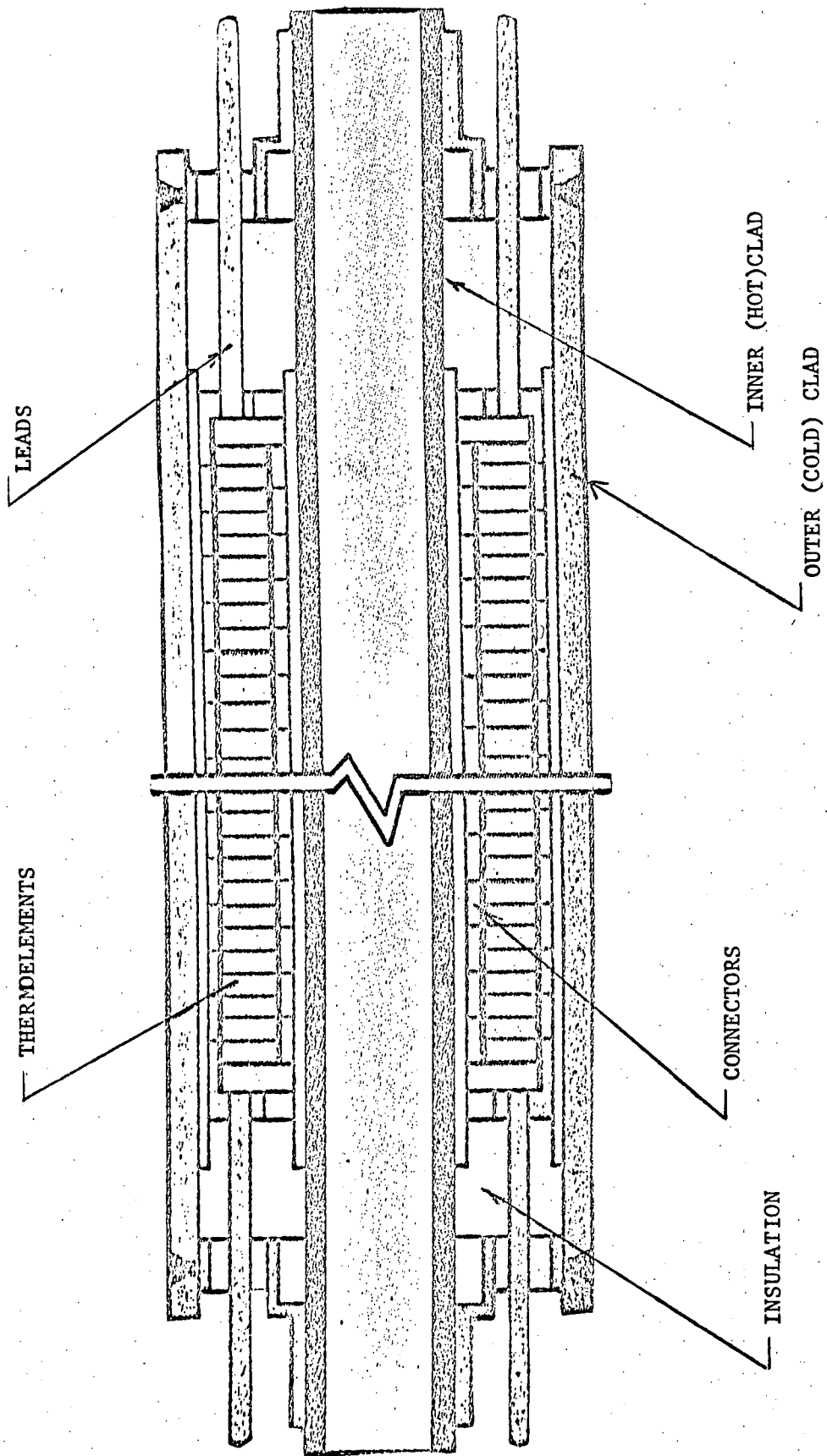
$$E_L = 30 \text{ V}$$

$$A_N = A_p = 0.1755 \text{ cm}^2$$

OPT . Design w/fins

REF. Design w/ribs only

FIGURE 50 MHW-RTG POWER OUTPUT

155.

FIGURE 51 LEAD-TELLURIDE MODULE CROSS-SECTION

LEADS

THERMOELEMENTS

INNER (HOT) CLAD

OUTER (COLD) CLAD

CONNECTORS

INSULATION

was electrically isolated from the inner Inconel 718 and outer stainless steel cladding by thin boron nitride sleeves. End closures complete the assembly.

The hot stage of the cascaded converted consisted of silicon-germanium Air-Vac thermocouples arranged circumferentially around the evaporator section of the heat pipe. The thermal energy from the electrical heater was radiated to the silicon-molybdenum hot shoes and then conducted to the hot junctions. The waste heat from the thermocouples was conducted by way of copper wedges to the heat pipe evaporator and from there was transferred by the heat pipe to the PbTe stage. All of the silicon-germanium thermocouples were connected electrically in series. The space between thermocouples was insulated with Micro-quartz and Min K-2020 fibrous insulation. Figure 52 shows a cross-section of the silicon-germanium hot stage. Since no test data were available for the silicon-germanium stage, the performance characteristics of the stage were calculated from the property data of the 63 a/o Si - 37 a/o Ge alloy.

The hot and cold stages just described were combined to form a cascaded generator. The two stages were thermally connected by a heat pipe. A radiant heater provided the thermal input to the silicon-germanium hot stage and a water-cooled system absorbed the waste heat from the lead telluride cold stage. The electrical output of each stage was connected to a separate external load and therefore the load voltage of each stage was independently adjustable.

A computer program was used to evaluate the performance of cascaded thermoelectric generators. This program called CASCADE was especially designed for analysis of cascaded generators consisting of two stages which may or may not be electrically connected. The heat input to the cascaded generator is specified and the power output of each stage is computed for a given value of load voltage for each stage.

THERMOELEMENT

HOT SHOE

COPPER
WEDGE

INSULATION
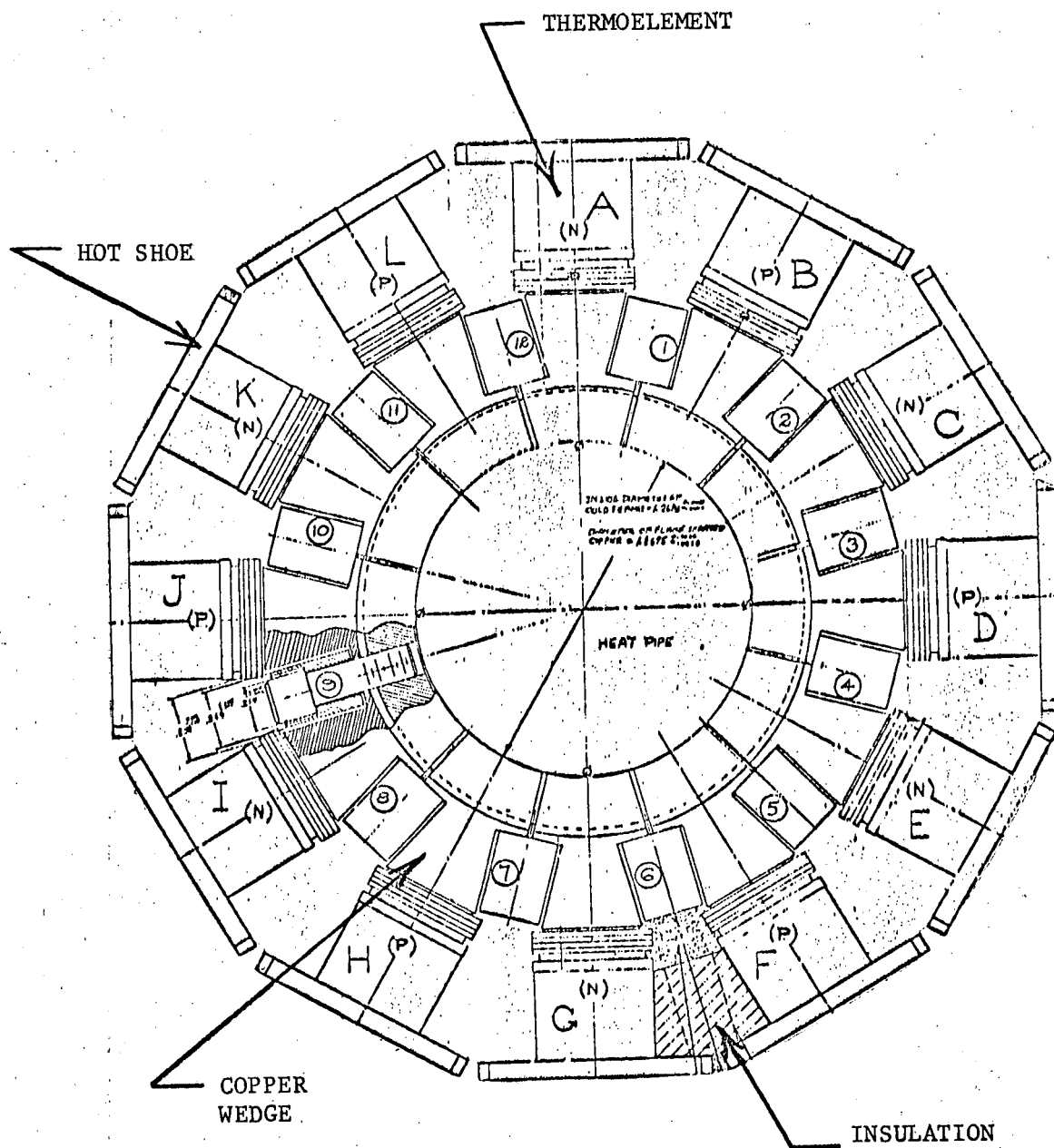
SILICON-GERMANIUM STAGE CROSS-SECTION

Figure 52

The analysis was conducted for four different values of heat input ranging from 3000 to 3900 watts, for four values of silicon-germanium stage load voltage ranging from eight to 14 volts and for four values of lead telluride state load voltage ranging from two to five volts. As expected, the PbTe stage hot clad temperature was almost independent of the silicon-germanium stage load voltage. Since the PbTe stage cold clad temperature was nearly independent of the silicon-germanium stage load voltage and because the PbTe stage cold clad temperature was fixed, it was only the PbTe stage and the total heat input to the generator that affected the PbTe stage hot clad temperature. The silicon-germanium stage effected the PbTe stage hot clad temperature only as the silicon-germanium stage load voltage changed. This, however, was a minor effect. Over the range of heat inputs and load voltages investigated, the PbTe stage hot clad temperature varies from 445 to 950°C.

Likewise, the silicon-germanium stage cold junction temperature was relatively independent of the silicon-germanium stage load voltage. On the other hand, the hot junction temperatures of the silicon-germanium stage thermocouples reflected changes in the load voltage of both stages. At heat input levels above 3300 watts and at the higher load voltages, the hot junction temperatures of the silicon-germanium stage thermocouples exceeded 1000°C. At a heat input level of 3900 watts, a silicon-germanium stage load voltage of 14 volts and a PbTe stage load voltage of five volts, the average hot junction temperature of the silicon-germanium stage thermocouples was calculated to be 1088°C. The melting point of the 63 a/o Si - 37 a/o Ge alloy was only about 100 degrees higher; thus care was exercised in this region of operation.

Just as the PbTe stage temperatures were not significantly influenced by the silicon-germanium stage, the power output of the PbTe stage was not significantly influenced by the silicon-germanium stage. The peak power output of the

PbTe stage occurred at a load voltage of about three volts. The precise value

depends upon the heat input level at which the generator is operated; the optimum

PbTe stage voltage increased with increasing heat input.

The peak power of the silicon-germanium stage occurred at load voltages

in the range of nine to 11 volts, the precise value depending on the heat input

level. As with the PbTe stage, the silicon-germanium stage load voltage at which

peak power occurred increased with increasing heat input. Note that the silicon-

germanium stage power output also increased with decreasing PbTe stage load

voltage. This happened because of a slightly larger temperature differential

across the silicon-germanium stage at the lower PbTe stage load voltages. This,

in turn, was due to lower heater losses at the lower temperatures.

Some of the results of the parametric analyses conducted as a part of

this special study are shown in Figure 53. The parametrics shown in Figure 53

represent the performance of the cascaded generator at the maximum power point

at each value of heat input shown. Extrapolation of the data shown in Figure

53 beyond the heat input of 3900 watts is not recommended because the silicon-

germanium temperatures approach unacceptable values.

J.   Memorandum #14

The special study summarized in Memorandum #14, titled Mathematical Model

and Computer Program for the Design and Analysis of Silicon-Germanium Air-Vac

RTG's, concerned itself with the documentation of the results of the RTG Design

Study task of the contract. The documentation consisted of two parts. The first

part gave a detailed discussion of the mathematical model underlying the computer

program that enables the design and performance analysis of silicon-germanium

RTG's. The second part of the documentation pertains to the computer code and,

in essence serves as a user code to the computer program. As mentioned in

Section II of this report, the computer code of the RTG design procedure is called

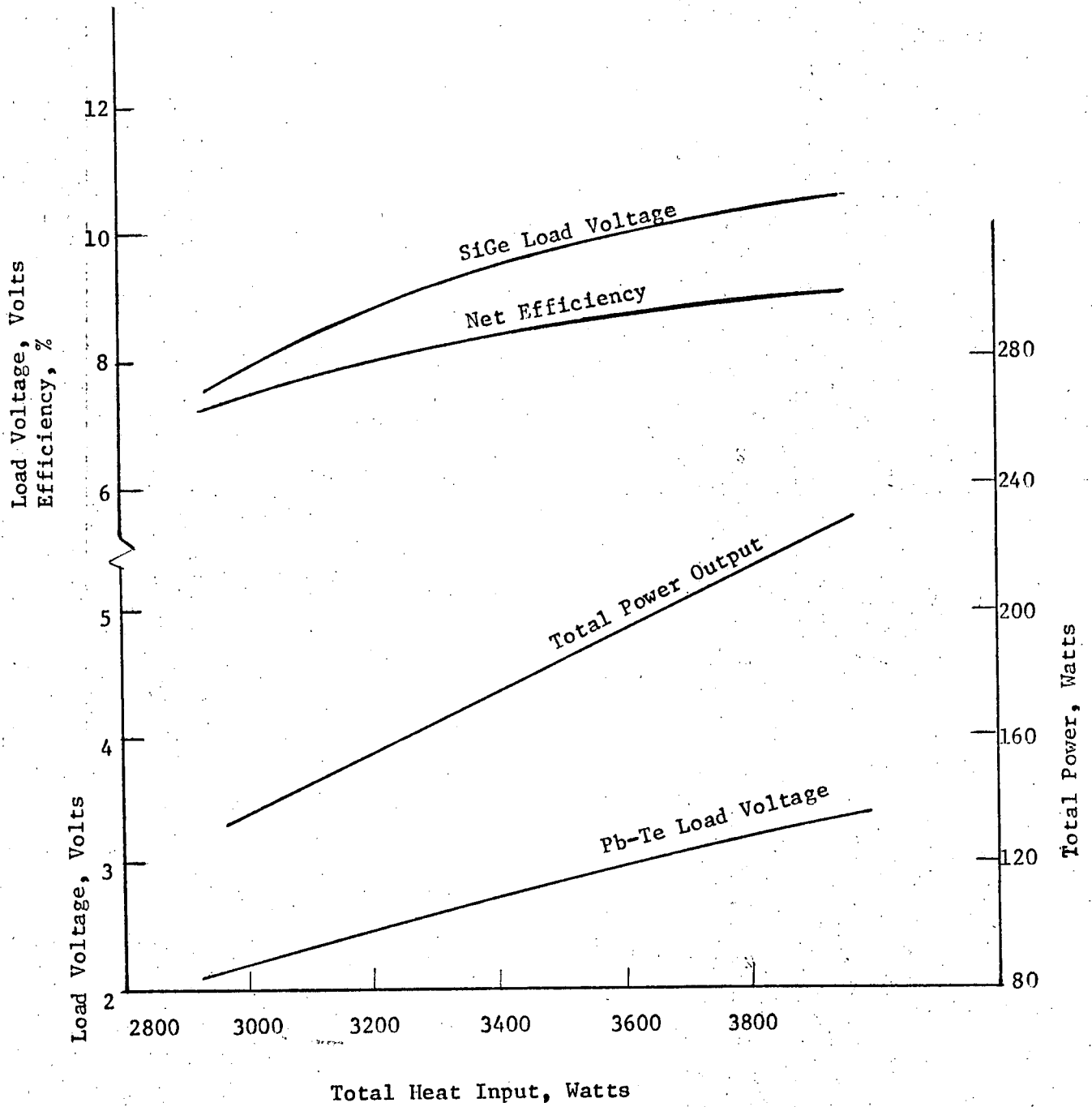CASCADED GENERATOR PARAMETERS

FIGURE 53

RATEG and has been made operational both at Resalab as well as at JPL. The code is available on punch cards and paper tape.

The mathematical basis of the RTG model and the associated computer code were discussed in Section II and the discussion will not be repeated here. The code has been used on the present contract to conduct parametric analyses, such as its use on the special study discussed under Part H.

VI. REFERENCES

1. P. E. Gray, <u>The Dynamic Behavior of Thermoelectric Devices</u>, (The Technology Press of MIT, Cambridge, 1960).

2. V. Raag, Eng. Conv. <u>8</u>, 169 (1968).

3. V. Raag, Proceedings 4th IECEC, Washington, D.C., September, 1969.

4. L. Ekstrom and J. P. Dismukes, J. Phys. Chem. Solids <u>27</u>, 857 (1966).

5. J. P. Dismukes, L. Ekstrom, E. F. Steigmeier, I. Kudman and D. S. Beers, J.Appl. Phys. <u>35</u>, 2899 (1964).

6. V. Raag, <u>The Performance Characteristics of Silicon-Germanium Alloys in Thermoelectric Applications</u>, Resalab Energy Conversion, 1969.

7. V. Raag, Memorandum #8, Resalab Energy Conversion, October, 1970.

8. V. Raag, Contract #NAS 5-3410, December, 1963.

9. RCA, Twenty-Third Monthly Report on AEC Contract #AT (29-2)-2510, November, 1969.

10. RCA, Twenty-Fourth Monthly Report on AEC Contract #AT (29-2)-2510, December, 1969.

11. I. M. Lifshitz and V. V. Slyozov, J.Phys.Chem. Solids <u>19</u>, 35 (1961).

12. NASA SP-8010, May, 1968.

13. NASA SP-8020, May, 1969.

14. Appendix B, RS-3703001, DRL Control #S1-0004, May 27, 1970.

15. J. R. Moszynski, <u>Proceedings of the Fourth Symposium on Thermophysical Properties</u>, ASME Publication, 1968.

16. Y. S. Touloukian, <u>Thermodynamic and Transport Properties of Gases, Liquids and Solids</u>, ASME Publication, McGraw Hill, New York, 1959.

17. S. Chapman and T. Cowling, <u>The Mathematical Theory of Non-Uniform Gases</u>, Cambridge, 1960.

18. J. O. Hirschfelder, C. F. Curtiss, and R. B. Bird, <u>Molecular Theory of Gases and Liquids</u>, John Wiley & Sons, Inc., New York, N.Y., 1954.

19. JPL Memorandum #342-70-B-549, W. D. Leonard, April 28, 1970.

20. W. D. Leonard et al, Memorandum #7, Resalab Scientific,
     May 20, 1970.